TÜBİTAK

Turkish Journal of Earth Sciences

http://journals.tubitak.gov.tr/earth/

Research Article

Turkish J Earth Sci
(2015) 24: 111-164
© TÜBİTAK
doi:10.3906/yer-1412-31

Origin, evolution, and tectonic setting of the eastern part of the Mexican Volcanic Belt and comparison with the Central American Volcanic Arc from conventional multielement normalized and new multidimensional discrimination diagrams and discordancy and significance tests

Surendra P. VERMA*
Renewable Energy Institute, Universidad Nacional Autónoma de México, Temixco, Morelos, Mexico

Received: 28.12.2014 • **Accepted/Published Online:** 17.02.2014 • **Printed:** 10.04.2015

Abstract: If both the Mexican Volcanic Belt (MVB) and the Central American Volcanic Arc (CAVA) have been related to the subduction of the Cocos plate beneath the North American and Caribbean plates, respectively, their magmas, and especially the less evolved basic varieties, should show considerable similarities. The conventional multielement normalized diagrams indicate more complex petrogenetic processes for the MVB than the CAVA. Forty-five statistically coherent tectonomagmatic discrimination diagrams were used to infer the tectonic setting of the controversial geological subprovince of the eastern part of the MVB (E-MVB). Basic rocks from the E-MVB indicated a continental rift setting, whereas the intermediate rocks were more consistent with a transitional setting of rift to collision. The acid rocks, presumably having a larger crustal component than the intermediate and basic rocks, showed inconclusive results. The volcanic rock data from the CAVA were used to successfully test these diagrams. The expected arc setting was consistently indicated for the CAVA from basic, intermediate, and acid rocks, confirming the satisfactory functioning of the diagrams. The data for all three types of rocks from the E-MVB and CAVA were then objectively compared for their similarities and differences. Specially designed computer programs were used to efficiently apply discordancy and significance tests at the strict 99% confidence level. Most (43 out of 50) chemical elements and (25 out of 28) log-ratio parameters in basic rocks from the E-MVB and CAVA showed statistically significant differences. For intermediate rocks and, to a lesser extent, for acid rocks, a large number of parameters also showed differences between the E-MVB and CAVA. The differences in the inferred tectonic settings for basic and evolved rocks from the E-MVB are likely related to the different magmatic sources.

Key words: Tectonomagmatic discrimination diagrams, discordancy tests, significance tests, continental rift, continental arc, collision tectonic setting

1. Introduction

Geochemistry is concerned mainly with the elucidation of geological processes through the determination and interpretation of chemical compositions of earth materials (Wedepohl, 1971; Cox et al., 1979; Taylor and McLennan, 1985; Ragland, 1989; Wilson, 1989; Rollinson, 1993). The common practice of data visualization and interpretation currently followed is still the same as that used for several decades, and it consists of the use of bivariate, ternary, and normalized multielement diagrams prepared from the data resulting from sample collection, preparation, and laboratory analysis (Wedepohl, 1971; Cox et al., 1979; Freeze and Cherry, 1979; Taylor and McLennan, 1985; Ragland, 1989; Wilson, 1989; Rollinson, 1993; Tatsumi and Eggins, 1995; Hall, 1996; Ottonello, 1997). The statistical methods are generally limited to the conventional univariate, bivariate, or multivariate techniques inappropriate for handling of compositional data (e.g., Pearson, 1897; Chayes, 1960; Aitchison, 1981, 1982, 1984, 1986; Aitchison et al., 2000; Egozcue et al., 2003; Aitchison and Egozcue, 2005; Buccianti et al., 2006; Agrawal and Verma, 2007; Verma, 2010). In spite of such a criticism, it is unfortunate that the traditional diagrams and related inappropriate statistical methods are still in wide use.

For the classification of fresh volcanic rocks, the well-known total alkalis versus silica (TAS) diagram (Le Bas et al., 1986; Le Bas and Streckeisen, 1991; Le Bas, 2000; Le Maitre et al., 2002) proposed by the International Union of Geological Sciences (IUGS) is extensively used (nearly

* Correspondence: spv@ier.unam.mx

2100 citations of Le Bas et al. (1986) alone in international journals, as confirmed on 15 July 2014 in the Science Citation Index). The computer program SINCLAS, written in Visual Basic, for rock classification based on the IUGS scheme and CIPW norm computation (Verma et al., 2002, 2003) is now superseded by IgRoCS (Verma and Rivera-Gómez, 2013b, written in VisualNet). For the classification of altered rocks, however, the TAS diagram is not recommended (Le Bas et al., 1986). Other bivariate diagrams based on the so-called immobile elements has been proposed (Floyd and Winchester, 1975, 1978; Winchester and Floyd, 1976, 1977). These diagrams are in extensive use for the classification of altered rocks (with >2500 citations in international journals), but they have been shown to be unsuitable and inconsistent with the IUGS scheme for rock classification (Verma et al., 2010).

New multidimensional discrimination diagrams based on a coherent statistical treatment of compositional data (Aitchison, 1986) and use of linear discriminant analysis (Agrawal, 1999) are now available for all kinds of magmas from ultrabasic and basic to acid (Verma et al., 2006b, 2012, 2013b; Agrawal et al., 2008; Verma and Agrawal, 2011; Verma SP and Verma SK, 2013).

The Mexican Volcanic Belt (MVB; also called the Trans-Mexican Volcanic Belt) is a major geological province in central Mexico, which extends approximately east-west from Veracruz (V) to Puerto Vallarta (Pu; Figure 1, modified after Verma, 2002). This Miocene to Recent province, more than 1000 km long and about 200–500 km wide, houses over 8000 volcanoes (some being active) and several geothermally promising areas, two of which are already producing electricity, as well as numerous

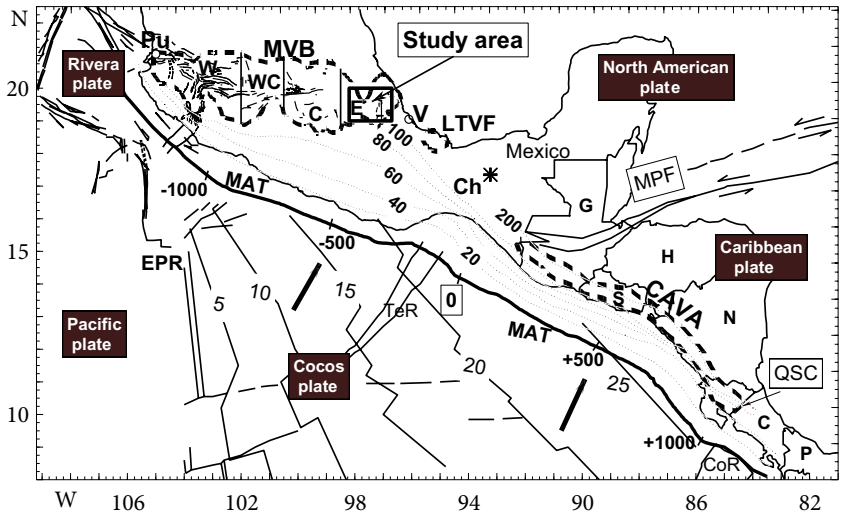

Figure 1. Simplified regional tectonics of southern Mexico and Central America showing the approximate location of the Mexican Volcanic Belt (MVB) and Central American Volcanic Arc (CAVA), map modified after Verma (2002). The MVB is approximately subdivided into W–western, WC–west-central, C–central, and E–eastern parts. The box in the eastern part of the MVB is the main study area. The location of the Middle America Trench (MAT) is shown by thick blue curve. Other tectonic and volcanic features are: EPR–East Pacific Rise; TeR–Tehuantepec Ridge; CoR–Cocos Ridge; MPF–Motagua-Polochic fault system; QSC–Quesada sharp contortion; and LTVF–Los Tuxtlas Volcanic Field. The countries are: G–Guatemala; S–El Salvador; H–Honduras; N–Nicaragua; C–Costa Rica; P–Panama. The Mexican cities are: Pu–Puerto Vallarta; V–Veracruz. The traces marked by numbers 5 to 25 on the oceanic Cocos plate give the approximate age of the oceanic plate; the dashed-dotted lines marked by numbers 20 to 200 on the continental (North American and Caribbean) plates indicate the approximate depth of the subducted Cocos plate (note the truncation of 80-km and 100-km depth contours in the study area; even the correctness of the contours in front of the LTVF has been criticized by Verma (2006, 2009); the numbers –1000, –500, 0, +500, and +1000 represent the approximate horizontal distance in kilometers from the triple junction represented by the intersection of three plates (Cocos, North American, and Caribbean); the negative numbers are for Mexico whereas the positive numbers are for Central America. These distances were used by Verma (2002) to compare and contrast the volcanism in southern Mexico with the CAVA. Simplified fracture and fault main patterns are also shown schematically using dashed curves.

mineralized areas under exploitation. The tectonic models include the conventional subduction-related origin (e.g., Molnar and Sykes, 1969; Negendank et al., 1981, 1985; Suarez and Singh, 1986; Pardo and Suárez, 1995; Gómez-Tuena et al., 2003; Carrasco-Núñez et al., 2005). Alternative models have been proposed since the early days of Alexander von Humboldt in 1808. These include fracture-related origin (e.g., von Humboldt, 1808; Mooser and Maldonado-Koerdell, 1961; Mooser, 1969; De Cserna, 1971), transtension or intraplate transform (e.g., Shurbet and Cebull, 1984; Cebull and Shurbet, 1987), plume-related origin (e.g., Moore et al., 1994; Márquez et al., 1999a), extension or rift-related origin (e.g., Sheth et al., 2000; Márquez et al., 2001; Verma, 2002, 2004, 2009), and a slab-detachment model (e.g., Ferrari, 2004). Thus, its origin has been highly debated (e.g., Ferrari and Rosas-Elguera, 1999; Márquez et al., 1999b; Blatter et al., 2001; Ferrari et al., 2002; Verma, 2002, 2004, 2009; Torres-Alvarado and Verma, 2003; Gómez-Tuena et al., 2007; Pérez-Campos et al., 2008; Pacheco and Singh, 2010; Verma et al., 2011).

The MVB contains mainly late Neogene to Quaternary (late Miocene to Holocene and even historic) eruptive products. Unfortunately, the samples for geochemistry are seldom specifically dated, although ages can be assumed for most of them based on other dated samples. This study is concerned with the eastern part of the MVB (E-MVB), where the analyzed and compiled samples mostly span a narrow range of less than 5 m.y. and all of them can be treated together. Similarly, there is no age-specific difference between the basic and evolved (intermediate and acid) rocks; they are considered as contemporary.

However, to the south of Mexico, the Central American Volcanic Arc (CAVA) from Guatemala to northwestern Costa Rica, located in the Caribbean Plate, presumably originated from the subduction of the same oceanic Cocos plate that subducts beneath the North American plate (Figure 1). The CAVA, a continental arc subparallel to the Middle America Trench (MAT; see the orientations of the CAVA and MAT in Figure 1), is considered a classic arc-trench system (e.g., Carr et al., 1982; Carr and Rose, 1986; Feigenson and Carr, 1993; Leeman and Carr, 1995; Carr et al., 2007). The compiled samples also are of similar ages as those from the MVB, namely late Neogene to Quaternary.

On the other hand, highly efficient and appropriate computational tools such as DODESSYS (Verma and Díaz-González, 2012), OYNYL (Verma et al., 2006a), and UDASYS (Verma et al., 2013a) for applying discordancy and significance tests (Barnett and Lewis, 1994; Jensen et al., 1997; Miller and Miller, 2005; Verma, 2005) have recently been developed. The statistical inference in these programs is made through the new, highly precise, and accurate critical values obtained from Monte Carlo simulations (Verma and Quiroz-Ruiz, 2008, 2011; Verma et al., 2008; Cruz-Huicochea and Verma, 2013; Verma and Cruz-Huicochea, 2013).

Besides the conventional techniques of multielement normalized diagrams, my aim is to illustrate the use of the new geochemical tools of multidimensional tectonomagmatic diagrams, log-ratio transformed variables, and discordancy and significance tests, thus providing further constraints on the origin and tectonic setting of the E-MVB and comparing this subprovince with the CAVA. This paper should reinforce new guidelines in geological and geochemical research.

2. New analytical data

I present new geochemical data for 1 volcanic rock sample from the Acoculco caldera area, 6 from the La Malinche volcano, and 18 from the Domos Las Derrumbadas area (Tables 1 and 2). Major and trace elements were obtained from X-ray fluorescence spectrometry at the Johannes Gutenberg University, Mainz, Germany, and rare-earth elements from high-performance liquid chromatography at the Max Planck Institute for Chemistry (MPI), Mainz, Germany. The analytical details and accuracy estimates were given by Verma (1991a, 1991b) and Verma et al. (1992). Radiogenic isotopes were analyzed on two fully automated MAT 261 mass spectrometers at the MPI using procedures summarized by Verma (1992): (i) triple-collector for Nd and Pb, and (ii) double-collector later transformed to multicollector for Sr.

3. Databases and procedures

3.1. Database for the E-MVB

The database for the eastern part of the MVB was constructed from several sources (approximately from west to east): the Tecocomulco area (Santiago Tetlapayac–El Tepozán–Santa Cruz, Hidalgo State; Correa Tello, 2011), the La Malinche volcano area (~98.03°W, ~19.31°N; Castro Govea, 1999, 2007; Verma, 2002; this work), the Tulancingo-Acoculco caldera area (~98.16°W, ~19.90°N; Verma, 2001a, 2002; López Hernández, 2009; this work), the Domos Las Derrumbadas area (~98.03°W, ~19.31°N; Negendank et al., 1985; Siebe and Verma, 1988; Verma, 2002; this work), Los Humeros caldera (Verma and Lopez, 1982; Verma, 1983, 1984, 2000a; Ferriz and Mahood, 1987; Carrasco-Núñez and Branney, 2005; Carrasco-Núñez et al., 2012), the Citláltepetl or Pico de Orizaba volcano area (Kudo et al., 1985; Siebe et al., 1993; Carrasco-Núñez and Rose, 1995; Carrasco-Núñez, 2000; Rossotti et al., 2006; Schaaf and Carrasco-Núñez, 2010), the Quezalapa-Las Cumbres area (Rodríguez et al., 2002), the Cofre de Perote area (Carrasco-Núñez et al., 2005, 2010), Mesa Buen País (Dávalos Elizondo, 2009), the Palma Sola area (Negendank et al., 1985; Orozco-Esquivel, 1995; Gómez-Tuena et al., 2003), the Southern volcanic area (Orozco-Esquivel et al.,

Table 1. New geochemical and isotopic data for volcanic rock samples from the Acoculco caldera and La Malinche volcano, eastern part of the Mexican Volcanic Belt (E-MVB), Mexico.

Sample:	CHG03	MAL02	MAL03	MAL04	MAL05	MAL06	MAL07
Long. (°W):	–98.18500	–98.0319	–98.03194	–98.0319	–98.0319	–98.0319	–98.0319
Lat. (°N):	+19.91667	+19.2308	+19.23083	+19.2308	+19.2308	+19.2308	+19.2308
Area	Acoculco caldera	La Malinche volcano	La Malinche volcano	La Malinche volcano	La Malinche volcano	La Malinche volcano	La Malinche volcano
Age	Quaternary	Quaternary	Quaternary	Quaternary	Quaternary	Quaternary	Quaternary
n1, n2, n3, n4	1, —, 1, 1	2, —, 1, 1	2, 2, 1, 1	6, 2, 1, 2	6, 2, 2, 2	6, 2, 3, 2	2, 2, 2, 2
Magma type:	Basic	Acid	Acid	Acid	Acid	Acid	Acid
Rock type:	Subalkali basalt	Dacite	Dacite	Dacite	Dacite	Dacite	Dacite
SiO_2	49.58	64.2	65.66	62.64	62.85	63.03	63.95
TiO_2	1.78	0.66	0.58	0.70	0.70	0.68	0.68
Al_2O_3	18.18	16.21	16.47	16.84	16.66	16.86	16.58
$Fe_2O_3^T$	10.82	4.39	3.82	4.93	4.98	4.81	4.59
MnO	0.159	0.073	0.066	0.084	0.087	0.082	0.080
MgO	6.11	2.31	2.10	2.90	3.01	2.87	2.52
CaO	8.85	4.34	4.24	4.93	5.04	5.095	4.74
Na_2O	3.7	4.44	4.52	4.22	4.13	4.18	4.62
K_2O	0.83	2.11	1.89	1.90	1.90	1.86	1.98
P_2O_5	0.280	0.172	0.152	0.159	0.162	0.156	0.178
LOI	0.00	1.27	0.24	0.58	0.21	0.21	0.60
Sum	100.29	100.18	99.74	99.87	99.74	99.83	100.52
$(SiO_2)_{adj}$	49.894	65.124	66.177	63.324	63.380	63.493	64.220
$(Na_2O + K_2O)_{adj}$	4.559	6.644	6.455	6.183	6.079	6.084	6.628
Q	0.00	17.23	19.38	15.23	15.62	15.76	15.31
Or	4.94	12.65	11.26	11.35	11.29	11.10	11.75
Ab	31.51	38.11	38.51	36.07	35.27	35.59	39.26
An	30.74	18.33	19.25	21.63	21.50	21.91	18.73
Di	9.50	1.93	0.78	1.65	2.14	2.054	3.02
Hy	3.22	8.36	7.89	10.46	10.51	10.07	8.45
Ol	13.63	0.00	0.00	0.00	0.00	0.00	0.00
Mt	2.41	1.71	1.48	1.91	1.93	1.86	1.77
Il	3.40	1.27	1.11	1.33	1.35	1.30	1.30
Ap	0.65	0.40	0.35	0.37	0.38	0.36	0.41
Mg#	56.90	58.64	59.61	61.31	61.92	61.66	59.66
FeO^T/MgO	1.59	1.71	1.64	1.53	1.49	1.51	1.64
Ba	—	—	500	487	481	476	518
Co	—	—	20	18	20	23	18
Cr	—	—	44	74	58	46	44
Cu	—	—	4	5	6	6	6
Nb	—	—	3.7	4.9	4.1	4.8	4.2
Ni	—	—	12	18	13	11	12
Rb	—	—	36	43	43	41	45
Sr	—	—	611	558	558	571	600

Table 1. (Continued).

Sample:	CHG03	MAL02	MAL03	MAL04	MAL05	MAL06	MAL07
Long. (°W):	–98.18500	–98.0319	–98.03194	–98.0319	–98.0319	–98.0319	–98.0319
Lat. (°N):	+19.91667	+19.2308	+19.23083	+19.2308	+19.2308	+19.2308	+19.2308
Area	Acoculco caldera	La Malinche volcano	La Malinche volcano	La Malinche volcano	La Malinche volcano	La Malinche volcano	La Malinche volcano
Age	Quaternary	Quaternary	Quaternary	Quaternary	Quaternary	Quaternary	Quaternary
n1, n2, n3, n4	1, –––, 1, 1	2, –––, 1, 1	2, 2, 1, 1	6, 2, 1, 2	6, 2, 2, 2	6, 2, 3, 2	2, 2, 2, 2
Magma type:	Basic	Acid	Acid	Acid	Acid	Acid	Acid
Rock type:	Subalkali basalt	Dacite	Dacite	Dacite	Dacite	Dacite	Dacite
V	–––	–––	66	94	90	105	66
Y	–––	–––	12.2	16.3	16.4	17.0	15.2
Zn	–––	–––	54	58	58	60	64
Zr	–––	–––	130	136	141	132	128
$(^{87}Sr/^{86}Sr)_m$	0.703953	0.704976	0.704493	0.704576	0.704591	0.704629	0.704554
$(^{143}Nd/^{144}Nd)_m$	0.512828	0.512632	0.512758	0.512692	0.512741	0.512729	0.5127125

Abbreviations: The subscript adj refers to adjusted data (anhydrous 100% adjusted basis); Mg# = 100 $Mg^{2+}/(Mg^{2+} + Fe^{2+})$, atomic; FeO^T = total iron expressed as FeO; computer program for adjustments and norm calculations can be either SINCLAS by Verma et al. (2002) or IgRoCS by Verma and Rivera-Gómez (2013a). Replicate analyses of major elements were performed for most samples; n1–number of analyses for major elements; n2–number of analyses for trace elements; n3–number of analyses for Sr isotopes ($^{87}Sr/^{86}Sr$); n4–number of analyses for Nd isotopes ($^{143}Nd/^{144}Nd$). Rounded concentration values were reported; the sum may not be consistent sometimes. The $^{87}Sr/^{86}Sr$ ratios are normalized to $^{86}Sr/^{88}Sr = 0.11940$ and adjusted to SRM987 $^{87}Sr/^{86}Sr$ of 0.710230. The $^{143}Nd/^{144}Nd$ are normalized to $^{146}Nd/^{144}Nd = 0.72190$ and adjusted to La Jolla $^{143}Nd/^{144}Nd$ of 0.511860. The measured $^{87}Sr/^{86}Sr$ for the SRM987 standard was 0.710216 ± 11 (1s; n = 36) and the measured $^{143}Nd/^{144}Nd$ for the La Jolla standard was 0.511833 ± 12 (1s; n = 82) during the period of measurement of about 1 year. Note the measured isotopic ratios were adjusted following the convention of Mainz (see, e.g., Verma, 2002).

Table 2. New geochemical and isotopic data for 18 volcanic rock samples from the Domos Las Derrumbadas area, eastern part of the Mexican Volcanic Belt (E-MVB), Mexico.

Sample:	E30	E27	E31	E22	E20	E21	E19	E17	E16
Long. (°W):	–97.4752	–97.47517	–97.47517	–97.47517	–97.47517	–97.47517	–97.47517	–97.47517	–97.47517
Lat. (°N):	+19.3305	+19.3305	+19.3305	+19.3305	+19.3305	+19.3305	+19.3305	+19.3305	+19.3305
n1, n2, n3, n4	2, 2, 2, 2	2, 2, 1, 2	2, 2, 2, 2	2, 2, 1, 3	2, 2, 5, 3	2, 2, 3, 6	2, 2, 1, 1	6, 2, 2, 2	6, 2, 2, 1
Magma type:	Basic	Intermediate	Intermediate	Intermediate	Intermediate	Intermediate	Intermediate	Intermediate	Acid
Rock type:	Subalkali basalt	Basaltic andesite	Basaltic andesite	Basaltic andesite	Trachyandesite, benmorite	Andesite	Andesite	Andesite	Rhyolite
SiO_2	51.20	52.46	53.89	56	59.5	60.2	61.28	61.32	70.2
TiO_2	1.43	1.14	1.00	0.86	0.77	0.85	0.80	0.60	0.15
Al_2O_3	16.85	15.76	15.46	16.58	17.73	17.9	15.66	16.06	15.48
$Fe_2O_3^T$	9.86	8.68	7.82	7.39	6.96	5.92	5.96	5.13	2.64
MnO	0.156	0.14	0.122	0.12	0.141	0.093	0.099	0.086	0.043
MgO	6.89	8.6	8.51	5.68	1.82	2.80	4.64	3.56	0.32
CaO	9.29	8.8	7.98	7.26	4.74	6.20	5.36	5.46	1.82

Table 2. (Continued).

Sample:	E30	E27	E31	E22	E20	E21	E19	E17	E16
Long. (°W):	–97.4752	–97.47517	–97.47517	–97.47517	–97.47517	–97.47517	–97.47517	–97.47517	–97.47517
Lat. (°N):	+19.3305	+19.3305	+19.3305	+19.3305	+19.3305	+19.3305	+19.3305	+19.3305	+19.3305
n1, n2, n3, n4	2, 2, 2, 2	2, 2, 1, 2	2, 2, 2, 2	2, 2, 1, 3	2, 2, 5, 3	2, 2, 3, 6	2, 2, 1, 1	6, 2, 2, 2	6, 2, 2, 1
Magma type:	Basic	Intermediate	Intermediate	Intermediate	Intermediate	Intermediate	Intermediate	Intermediate	Acid
Rock type:	Subalkali basalt	Basaltic andesite	Basaltic andesite	Basaltic andesite	Trachyandesite, benmorite	Andesite	Andesite	Andesite	Rhyolite
Na_2O	3.61	3.25	3.52	3.53	4.86	4.44	3.98	4.09	4.30
K_2O	1.01	1.15	1.34	1.68	2.2	1.66	2	1.83	3.36
P_2O_5	0.294	0.276	0.311	0.219	0.51	0.212	0.232	0.199	0.083
LOI	0.04	0.12	0.34	0.75	0.64	0.17	0.03	1.01	1.28
Sum	100.630	100.376	100.293	100.069	99.871	100.445	100.041	99.345	99.676
$(SiO_2)_{adj}$	51.327	52.686	54.250	56.717	60.273	60.306	61.553	62.607	71.477
$(Na_2O + K_2O)_{adj}$	4.631	4.419	4.892	5.277	7.152	6.111	6.007	6.044	7.799
Q	0.00	0.00	0.00	4.64	8.82	10.04	11.74	13.5	27.70
Or	5.98	6.83	7.97	10.06	13.17	9.83	11.87	11.04	20.22
Ab	30.62	27.62	29.98	30.25	41.66	37.64	33.83	35.33	37.05
An	26.86	25.12	22.58	24.75	20.32	24.05	19.04	20.48	8.64
Di	14.19	13.59	12.22	8.33	0.10	4.40	4.96	4.74	0.00
Hy	5.93	16.63	20.35	17.50	10.54	9.88	14.41	11.45	3.01
Ol	10.83	4.71	1.84	0.00	0.00	0.00	0.00	0	0.00
Mt	2.19	2.69	2.43	2.31	2.71	2.06	2.08	1.82	1.21
Il	2.72	2.17	1.91	1.65	1.48	1.62	1.53	1.16	0.29
Ap	0.68	0.64	0.73	0.51	1.20	0.49	0.54	0.47	0.20
Mg#	62.03	71.37	73.25	65.91	41.33	55.20	66.97	64.38	25.82
FeO^T/MgO	1.29	0.91	0.83	1.17	3.44	1.90	1.16	1.3	7.42
Ba	262	389	440	464	779.5	471	799	712	924
Co	32	36	34	26	12.5	15.5	20	16	3
Cr	135	396	360	228	4.5	21.5	176	98	7
Cu	25	43	30.5	22	5.5	9.5	17.5	12	3
Nb	10.0	6.8	9.9	5.5	14.1	5.35	11.05	4.4	12.8
Ni	39	136	188.5	57	5.5	10.5	91	29	4.5
Rb	17.5	19.5	24.1	31	56.35	39.8	40.55	28.8	99.25
Sr	474	573	705	532	523.8	604.7	482	779	277
V	162	163	154	138	40.5	98.5	86.5	77	5
Y	24.1	22.2	20.4	20.45	30.35	20	18.35	15.5	7.7
Zn	74	80	84.5	77	87.5	66.5	66.5	62	71
Zr	153	162	155	140	296.9	166.45	150	138	155
La	6.9	19.1	22.2	13.1	28.4	14.2	–––	17	–––
Ce	17.1	42.5	48.3	25.8	62.9	28.4	–––	33.7	–––
Pr	2.14	5.34	5.99	4.69	7.67	3.69	–––	4.39	–––
Nd	9.86	22.3	24.5	15.9	32.5	15.5	–––	18.5	–––
Sm	2.2	4.7	4.86	3.43	6.38	3.41	–––	3.61	–––
Eu	0.7	1.48	1.47	1.74	1.81	1.09	–––	1.09	–––
Gd	2.3	4.29	4.2	6.75	5.76	3.49	–––	3.34	–––
Tb	0.34	0.61	0.66	0.49	0.81	0.61	–––	0.48	–––
Ho	0.42	0.72	0.62	0.55	0.94	0.62	–––	0.58	–––
Er	1.27	2.12	2	1.68	2.95	1.87	–––	1.82	–––
Tm	0.19	0.3	0.41	0.27	0.49	0.31	–––	0.31	–––
Yb	1.29	2.08	2.21	1.67	3.27	2.09	–––	1.9	–––
Lu	0.23	0.39	0.36	0.31	1.02	0.26	–––	0.29	–––
$(^{87}Sr/^{86}Sr)_m$	0.704206	0.704123	0.704295	0.704965	0.704626	0.704630	0.704459	0.704243	0.705167
$(^{143}Nd/^{144}Nd)_m$	0.512774	0.512776	0.512680	0.512593	0.512660	0.512642	0.512651	0.512496	0.512527

Table 2. (Continued).

Sample	E13	E15	E08	E14	E07	E04	E11	E12	E01
Long. (°W):	–97.53017	–97.47517	–97.27350	–97.47517	–97.50867	–97.47850	–97.57933	–97.52683	–97.45367
Lat. (°N):	+19.2823333	+19.3305	+19.2416667	+19.3305	+19.2795	+19.3316667	+19.2826667	+19.299	+19.2243333
n1, n2, n3, n4	2, 2, 1, 2	2, 2, 1, 1	2, 2, 1, 2	2, 2, 1, 1	2, 2, 1, 2	2, 2, 2, 1	2, 2, 1, 3	2, 2, 1, 2	6, 2, 1, 1
Rock type:	Acid	Acid	Acid	Acid	Acid	Acid	Acid	Acid	Acid
Magma type:	Rhyolite	Rhyolite	Rhyolite	Rhyolite	Rhyolite	Rhyolite	Rhyolite	Rhyolite	Rhyolite
SiO_2	71.44	71.1	71.66	71.5	71.06	72.82	73.66	74.43	73.48
TiO_2	0.14	0.15	0.15	0.15	0.15	0.06	0.06	0.06	0.04
Al_2O_3	15.64	15.52	15.64	15.61	15.54	14.05	14.18	14.3	14.09
$Fe_2O_3^T$	2.58	2.62	2.63	2.56	2.49	1.35	1.48	1.42	1.43
MnO	0.046	0.046	0.047	0.044	0.043	0.056	0.058	0.056	0.052
MgO	0.24	0.24	0.25	0.24	0.25	0.1	0.1	0.11	0.14
CaO	1.84	1.8	1.83	1.81	1.88	1.09	0.97	0.96	0.81
Na_2O	4.67	4.58	4.58	4.63	4.46	4.31	4.44	4.42	4.17
K_2O	3.42	3.4	3.42	3.42	3.42	3.78	3.81	3.84	4.11
P_2O_5	0.080	0.082	0.082	0.082	0.084	0.06	0.06	0.058	0.054
LOI	0.23	0.59	0	0	0.2	2.14	1.02	0.11	1.13
Sum	100.326	100.128	100.289	100.046	99.577	99.816	99.838	99.764	99.506
$(SiO_2)_{adj}$	71.496	71.5601659	71.5832189	71.5980188	71.6295006	74.6238739	74.6183013	74.7620369	74.7726821
$(Na_2O+ K_2O)_{adj}$	8.096	8.03164732	7.99142829	8.06103568	7.94315318	8.29040291	8.35733079	8.29684838	8.42566424
Q	26.16	26.66	26.85	26.56	27.16	31.18	30.99	31.53	31.65
Or	20.23	20.22	20.19	20.24	20.37	22.89	22.81	22.79	24.72
Ab	39.55	39.01	38.71	39.23	38.04	37.37	38.06	37.57	35.91
An	8.61	8.45	8.53	8.47	8.85	5.14	4.48	4.40	3.76
Di	0.00	0.00	0.00	0.00	0.00	0.00	0.00	0.00	0.00
Hy	2.74	2.77	2.78	2.69	2.68	1.48	1.58	1.54	1.67
Ol	0.00	0.00	0.00	0.00	0.00	0.00	0.00	0.00	0.00
Mt	1.16	1.19	1.18	1.15	1.13	0.62	0.67	0.64	0.65
Il	0.27	0.29	0.28	0.29	0.29	0.12	0.12	0.11	0.08
Ap	0.19	0.19	0.19	0.19	0.20	0.14	0.14	0.13	0.12
Mg#	21.09	20.83	21.45	21.22	22.38	17.54	16.25	18.20	21.95
FeO^T/MgO	9.67	9.82	9.47	9.60	8.96	12.15	13.32	11.62	9.19
Ba	958	906	961	954.5	946.5	1008	1019	1055	1024
Co	1	2.5	2.5	2	5	1	1.5	1	1
Cr	6	3	7	2.5	4.5	4.5	6.5	5.5	7.5
Cu	2.5	1.5	1.5	1.5	1		1		
Nb	13.2	12.9	13.4	13.35	12.35	15.25	13.85	14	14.35
Ni	5	4.5	4.5	4	4.5	4	5	3.5	4
Rb	101.55	101.85	102.6	103.55	103.2	114.3	112.3	114.75	121
Sr	282	280.1	285.4	282.6	288.8	132.6	130.85	131.2	97.65
V	6.5	7	7	5.5	14	6	5.5	5.5	5
Y	6.9	7.8	8.1	7.45	7.7	6.75	6.65	6.5	4.05
Zn	71.5	75.5	69	68	73.5	60.5	63.5	56.5	61.5
Zr	153	157.7	154.9	155	155.55	61.65	61.85	62.55	47.9
La	–––	8.26	10.2	–––	14.8	5.71	–––	–––	4.8
Ce	–––	15.7	27	–––	31.6	11.2	–––	–––	10
Pr	–––	2.18	2.47	–––	3.78	1.38	–––	–––	1.3
Nd	–––	8.87	9.5	–––	14.8	4.95	–––	–––	4.2
Sm	–––	1.73	1.73	–––	2.6	0.96	–––	–––	1
Eu	–––	0.4	0.46	–––	0.59	0.25	–––	–––	0.2
Gd	–––	1.42	1.38	–––	1.84	0.87	–––	–––	0.9
Tb	–––	0.22	0.2	–––	0.24	0.17	–––	–––	0.2
Ho	–––	0.19	0.18	–––	0.21	0.19	–––	–––	0.22
Er	–––	0.48	0.48	–––	0.49	0.5	–––	–––	0.38
Tm	–––	0.09	0.1	–––	0.1	0.11	–––	–––	0.08
Yb	–––	0.5	0.58	–––	0.45	0.53	–––	–––	0.38
Lu	–––	0.1	0.07	–––	0.11	0.12	–––	–––	0.08
$(^{87}Sr/^{86}Sr)_m$	0.705238	0.705225	0.705253	0.705218	0.705221	0.705172	0.704965	0.704987	0.704976
$(^{143}Nd/^{144}Nd)_m$	0.512536	0.512556	0.512556	0.512520	0.512524	0.512568	0.512613	0.512624	0.512563

More explanation is given in the footnote of Table 1.

2007), the Xapala-Naolinco area (Siebert and Carrasco-Núñez, 2002; Morales Barrera, 2009), and several other localities of the E-MVB (Demant, 1981; Negendank et al., 1985).

3.2. Database for the CAVA

Relatively fresh rock data for samples from the known continental arc tectonic setting were compiled from numerous sources: for Guatemala, localities or volcanoes such as Cerro Chiquito, Cuilapa, Guatemala, Moyuta, Pacaya, Santa María, Tecuamburro, and the Tacaná volcano partly located in Mexico (Carr, 1984; Bardintzeff and Deniel, 1992; Duffield et al., 1992; Carr et al., 1990; Chan et al., 1999; Patino et al., 1997; Walker et al., 2000; Cameron et al., 2002; Mora et al., 2004; Singer et al., 2011); for El Salvador, localities or volcanoes such as Ahuachapán, Berlín, Boqueron, Cerro Rico, Cerro Nejapa, Chichontepec, IIopango, Izalco, La Concepción caldera, Santa Ana, San Miguel, and San Salvador (Carr, 1984; González Partida et al., 1997; Patino et al., 1997; Rotolo and Castorina, 1998; Chan et al., 1999; Walker et al., 2000; Agostini et al., 2006); for Honduras, localities or volcanoes such as Tegucigalpa, Yojoa, and Zacate (Patino et al., 1997, 2000; Walker et al., 2000); for Nicaragua, localities or volcanoes such as Apoyo, Asososca, Cerro Negro, Coseguina, El Hormigón, Granada, Managua, Masaya, Momotombo, Nejapa, San Cristobal, Telica, and Ticomo (Carr, 1984; Sussman, 1985; Hazlett, 1987; Carr et al., 1990; Walker et al., 1990, 2001; Chan et al., 1999; Patino et al., 1997; Pardo et al., 2008; Avellán et al., 2012); and for Costa Rica, localities or volcanoes such as Arenal, Irazu, Guayacan, Platanar, Tenorio, and Turrialba (Reagan and Gill, 1989; Carr et al., 1990; Chan et al., 1999; Patino et al., 1997; Alvarado et al., 2006; Bolge et al., 2006; Ryder et al., 2006). Clearly altered samples, such as hydrothermally altered or intensely weathered samples and those described as altered by the original authors (from petrographic observations), were avoided in the present compilation.

Honduras (H) lies behind the trace of the CAVA (the main arc location) as well as far away from the MAT as outlined in Figure 1. Honduran samples are not strictly from the CAVA, but they could be called back-arc rocks (Figure 1). These samples are included here to understand how the continental back-arc or behind-the-arc data would behave in these new multidimensional diagrams.

3.3. Data processing procedures

All data were processed in the SINCLAS module (Verma et al., 2002) of the IgRoCS software (Verma and Rivera-Gómez, 2013b) to automatically determine the magma and rock types under the Middlemost (1989) option for Fe-oxidation adjustment, which allowed me to strictly follow the IUGS recommendations for rock classification and nomenclature (Le Bas et al., 1986; Le Bas, 2000; Le Maitre et al., 2002) and treat all major element data in exactly the same manner. The use of 100% adjusted data on an anhydrous basis and after Fe-oxidation adjustment helps minimize the effect of analytical errors and element mobility and makes the use of the TAS diagram more consistent with the IUGS scheme.

Commercial software Statistica was used for data compilation and calculation of DF1 and DF2 functions from complex equations and for graphics. The 90 equations for 45 diagrams were presented by the original authors (Verma et al., 2006b; Agrawal et al., 2008; Verma and Agrawal, 2011; Verma et al., 2012, 2013b; Verma SP and Verma SK, 2013), were also reproduced recently in a single source (Verma SP et al., 2015), and, therefore, are not reproduced here. Individual sample probability values were computed from the method outlined by Verma and Agrawal (2011) and complemented by Verma (2012). Computer program TecD (Verma and Rivera-Gómez, 2013b) was used for automatic sample counting in the four tectonic fields of the diagrams for basic and ultrabasic rocks (Verma et al., 2006b; Agrawal et al., 2008; Verma and Agrawal, 2011). Similarly, for the probability-based counting (concepts explained in Verma and Agrawal, 2011; Verma, 2012) of intermediate and acid rock samples in different diagrams (Verma SP and Verma SK, 2013; Verma et al., 2012, 2013b), an unpublished computer program, TecDIA (Verma SP et al., in preparation), was employed.

An objective comparison of the data for similar magma types from the E-MVB and CAVA was achieved through the application of discordancy and significance tests (Fisher F and Student t) (Barnett and Lewis, 1994; Jensen et al., 1997; Miller and Miller, 2005; Verma, 2005; Verma and Díaz-González, 2012; Verma et al., 2013a).

Conventional petrogenetic interpretation was achieved through multielement normalized diagrams and Sr-Nd radiogenic isotopes.

4. Results and discussion

All E-MVB compiled samples, including the newly analyzed ones, are classified from the TAS diagram (Figure 2a). The compiled rocks from the CAVA are also plotted in the TAS diagram (Figure 2b). In both areas, the compiled rocks vary mainly from basalt to rhyolite, representing all three types of magmas (basic, intermediate, and acid). The E-MVB rocks, however, are more alkali-rich as compared to the CAVA rocks (Figures 2a and 2b).

The total numbers of samples compiled from the E-MVB were 51, 115, and 91, respectively, for basic, intermediate, and acid rocks; for the CAVA, these were 180, 413, and 36 samples, respectively (Tables 3–8).

Tables 3, 5 and 7 present a geochemical synthesis of major and trace elements and CIPW normative minerals for the E-MVB, whereas Tables 4, 6 and 8 provide a summary of the data for the CAVA. The final column in each table includes the overall mean and standard

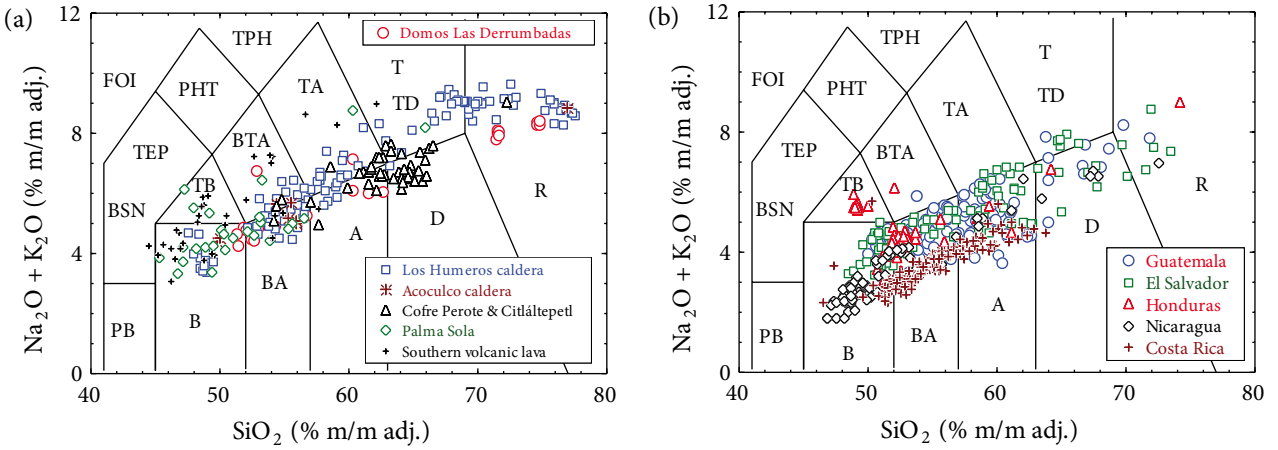

Figure 2. The total alkalis versus silica (TAS: $(SiO_2)_{adj}$ – $(Na_2O+K_2O)_{adj}$) bivariate diagram for volcanic rock classification recommended by the International Union of Geological Sciences (IUGS) showing samples from the **(a)** eastern part of the Mexican Volcanic Belt (E-MVB) and **(b)** Central American Volcanic Arc (CAVA). The rock types (fieldnames) are as follows: A–andesite; B–basalt; BA–basaltic andesite; BSN–basanite; BTA–basaltic trachyandesite; D–dacite; FOI–foidite; PB–picrobasalt; PHT–phonotephrite; R–rhyolite; T–trachyte; TA–trachyandesite; TB–trachybasalt; TD–trachydacite; TEP–tephrite; TPH–tephriphonolite. The magma types are as follows: ultrabasic–<45%, 35%–45% $(SiO_2)_{adj}$; basic–45%–52% $(SiO_2)_{adj}$; intermediate–52%–63% $(SiO_2)_{adj}$; acid–>63%, 63%–80% $(SiO_2)_{adj}$. The symbols for rock samples are explained as insets.

deviation values for the E-MVB or CAVA; these results are reported as rounded values according to the flexible rules put forth by Verma (2005). The total number of samples compiled from each area is also given; the number of data from a given parameter is generally less than this number, or equal to it especially for major elements (Tables 3–8). The mean geochemical data for individual areas are for all compiled samples, whereas the synthesis for each province (the E-MVB or CAVA) was obtained after the separation of discordant outliers from single-outlier type tests applied at the strict 99% confidence level (Verma, 2005; Verma et al., 2009).

4.1. Application of multielement normalized diagrams

Chondrite-normalized rare-earth element (REE) plots are shown in Figures 3a–3c for the average data for the La Malinche, Las Derrumbadas, and Los Humeros areas, respectively. Figure 3d, on the other hand, presents normalized average data for the E-MVB crustal rocks. Evolved acid rocks from the La Malinche and Las Derrumbadas areas (Figures 3a and 3b) show significantly lower concentrations of all REEs, which will be difficult to explain from a simple fractional crystallization process because all partition coefficients are >1 for most, if not all, common rock-forming minerals (e.g., Rollinson, 1993; Torres-Alvarado et al., 2003). Even the intermediate rocks do not have significantly higher REE concentrations than basic rocks from these two areas (Figures 3a and 3b). For the Los Humeros caldera area, both acid and intermediate rocks show significantly higher concentrations for most REEs than the basic rocks; however, the average values of the REEs for acid and intermediate rocks do not show significant differences (Figure 3c). These observations (Figures 3a–3c) require a crustal component in the genesis of the evolved magmas. The average crustal rock data from the E-MVB are presented in Figure 3d. The basic crust seems to have low concentrations of all REEs as compared to the E-MVB volcanic rocks. Therefore, in principle, such an assimilant could provide a suitable endmember for an assimilation combined with a fractional crystallization model for the generation of the evolved E-MVB magmas. The REE data would also be consistent with the E-MVB evolved magmas to represent near complete (anatectic) melts of the underlying intermediate and acid crust (Figures 3a–3d; DePaolo, 1981; Verma, 2001b; Torres-Alvarado et al., 2003). Quantitative models can be easily worked out, but it would be better to present and discuss other geochemical and isotopic constraints, especially those from the new multidimensional diagrams.

The average concentration data are also plotted in a multielement primitive mantle normalized diagram for the E-MVB in Figure 4a and the CAVA in Figure 4b. The E-MVB basic rocks do not show the conventional anomaly of high-field strength elements (HFSEs) Nb and Th with respect to the large ion lithophile elements (LILEs) Ba and K (Figure 4a), whereas the CAVA basic rocks clearly show such a negative anomaly (Figure 4b). The intermediate and acid rocks from both provinces (the E-MVB and CAVA) show similar negative Nb anomalies (Figures 4a and 4b). Again, the basic crust from the E-MVB could provide an appropriate assimilant for explaining also the LILEs and HFSEs.

Table 3. Geochemical composition of basic volcanic rock samples from the eastern part of the Mexican Volcanic Belt (E-MVB) obtained from Statistica, DODESSYS (Verma and Díaz-González, 2012), and UDASYS (Verma et al., 2013a).

Chemical parameter	Derrumbadas area	Los Humeros caldera	Acoculco caldera	Cofre Perote & Citláltepetl	Palma Sola area	Southern volcanic area	E-MVB
Long. (°W):	–97.4656	–97.4932	–98.1314		–96.7939	–96.6706	See
Lat. (°N):	19.2866	19.6697	19.8040		19.6780	19.7505	Figure 1
No. of samples (data)	4 (≤4)	12 (≤12)	2 (≤2)	0	15 (≤15)	21 (≤21)	54 (≤54)
$(SiO_2)_{adj}$	51.63	48.82	49.90		48.57	47.72	48.60 ± 1.67
$(TiO_2)_{adj}$	1.38	1.77	1.71		2.01	2.20	1.96 ± 0.51
$(Al_2O_3)_{adj}$	16.12	17.16	17.73		16.48	16.32	16.54 ± 1.15
$(Fe_2O_3)_{adj}$	1.458	1.733	1.6715		1.842	2.055	1.874 ± 0.338
$(FeO)_{adj}$	7.29	8.66	8.36		8.41	8.92	8.56 ± 0.95
$(MnO)_{adj}$	0.150	0.157	0.16		0.166	0.175	0.1695 ± 0.0148
$(MgO)_{adj}$	8.12	7.88	7.00		7.64	7.77	7.76 ± 1.91
$(CaO)_{adj}$	8.87	9.59	8.71		10.01	9.62	9.65 ± 0.89
$(Na_2O)_{adj}$	3.37	3.37	3.70		3.13	3.46	3.34 ± 0.48
$(K_2O)_{adj}$	1.26	0.57	0.76		1.28	1.14	1.06 ± 0.48
$(P_2O_5)_{adj}$	0.358	0.283	0.306		0.470	0.609	0.477 ± 0.280
$(Na_2O+ K_2O)_{adj}$	4.63	3.94	4.46		4.41	4.60	4.41 ± 0.74
Q	0	0	0		0	0	–––
Or	7.44	3.36	4.46		7.57	6.71	6.29 ± 2.81
Ab	28.5	28.1	31.3		23.8	24.5	25.6 ± 5.2
An	25.14	30.02	29.54		27.12	25.64	27.00 ± 3.15
Di	13.39	12.80	9.53		15.83	14.74	14.43 ± 3.78
Hy	9.53	2.14	4.13		1.84	0.45	1.97 ± 3.25
Ol	10.42	16.82	14.63		14.83	16.79	15.67 ± 3.64
Mt	2.11	2.51	2.42		2.67	2.98	2.72 ± 0.49
Il	2.62	3.35	3.26		3.81	4.18	3.74 ± 0.96
Ap	0.83	0.66	0.71		1.09	1.41	1.11 ± 0.65
Mg#	66.4	61.4	59.9		61.1	59.8	61.0 ± 6.4
FeO^T/MgO	1.07	1.36	1.41		1.40	1.50	1.41 ± 0.42
Ba	419	136	191		450	434	380 ± 156
Co	35.2	41.0	37.5		40.0	40.1	39.6 ± 8.9
Cr	303	126	78		253	243	235 ± 170
Cu	33.2	31.5	31.5		49.2		44.4 ± 15.1
Nb	13.8	12.5	13.2		24.1	22.4	19.9 ± 8.7
Ni	129	62	62		97	112	91 ± 58
Rb	24.1	8.9	8.8		28.8	21.8	19.9 ± 9.5
Sr	578	467	570		708	761	684 ± 227
Th		1.18			4.45	4.01	3.56 ± 1.68
U		0.45			1.28	1.20	1.06 ± 0.45
V	176	178	184		243		220.0 ± 41.1
Y	23.8	26.4	24.5		28.0	26.6	26.85 ± 4.29
Zn	80.5	84.5	84.5		85.8		84.7 ± 14.7
Zr	171	157	157		209	195	193 ± 51
La	18.3	9.2	10.1		30.1	29.6	25.4 ± 13.0
Ce	38.2	23.2	27.5		63.6	60.4	53.4 ± 24.8
Pr	4.85	2.77	3.2		8.05	8.9	7.04 ± 3.27
Nd	19.4	13.9	14.2		33.7	33.3	29.0 ± 12.5
Sm	4.09	3.47	3.25		7.22	7.36	6.38 ± 2.38
Eu	1.26	1.26	1.12		2.21	2.32	2.01 ± 0.66
Gd	3.64	3.60	3.35		6.52	6.80	5.94 ± 1.88
Tb	0.52	0.65	0.53		0.95	0.99	0.881 ± 0.239
Ho	0.57	0.72	0.61		0.99	1.02	0.930 ± 0.222
Er	1.62	2.04	1.64		2.58	2.70	2.41 ± 0.51
Tm	0.25	0.28	0.21			0.38	0.343 ± 0.087
Yb	1.53	1.91	1.54		2.26	2.17	2.104 ± 0.419
Lu	0.24	0.28	0.25		0.34	0.31	0.308 ± 0.064

Table 4. Geochemical composition of basic volcanic rock samples from the Central American Volcanic Arc (CAVA) obtained from Statistica, DODESSYS (Verma and Díaz-González, 2012), and UDASYS (Verma et al., 2013a).

Chemical parameter	Guatemala	El Salvador	Honduras	Nicaragua	Costa Rica (NW)	CAVA
Long. (°W) and Lat. (°N):	See Figure 1.					
No. of samples (data)	25 (≤25)	26 (≤26)	25 (≤ 25)	72 (≤72)	32 (≤32)	180 (≤180)
$(SiO_2)_{adj}$	51.08	50.79	50.30	49.00	51.19	50.16 ± 1.45
$(TiO_2)_{adj}$	1.133	1.086	1.664	0.934	0.700	0.945 ± 0.239
$(Al_2O_3)_{adj}$	19.26	18.99	18.40	17.27	20.26	18.43 ± 1.86
$(Fe_2O_3)_{adj}$	1.530	1.666	2.047	1.758	1.479	1.661 ± 0.203
$(FeO)_{adj}$	7.65	8.19	7.52	8.79	7.28	8.12 ± 0.85
$(MnO)_{adj}$	0.151	0.175	0.170	0.192	0.164	0.1742 ± 0.0168
$(MgO)_{adj}$	4.84	5.06	5.31	7.15	5.60	5.68 ± 1.53
$(CaO)_{adj}$	9.87	9.76	9.29	12.14	10.26	10.56 ± 1.21
$(Na_2O)_{adj}$	3.40	3.11	3.49	2.23	2.40	2.72 ± 0.60
$(K_2O)_{adj}$	0.837	0.948	1.365	0.391	0.505	0.508 ± 0.255
$(P_2O_5)_{adj}$	0.247	0.238	0.434	0.133	0.149	0.156 ± 0.068
$(Na_2O+ K_2O)_{adj}$	4.23	4.05	4.85	2.62	2.90	3.29 ± 0.92
Q	0.0244	0.330	0.216	0.164	2.840	−−−
Or	4.95	5.60	8.07	2.31	2.98	3.00 ± 1.51
Ab	28.7	26.3	27.3	18.8	20.1	22.7 ± 4.8
An	34.8	35.1	30.5	35.9	41.4	35.9 ± 5.8
Di	10.3	9.7	10.4	19.2	7.0	12.2 ± 5.8
Hy	10.8	12.4	7.9	10.8	19.3	12.2 ± 7.1
Ol	5.4	5.5	7.2	8.1	1.8	5.2 ± 5.2
Mt	2.219	2.415	2.967	2.549	2.145	2.409 ± 0.294
Il	2.15	2.06	3.16	1.77	1.33	1.80 ± 0.45
Ap	0.573	0.550	1.006	0.309	0.346	0.361 ± 0.158
Mg#	52.1	51.5	55.3	58.0	56.7	56.0 ± 6.5
FeO^T/MgO	1.99	2.07	1.82	1.60	1.66	1.72 ± 0.47
Ba	397	409	433	314	495	348 ± 137
Co		33.0		46.7	25.0	35.2 ± 12.6
Cr	81.9	85.9	82.5	137.7	79.4	33.2 ± 22.1
Cu	76	129	53	165	102	111 ± 56
Nb	4.04	4.51	26.09	4.11	6.44	3.86 ± 1.70
Ni	33.7	44.2	54.7	60.4	46.9	26.4 ± 15.7
Rb	12.4	14.0	16.0	8.8	9.2	10.3 ± 4.7
Sr	592	543	589	406	742	523 ± 131
Th	1.244	1.075	1.560	0.471	0.780	0.474 ± 0.212
U	0.517	0.462	0.555	0.351	0.276	0.321 ± 0.176
V	250	278	216	303	164	259 ± 60
Y	21.4	23.2	36.0	18.0	14.9	18.0 ± 4.5
Zn				71.50	75.41	73.44 ± 3.46
Zr	99.4	97.7	185.3	53.0	45.4	51.8 ± 20.4
La	9.89	10.48	21.13	4.43	14.10	6.56 ± 2.62
Ce	23.4	24.4	42.4	11.1	27.0	14.8 ± 5.0
Pr	2.86	3.74	1.12	2.40	2.86	2.32 ± 0.54
Nd	15.19	15.65	25.15	8.25	15.38	9.35 ± 2.24
Sm	3.832	3.900	6.007	2.430	3.360	2.485 ± 0.413
Eu	1.221	1.346	1.683	0.904	1.110	0.919 ± 0.129
Gd	4.11	4.29	5.99	3.12	3.02	3.05 ± 0.69
Tb	0.607	0.704		0.453	0.413	0.446 ± 0.092
Ho	0.794	0.878		0.610	0.504	0.584 ± 0.151
Er	2.221	2.360	3.313	1.797	1.541	1.767 ± 0.426
Tm	0.3800	0.3567		0.2433	0.2167	0.2137 ± 0.0307
Yb	1.958	2.223	2.886	1.550	1.489	1.547 ± 0.271
Lu	0.3015	0.3157		0.2400	0.2167	0.2348 ± 0.0437

Table 5. Geochemical composition of intermediate volcanic rock samples from the eastern part of the Mexican Volcanic Belt (E-MVB) obtained from Statistica, DODESSYS (Verma and Díaz-González, 2012), and UDASYS (Verma et al., 2013a).

Chemical parameter	Derrumbadas area	Los Humeros caldera	Acoculco caldera	Cofre Perote & Citláltepetl	Palma Sola area	Southern volcanic area	E-MVB
Long. (°W):	–97.2486	–97.2562	–98.1404	–97.2995	–96.6541	–97.0550	See
Lat. (°N):	19.4144	19.3855	19.7702	19.4324	19.7298	19.7619	Figure 1
No. of samples (data)	10 (≤10)	55 (≤55)	5 (≤5)	22 (≤22)	10 (≤10)	13 (≤13)	115 (≤115)
$(SiO_2)_{adj}$	56.66	57.00	55.41	60.34	54.60	55.35	57.09 ± 3.30
$(TiO_2)_{adj}$	0.974	1.337	1.128	0.942	1.314	1.542	1.247 ± 0.341
$(Al_2O_3)_{adj}$	16.62	17.78	17.44	17.15	17.27	17.45	17.35 ± 0.90
$(Fe_2O_3)_{adj}$	1.672	1.840	1.712	1.525	2.046	1.983	1.781 ± 0.316
$(FeO)_{adj}$	5.13	5.23	5.33	4.13	6.47	5.70	5.09 ± 1.01
$(MnO)_{adj}$	0.122	0.115	0.123	0.096	0.176	0.135	0.1192 ± 0.0280
$(MgO)_{adj}$	5.64	3.51	5.21	3.14	4.61	3.83	3.77 ± 1.42
$(CaO)_{adj}$	7.28	6.83	8.02	5.95	7.71	6.82	6.87 ± 1.49
$(Na_2O)_{adj}$	3.84	4.09	3.79	4.09	3.69	4.22	4.06 ± 0.55
$(K_2O)_{adj}$	1.754	1.925	1.528	2.362	1.729	2.359	1.814 ± 0.446
$(P_2O_5)_{adj}$	0.310	0.333	0.310	0.267	0.382	0.615	0.320 ± 0.084
$(Na_2O+ K_2O)_{adj}$	5.60	6.02	5.32	6.45	5.42	6.58	6.04 ± 1.03
Q	4.87	5.74	2.89	9.97	2.75	2.62	5.62 ± 4.24
Or	10.37	11.38	9.03	13.96	10.22	13.94	10.72 ± 2.64
Ab	32.5	34.6	32.1	34.6	31.2	35.3	34.3 ± 4.7
An	22.9	24.4	26.1	21.4	25.4	21.6	23.6 ± 5.4
Di	9.01	5.96	9.47	5.16	8.48	6.73	6.70 ± 3.61
Hy	12.70	11.72	15.13	10.25	15.22	11.14	11.89 ± 4.02
Ol	2.63	0.14	0	0.007	0.33	1.19	–––
Mt	2.42	2.67	2.48	2.21	2.97	2.88	2.58 ± 0.46
Il	1.85	2.54	2.14	1.79	2.50	2.93	2.37 ± 0.65
Ap	0.718	0.772	0.719	0.618	0.884	1.426	0.742 ± 0.195
Mg#	63.8	53.9	63.5	55.9	54.6	51.2	55.9 ± 6.8
FeO^T/MgO	1.42	2.05	1.33	1.93	2.06	2.98	1.87 ± 0.54
Ba	659	572	456		531	715	588 ± 204
Co	22.8	23.0	23.6		24.7	20.3	22.6 ± 7.2
Cr	169	24	97		87	96	23.7 ± 18.1
Cu	26.0	30.2	31.8		50.9		37.0 ± 23.1
Nb	11.1	12.5	11.5		20.9	30.1	11.68 ± 4.41
Ni	74	11	61		43	41	35.8 ± 32.0
Rb	39.5	44.4	28.5		39.9	59.6	38.3 ± 15.9
Sr	627	394	587		559	646	525 ± 168
Th	8.5	5.9			4.9	9.3	6.69 ± 4.29
U		1.8			1.4	2.8	1.92 ± 1.26
V	99	165	142		188		158 ± 52
Y	23.0	24.6	25.7		25.8	31.5	25.3 ± 5.8
Zn	76.1	86.3	81.4		88.7		82.9 ± 11.5
Zr	180	208	200		193	325	211 ± 84
La	21.7	24.5	19.3		30.3	44.0	25.1 ± 9.5
Ce	50.2	50.8	43.4		59.9	85.6	53.9 ± 19.8
Pr	5.30	5.84	5.26		7.60	12.7	4.27 ± 2.44
Nd	22.7	24.4	21.7		30.5	43.0	27.3 ± 9.2
Sm	4.63	5.31	4.44		6.16	8.69	5.80 ± 1.87
Eu	1.50	1.52	1.29		1.84	2.35	1.75 ± 0.54
Gd	4.64	5.19	4.14		5.52	8.17	5.42 ± 1.67
Tb	0.62	0.78	0.65		0.82	1.10	0.819 ± 0.238
Ho	0.67	0.87	0.67		0.91	1.14	0.873 ± 0.224
Er	2.07	2.54	1.88		2.48	3.36	2.39 ± 0.55
Tm	0.35	0.35	0.25			0.45	0.362 ± 0.093
Yb	2.23	2.34	1.69		2.32	2.85	2.35 ± 0.54
Lu	0.43	0.35	0.27		0.35	0.40	0.345 ± 0.074

Table 6. Geochemical composition of intermediate volcanic rock samples from the Central American Volcanic Arc (CAVA) obtained from Statistica, DODESSYS (Verma and Díaz-González, 2012), and UDASYS (Verma et al., 2013a).

Chemical parameter	Guatemala	El Salvador	Honduras	Nicaragua	Costa Rica (NW)	CAVA
Long. (°W) and Lat. (°N):						
No. of samples (data)	119 (≤119)	48 (≤48)	27 (≤27)	26 (≤26)	193 (≤193)	413 (≤413)
$(SiO_2)_{adj}$	56.18	57.38	53.79	55.18	55.32	54.49 ± 1.61
$(TiO_2)_{adj}$	0.855	0.863	1.052	1.166	0.602	0.637 ± 0.070
$(Al_2O_3)_{adj}$	18.52	18.04	17.92	16.59	19.54	18.76 ± 1.12
$(Fe_2O_3)_{adj}$	1.891	1.930	2.086	2.220	1.784	1.874 ± 0.219
$(FeO)_{adj}$	5.91	5.87	6.81	7.23	5.79	6.00 ± 0.84
$(MnO)_{adj}$	0.1482	0.1622	0.1675	0.1848	0.1665	0.1600 ± 0.0206
$(MgO)_{adj}$	3.69	3.16	4.63	4.45	4.11	3.95 ± 1.04
$(CaO)_{adj}$	7.63	7.09	8.72	8.67	8.85	8.28 ± 1.25
$(Na_2O)_{adj}$	3.69	3.72	3.22	3.05	3.08	3.32 ± 0.47
$(K_2O)_{adj}$	1.285	1.556	1.273	1.050	0.590	0.646 ± 0.170
$(P_2O_5)_{adj}$	0.2053	0.2424	0.3345	0.2110	0.1690	0.1901 ± 0.0402
$(Na_2O+ K_2O)_{adj}$	4.97	5.28	4.49	4.10	3.67	4.26 ± 0.81
Q	6.31	8.21	3.66	7.14	7.85	6.40 ± 3.53
Or	7.60	9.20	7.52	6.20	3.48	3.82 ± 1.01
Ab	31.21	31.47	27.21	25.85	26.07	28.05 ± 4.00
An	29.7	27.7	30.7	28.4	37.3	32.8 ± 5.5
Di	5.59	4.91	8.50	10.85	4.49	5.35 ± 2.97
Hy	14.55	13.39	16.31	15.60	16.51	15.61 ± 2.85
Ol	0.0280	0.068	0.297	0	0	–––
Mt	2.741	2.798	3.025	3.218	2.586	2.716 ± 0.318
Il	1.623	1.639	1.997	2.215	1.143	1.210 ± 0.133
Ap	0.476	0.562	0.775	0.489	0.392	0.441 ± 0.093
Mg#	52.0	48.2	54.2	51.4	55.1	53.2 ± 5.4
FeO^T/MgO	2.19	2.62	1.98	2.21	1.89	2.00 ± 0.54
Ba	541	663	658	806	505	541 ± 126
Co		23.3		34.4	21.5	22.2 ± 5.2
Cr	39.0	14.7	65.3	59.1	30.7	27.1 ± 20.5
Cu	42.1	106.1	95.2	157.2	71.1	74.2 ± 38.7
Nb	3.60	3.45	9.30	6.87	3.75	3.51 ± 0.76
Ni	23.3	9.4	46.1	29.9	22.4	21.3 ± 14.8
Rb	23.0	29.6	24.3	25.4	10.4	11.4 ± 3.32
Sr	498	437	558	443	678	597 ± 116
Th	1.622	2.080	1.635	1.421	0.941	0.996 ± 0.352
U	0.715	1.053	0.627	1.114	0.363	0.384 ± 0.126
V	184	167	229	253	148	166 ± 55
Y	24.7	29.4	35.4	26.1	15.8	16.4 ± 2.32
Zn				93.5	80.5	80.1 ± 8.8
Zr	113.8	119.5	128.5	100.7	50.5	53.4 ± 12.5
La	10.85	13.86	18.51	7.81	11.37	10.90 ± 2.82
Ce	22.3	28.0	36.6	18.8	23.5	22.9 ± 5.1
Pr	3.67	3.83			3.13	3.11 ± 0.48
Nd	15.06	17.80	23.49	12.66	13.19	13.23 ± 1.92
Sm	3.768	4.504	5.621	3.597	3.022	2.984 ± 0.354
Eu	1.117	1.246	1.508	1.198	1.038	1.022 ± 0.098
Gd	3.948	4.655	5.569	4.246	2.951	2.970 ± 0.373
Tb	0.6471	0.7333		0.6875	0.4538	0.4467 ± 0.0429
Ho	0.831	0.910			0.552	0.549 ± 0.046
Er	2.403	2.707	3.278	2.510	1.576	1.557 ± 0.153
Tm	0.4350	0.3825			0.2382	0.2296 ± 0.0204
Yb	2.171	2.549	2.666	2.300	1.561	1.508 ± 0.140
Lu	0.3415	0.3867		0.3488	0.2417	0.2354 ± 0.0235

Table 7. Geochemical composition of acid volcanic rock samples from the eastern part of the Mexican Volcanic Belt (E-MVB) obtained from Statistica, DODESSYS (Verma and Díaz-González, 2012), and UDASYS (Verma et al., 2013a).

Chemical parameter	Derrumbadas area	Los Humeros caldera	Acoculco caldera	Cofre Perote & Citláltepetl	Palma Sola area	Southern volcanic area	E-MVB
Long. (°W):	–97.4776	–97.4189	–98.2186	–97.2716	–96.4100		See
Lat. (°N):	19.2933	19.6583	19.9558	19.2131	19.6630		Figure 1
No. of samples (data)	10 (≤10)	53 (≤53)	1 (≤1)	25 (≤25)	1 (≤1)	0	90 (≤90)
$(SiO_2)_{adj}$	72.81	71.53	76.90	65.10	65.96		69.82 ± 4.44
$(TiO_2)_{adj}$	0.112	0.391	0.15	0.623	0.37		0.434 ± 0.263
$(Al_2O_3)_{adj}$	15.14	14.70	12.36	16.80	16.88		15.31 ± 1.45
$(Fe_2O_3)_{adj}$	0.663	0.782	0.40	1.172	1.08		0.889 ± 0.368
$(FeO)_{adj}$	1.326	1.564	0.79	2.804	2.15		1.90 ± 0.86
$(MnO)_{adj}$	0.050	0.046	0.053	0.0774	0.130		0.059 ± 0.025
$(MgO)_{adj}$	0.200	0.555	0.07	1.639	1.60		0.74 ± 0.59
$(CaO)_{adj}$	1.493	1.457	0.43	4.659	3.42		2.38 ± 1.70
$(Na_2O)_{adj}$	4.497	4.354	3.91	4.497	5.69		4.41 ± 0.55
$(K_2O)_{adj}$	3.633	4.516	4.92	2.442	2.51		3.77 ± 1.12
$(P_2O_5)_{adj}$	0.073	0.103	0.015	0.189	0.210		0.122 ± 0.074
$(Na_2O+ K_2O)_{adj}$	8.13	8.87	8.84	6.94	8.20		8.23 ± 0.98
Q	28.6	24.6	34.0	17.0	13.5		22.8 ± 7.1
Or	21.5	26.7	29.1	14.4	14.8		22.3 ± 6.6
Ab	38.1	36.8	33.1	38.1	48.2		37.3 ± 4.7
An	6.9	6.1	1.6	18.4	13.1		9.9 ± 6.8
Di	0	0.337	0.34	2.887	2.02		—
Hy	2.29	2.88	0.98	5.96	5.70		3.76 ± 2.26
Ol	0	0	0	0	0		0
Mt	0.96	1.13	0.57	1.70	1.56		1.29 ± 0.53
Il	0.212	0.743	0.29	1.183	0.70		0.82 ± 0.50
Ap	0.169	0.239	0.040	0.438	0.49		0.283 ± 0.172
Mg#	20.7	34.6	13.8	50.1	57.1		38.6 ± 13.2
FeO^T/MgO	10.1	5.5	16.2	2.5	1.9		3.46 ± 1.39
Ba	976	742	61		2688		834 ± 150
Co	2.0	2.0	1.0		9.6		1.96 ± 1.47
Cr	5	6	10		18		6.00 ± 1.88
Cu	1	4	1		16		1.42 ± 1.24
Nb	13.5	12.9	42.3		26.5		13.05 ± 2.11
Ni	4	6	8		7		5.14 ± 1.42
Rb	107.4	111.5	167.0		66.2		110.9 ± 18.4
Sr	219	123	5		906		141 ± 88
Th		18.7			6.5		17.8 ± 4.8
U		4.8			4.6		4.83 ± 0.73
V	7.0	33	4		90		21.9 ± 17.5
Y	7.0	26.6	43.2		16.9		22.6 ± 9.0
Zn	67.0	42.2	54.0		43.4		54.1 ± 15.2
Zr	117	251	173		81		218 ± 94
La	8.8	32.8	16.2		46.3		28.6 ± 13.1
Ce	19.1	60.6	20.8		72.8		52.5 ± 22.4
Pr	2.22	5.01	2.82		9.23		4.27 ± 2.43
Nd	8.5	24.0	9.5		34.3		21.2 ± 9.2
Sm	1.60	4.61	1.61		5.96		4.04 ± 1.73
Eu	0.38	0.63	0.14		1.61		0.603 ± 0.401
Gd	1.28	4.39	1.4		4.68		3.66 ± 1.80
Tb	0.21	0.69	0.26		0.58		0.589 ± 0.248
Ho	0.20	0.75	0.31		0.49		0.532 ± 0.309
Er	0.47	2.45	0.96		1.19		1.66 ± 1.03
Tm	0.10	0.34	0.12				0.244 ± 0.139
Yb	0.49	2.73	1.02		1.00		2.22 ± 1.02
Lu	0.10	0.47	0.16		0.15		0.384 ± 0.165

Table 8. Geochemical composition of acid volcanic rock samples from the Central American Volcanic Arc (CAVA) obtained from Statistica, DODESSYS (Verma and Díaz-González, 2012), and UDASYS (Verma et al., 2013a).

Chemical parameter	Guatemala	El Salvador	Honduras	Nicaragua	Costa Rica (NW)	CAVA
Long. (°W) and Lat. (°N):	See Figure 1.					
No. of samples (data)	11 (≤11)	17 (≤17)	2 (≤2)	5 (≤5)	1 (≤1)	36 (≤36)
$(SiO_2)_{adj}$	66.77	67.68	69.15	67.72	63.74	67.38 ± 3.18
$(TiO_2)_{adj}$	0.506	0.490	0.449	0.489	0.362	0.489 ± 0.154
$(Al_2O_3)_{adj}$	16.32	16.09	15.39	15.79	17.46	16.17 ± 0.83
$(Fe_2O_3)_{adj}$	1.156	1.276	1.141	1.124	1.541	1.218 ± 0.326
$(FeO)_{adj}$	2.76	2.82	2.69	2.73	3.85	2.81 ± 0.84
$(MnO)_{adj}$	0.1101	0.1214	0.0765	0.1268	0.2283	0.1222 ± 0.0225
$(MgO)_{adj}$	1.33	1.07	0.65	1.26	1.91	1.18 ± 0.54
$(CaO)_{adj}$	3.83	3.16	2.39	4.11	6.25	3.51 ± 1.30
$(Na_2O)_{adj}$	4.20	4.32	5.05	4.07	3.89	4.28 ± 0.60
$(K_2O)_{adj}$	2.87	2.83	2.81	2.44	0.76	2.73 ± 0.89
$(P_2O_5)_{adj}$	0.156	0.144	0.197	0.139	0.0010	0.147 ± 0.081
$(Na_2O+ K_2O)_{adj}$	7.07	7.14	7.86	6.51	4.66	7.00 ± 0.93
Q	20.4	22.4	22.0	23.3	20.0	21.8 ± 5.6
Or	17.0	16.7	16.6	14.4	4.5	16.1 ± 5.3
Ab	35.5	36.5	42.7	34.4	32.9	36.2 ± 5.1
An	16.3	13.8	10.1	17.4	27.9	15.2 ± 5.3
Di	1.42	0.75	0.41	1.72	2.55	—
Hy	6.10	5.85	4.81	5.81	9.11	5.95 ± 2.29
Ol	0	0	0	0	0	0
Mt	1.68	1.85	1.65	1.63	2.23	1.77 ± 0.47
Il	0.961	0.931	0.853	0.928	0.688	0.929 ± 0.293
Ap	0.362	0.333	0.455	0.322	0.0023	0.340 ± 0.188
Mg#	45.0	38.6	25.2	45.0	46.9	40.9 ± 7.8
FeO^T/MgO	3.11	4.25	8.69	3.01	2.74	3.55 ± 0.99
Ba	852	1036	937	1255	592	1018 ± 197
Co		8.4				8.4 ± 5.2
Cr	4.05	4.00	5.56		2.483	4.17 ± 2.28
Cu		9.00	13.04		6.87	10.49 ± 3.54
Nb	5.55	4.40	5.73			5.03 ± 1.33
Ni	3.45	3.44	3.77		0.86	3.31 ± 1.21
Rb	74.2	60.4	22.3	42.5	16.4	51.6 ± 22.2
Sr	322	305	302	388	623	339 ± 125
Th	5.72	2.91			1.00	4.78 ± 1.97
U	2.19	1.56			0.55	1.90 ± 0.73
V		51.8	12.0		25.0	42.9 ± 35.8
Y	19.3	30.8	41.8		20.5	27.6 ± 9.8
Zn					94	—
Zr	179	165	187	145	61	162 ± 53
La	16.63	18.90	19.82		12.68	17.02 ± 3.22
Ce	34.02	35.57	38.77		29.01	29.88 ± 1.76
Pr	5.34	4.97			4.05	4.97 ± 0.66
Nd	15.5	23.5	22.7		17.0	20.3 ± 6.1
Sm	3.66	5.71	5.40		3.94	5.15 ± 1.77
Eu	0.73	1.47	1.36		1.27	1.21 ± 0.52
Gd	3.80	5.02	5.29		3.74	4.77 ± 1.53
Tb	0.520	0.825			0.566	0.731 ± 0.315
Ho	0.730	1.310			0.688	0.909 ± 0.348
Er	2.22	3.20	4.56		2.03	3.27 ± 1.34
Tm		0.560			0.326	0.443 ± 0.165
Yb	1.92	3.36	3.34		2.19	2.81 ± 1.03
Lu	0.310	0.490			0.355	0.419 ± 0.169

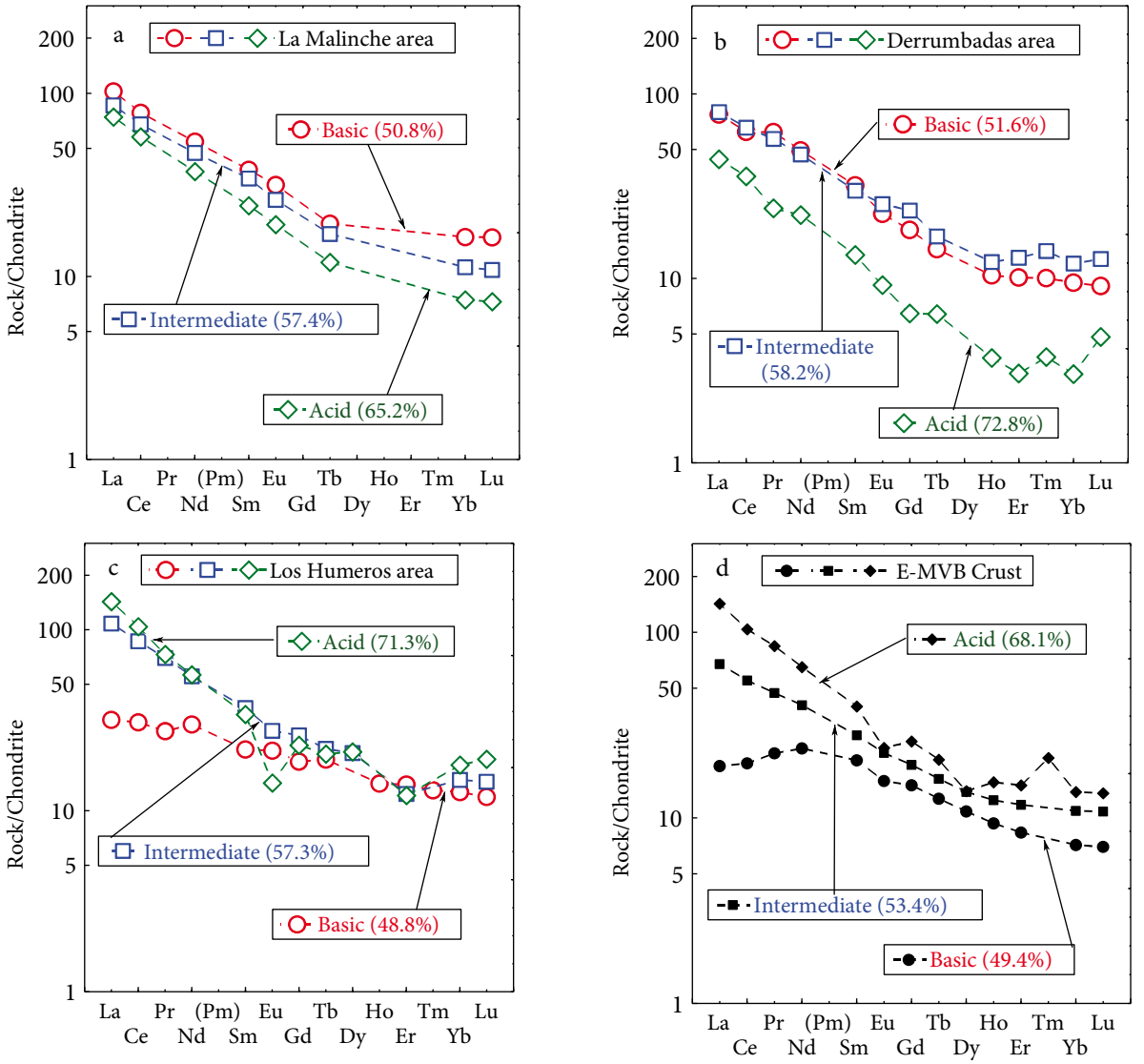

Figure 3. Chondrite-normalized REE patterns (chondrite values from McDonough and Sun, 1995) for average concentrations of basic, intermediate, and acid rocks from **(a)** La Malinche area, **(b)** Las Derrumbadas area, **(c)** Los Humeros area, and **(d)** E-MVB crustal rocks. The adjusted silica $(SiO_2)_{adj}$ values are also given in each plot. Approximate locations of these areas are given in the text in terms of coordinates.

The Sr-Nd isotope data from the E-MVB and CAVA are plotted in the conventional bivariate diagram (Figure 5), which also includes data from numerous island arcs and continental rifts (unpublished compilation of the author) as well as the mixing curve of basalts and sediments from the subducting slab (Verma, 2000b) and Mexican lower and upper crusts. The CAVA average data for basic, intermediate, and acid magmas plot close to each other and are shifted towards the down-going slab mixing curve, as are most of the island arc data. The samples from the E-MVB plot within the "mantle array", close to the continental rift samples (Figure 5). Furthermore, the average values for basic, intermediate, and acid E-MVB rocks show significantly different compositions, although all three compositions plot within the mantle array, away from the down-going slab. The acid rock composition is similar to the Mexican lower crust (Figure 5). These isotopic characteristics of the E-MVB magmas are inconsistent with their derivation from the same source; instead, they require that the basic and acid rocks originated from different sources (the basic rocks mainly in the mantle and the acid rocks in the underlying crust). The intermediate rocks may represent a mixture of these two types of magmas. The available geochemical evidence favors this general model for the E-MVB, although locally fractional crystallization may play a dominant role at some specific volcanic centers.

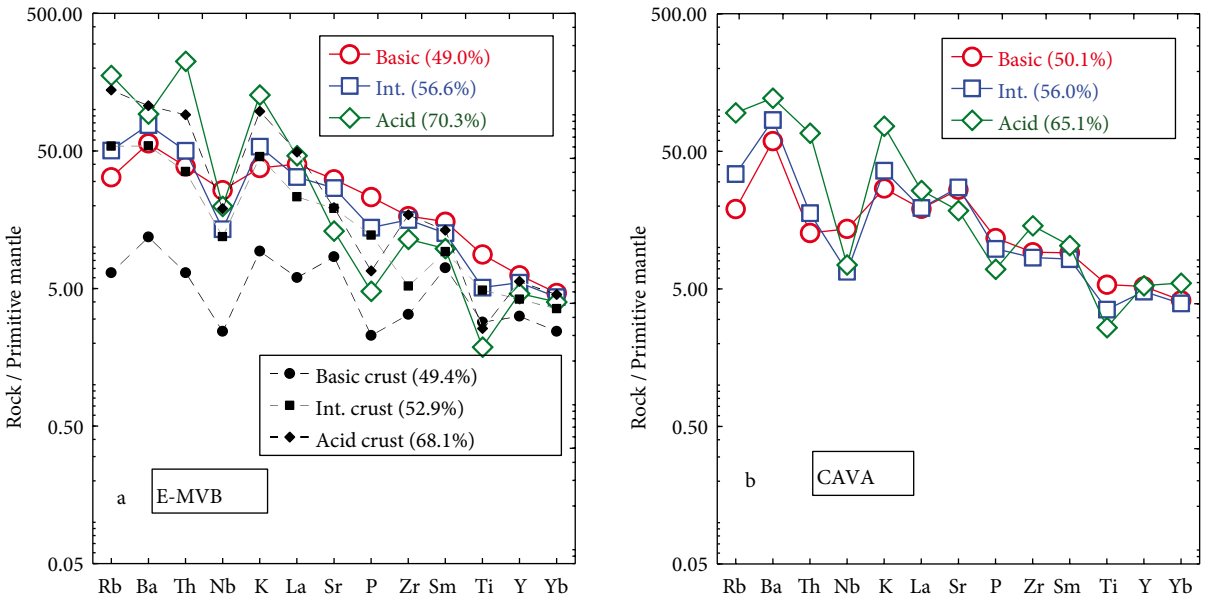

Figure 4. Multielement primitive mantle normalized diagram (normalizing values from Sun and McDonough, 1989) for average concentrations of basic, intermediate, and acid rocks from **(a)** E-MVB for volcanic as well as crustal rocks and **(b)** CAVA for volcanic rocks. The adjusted silica $(SiO_2)_{adj}$ values are also given in each plot.

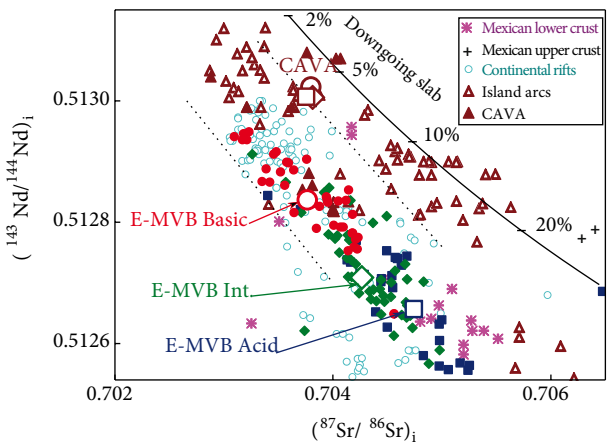

Figure 5. Conventional Sr-Nd isotope diagram for the E-MVB and CAVA rocks. The trace of the "mantle array" is from Faure (1986); the trace of the "Downgoing slab" is from Verma (2000b), in which the numbers 2% to 20% indicate the amount of sediment in the basalt-sediment mixture; other numerous island arc, continental rift, and Mexican lower and upper crust data are also shown for reference (Verma SP, unpublished compilation); the average values for basic, intermediate, and acid rocks from both the E-MVB and CAVA are shown using larger symbols.

4.2. Application of multidimensional diagrams

Appropriate multidimensional discrimination diagrams, specifically proposed for a given magma type, were applied to the compiled data from both areas. The respective plots are presented in Figures 6 to 11 for basic rocks, Figures 12 to 17 for intermediate rocks, and Figures 18 to 22 for acid rocks. The results are summarized in Tables 9 and 10, 11 and 12, and 13 and 14 for basic, intermediate, and acid rocks, respectively.

4.2.1. Basic rocks

Three sets of five diagrams each indicated a continental rift tectonic setting for the E-MVB (Figures 6, 8, and 10; Table 9) and an arc setting for the CAVA (Figures 7, 9, and 11; Table 10). Application of major element-based diagrams (Verma et al., 2006b) to basic rock data from the E-MVB showed that 44 to 50 out of 51 samples (equivalent to about 86% to 98%; see the first part of Table 9) plotted in the continental rift field. The remaining few samples (7 to 1) were distributed among the three remaining tectonic fields (Figure 6; Table 9). Therefore, a continental rift setting is clearly indicated by these diagrams (Figures 6a–6c, 6e), and the diagram from which this setting is absent (Figure 6d) can be considered as an inapplicable diagram (Table 9). The other two sets of diagrams based on log-ratios of immobile elements (Figures 8 and 10; Agrawal et al., 2008; Verma and Agrawal, 2011) confirm this conclusion because most samples plot in the tectonic field of continental rift (see the second and third parts of Table 9).

The same three sets of diagrams (Figures 7, 9, and 11; Verma et al., 2006b; Agrawal et al., 2008; Verma and Agrawal, 2011) indicated an arc setting for basic rocks from the CAVA, because most samples plotted in this field (Table 10). These diagrams (Figures 7, 9, and 11) cannot discriminate island arc from continental arc because, for

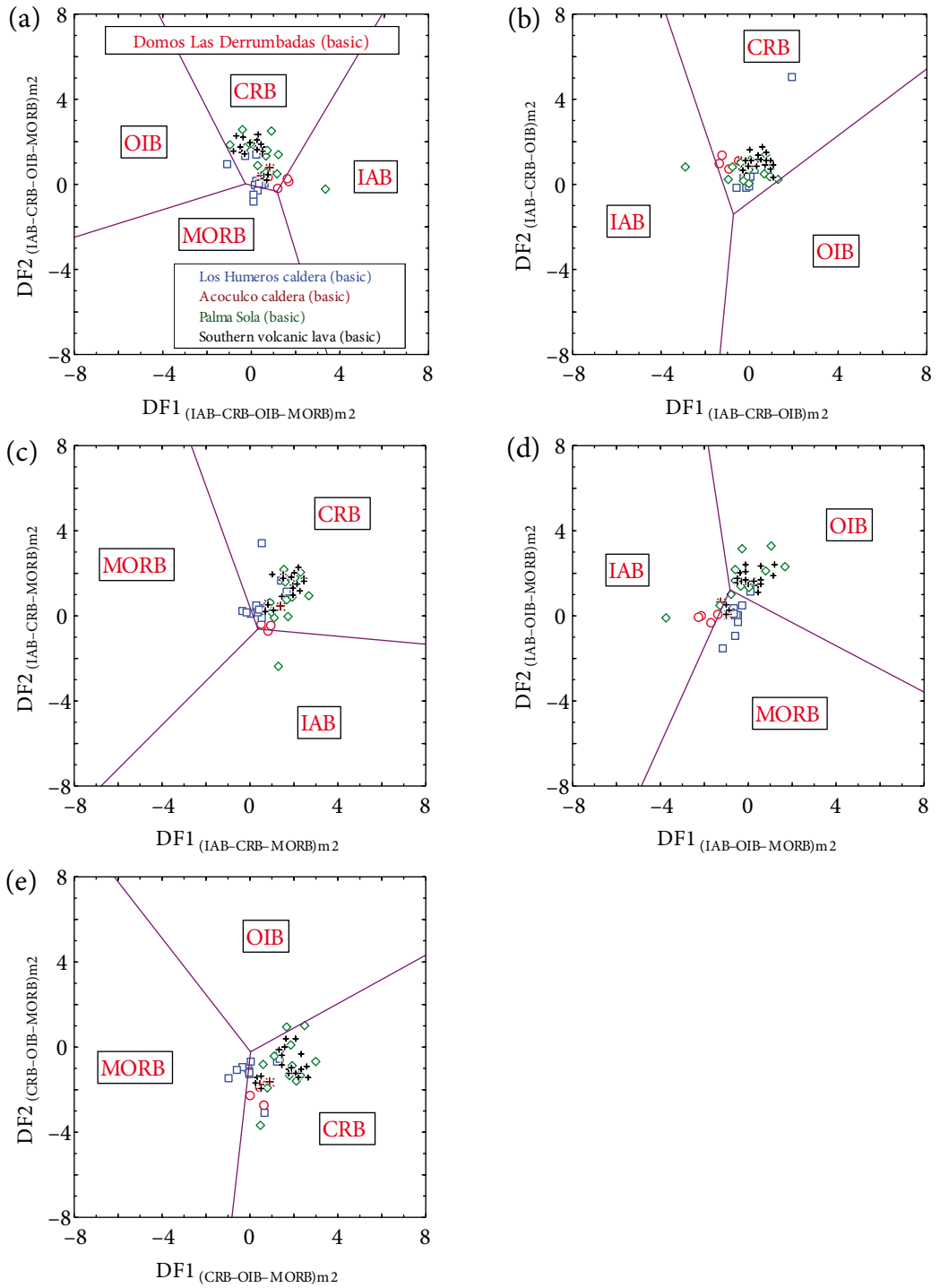

Figure 6. Application of the set of five multidimensional DF1–DF2 diagrams based on linear discriminant analysis of log-transformed major element ratios for the discrimination of four tectonic settings (arc, continental rift, ocean island, and mid-ocean ridge) for basic magmas from the eastern part of the Mexican Volcanic Belt (E-MVB). See the subscript m2 in all these diagrams (Verma et al., 2006b). Symbols are explained in insets. The letter B after the name of the tectonic field represents basic and ultrabasic rocks. **(a)** Four tectonic settings IA–CR–OI–MOR; **(b)** three tectonic settings IA–CR–OI; **(c)** three tectonic settings IA–CR–MOR; **(d)** three tectonic settings IA–OI–MOR; **(e)** three tectonic settings CR–OI–MOR.

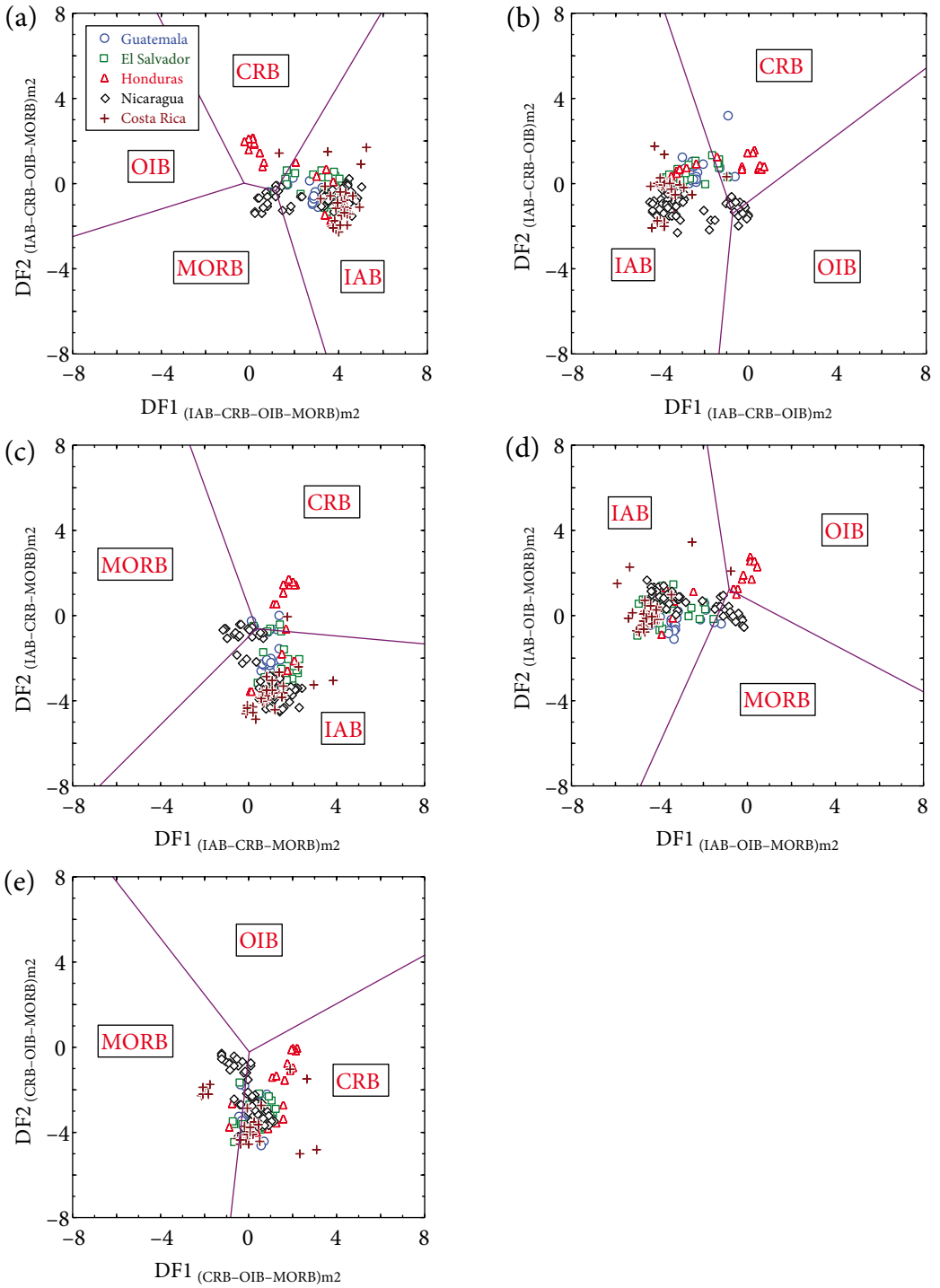

Figure 7. Application of the set of five multidimensional DF1–DF2 diagrams for basic magmas from the Central American Volcanic Arc (CAVA). More details are given in Figure 6.

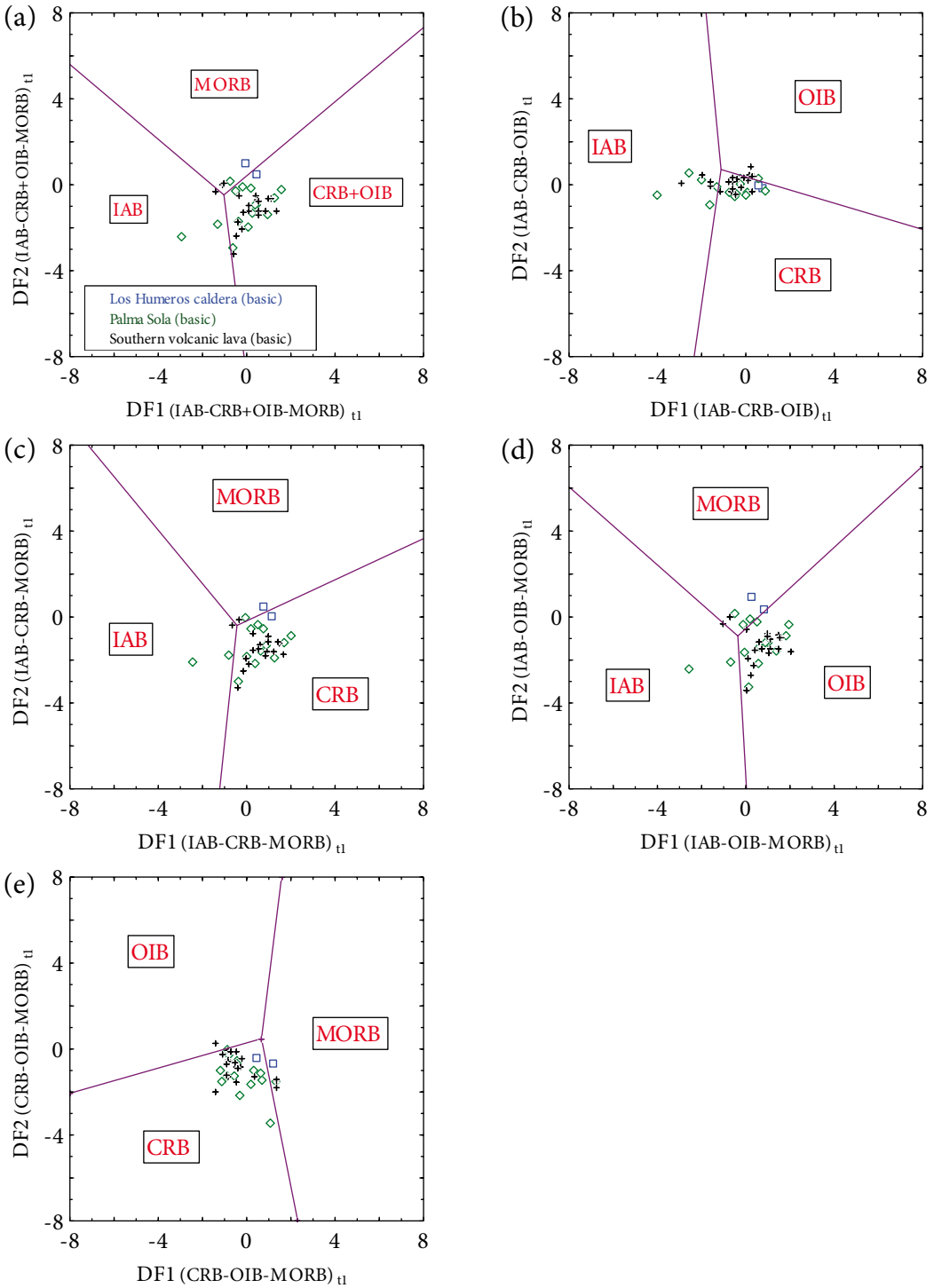

Figure 8. Application of the set of five multidimensional DF1–DF2 diagrams based on log-ratios of immobile trace elements (see the subscript t1 in all these diagrams; Agrawal et al., 2008) for basic rock samples from the eastern part of the Mexican Volcanic Belt (E-MVB). The symbols are shown as an inset in (a). **(a)** Three tectonic settings IA–CR+OI–MOR; **(b)** three tectonic settings IA–CR–OI; **(c)** three tectonic settings IA–CR–MOR; **(d)** three tectonic settings IA–OI–MOR; **(e)** three tectonic settings CR–OI–MOR.

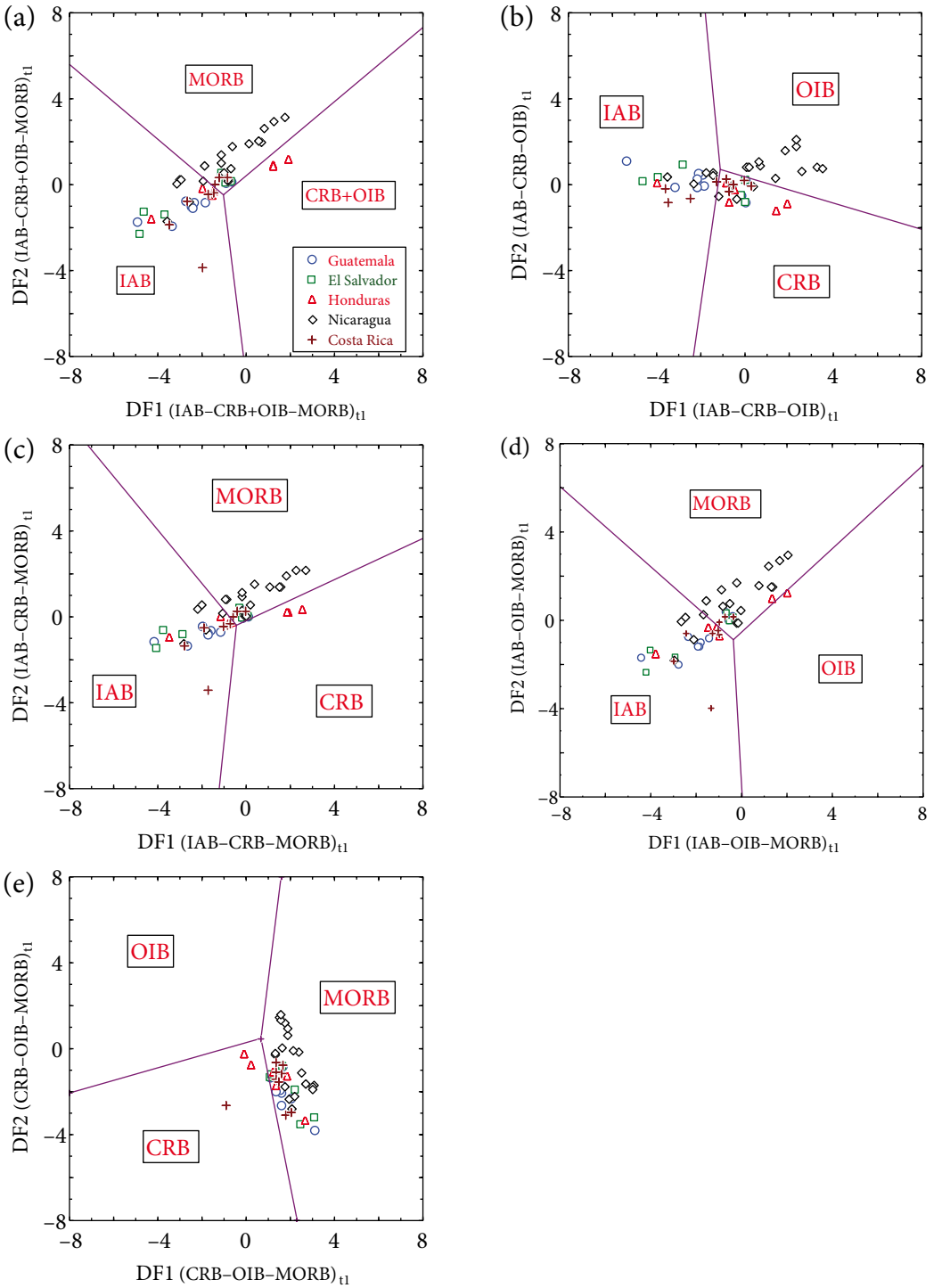

Figure 9. Application of the set of five multidimensional DF1–DF2 diagrams for basic rock samples from the Central American Volcanic Arc (CAVA). More details are given in Figure 8.

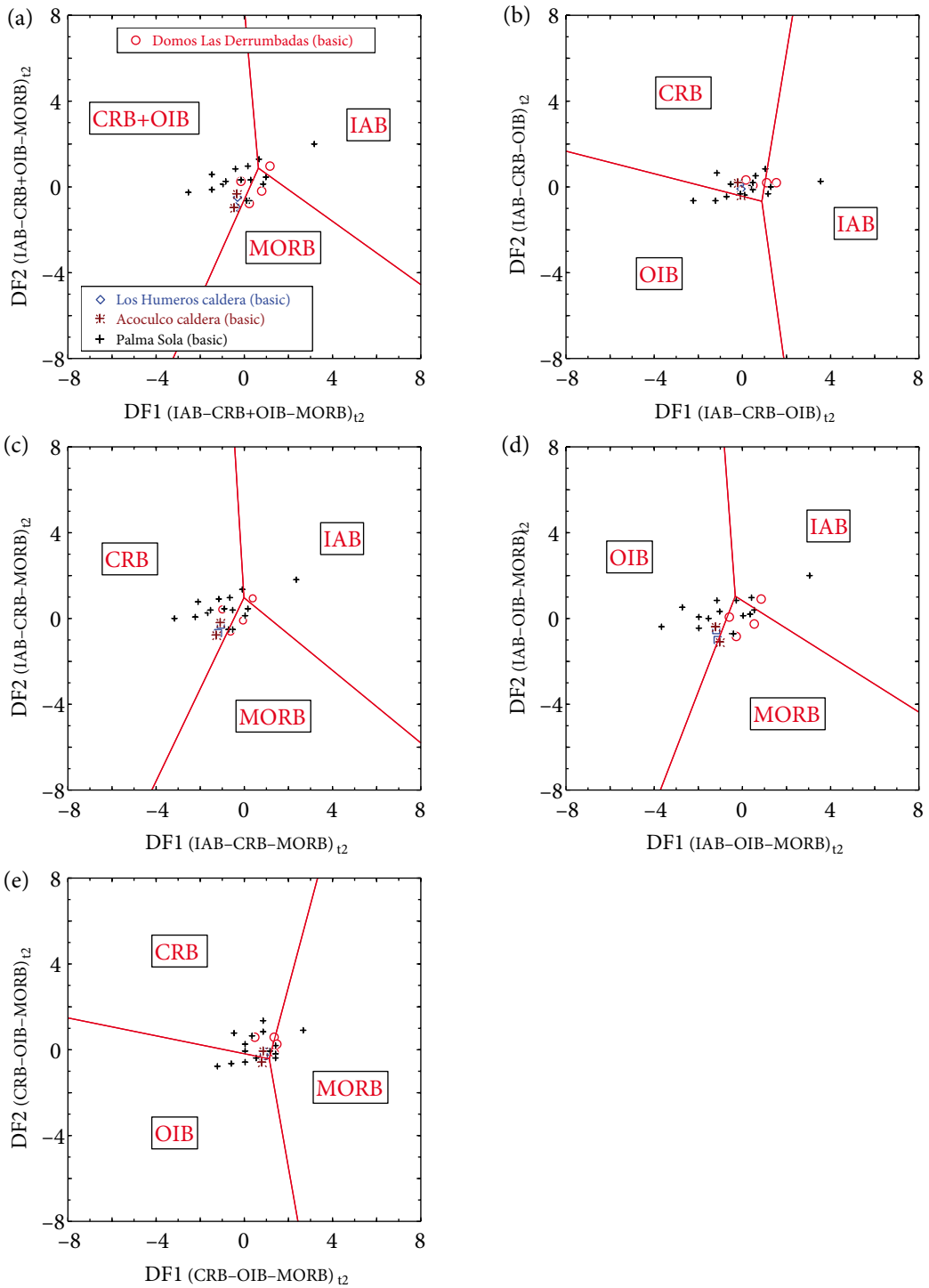

Figure 10. Application of the set of five multidimensional DF1–DF2 diagrams based on log-ratios of immobile major and trace elements (see the subscript t2 in all these diagrams; Verma and Agrawal, 2011) for basic rock samples from the eastern part of the Mexican Volcanic Belt (E-MVB). The symbols are shown as insets in (a). **(a)** Three tectonic settings IA–CR+OI–MOR; **(b)** three tectonic settings IA–CR–OI; **(c)** three tectonic settings IA–CR–MOR; **(d)** three tectonic settings IA–OI–MOR; **(e)** three tectonic settings CR–OI–MOR.

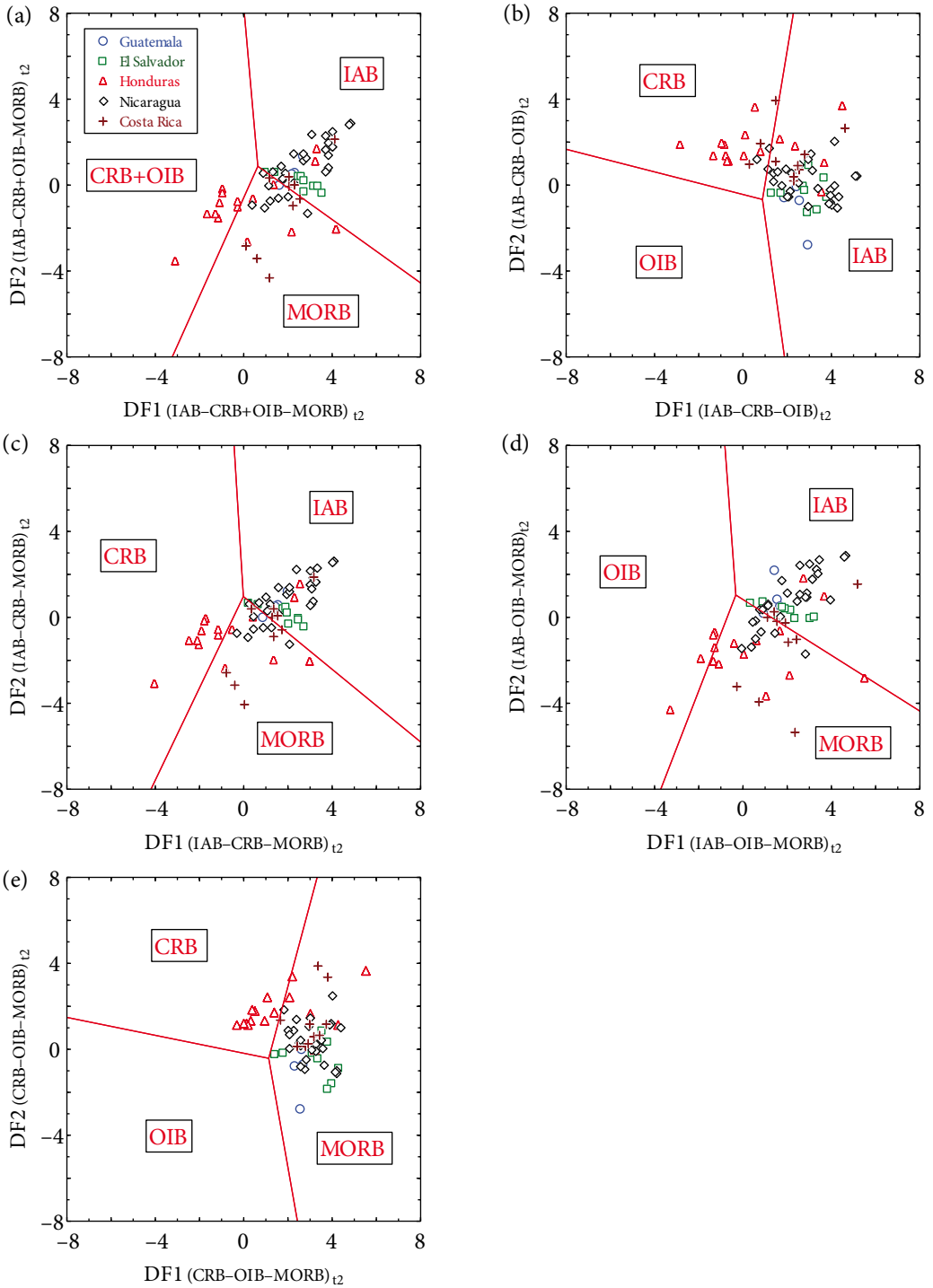

Figure 11. Application of the set of five multidimensional DF1–DF2 diagrams for basic rock samples from the Central American Volcanic Arc (CAVA). More details are given in Figure 10.

Table 9. Application of multidimensional diagrams for tectonic discrimination of basic rock samples from the eastern part of the Mexican Volcanic Belt (E-MVB).

Reference; figure type §; figure no.	Discrimination diagram §	Total no. of samples (%)	Predicted tectonic affinity and number of discriminated samples (%)				
			IAB	CRB+OIB	CRB	OIB	MORB
Verma et al. (2006b); major element log-ratios; Figure 6	IAB–CRB–OIB–MORB	51 (100)	3 (6)	–––	***44*** (86)	1 (2)	3 (6)
	IAB–CRB–OIB	51 (100)	1 (2)	–––	***50*** (98)	0 (0)	–––
	IAB–CRB+MORB	51 (100)	2 (4)	–––	***46*** (90)	–––	3 (6)
	IAB–OIB–MORB *	51 (100)	7 (14)	–––	–––	29 (57)	15 (29)
	CRB–OIB–MORB	51 (100)	–––	–––	***47*** (92)	1 (2)	3 (6)
Agrawal et al. (2008); log-ratios of immobile trace elements; Figure 8	IAB–CRB+OIB–MORB	38 (100)	3 (8)	***31*** (82)	–––	–––	4 (10)
	IAB–CRB–OIB	38 (100)	9 (24)	–––	***24*** (63)	5 (13)	–––
	IAB–CRB+MORB	38 (100)	3 (8)	–––	***31*** (82)	–––	4 (10)
	IAB–OIB–MORB *	38 (100)	3 (8)	–––	–––	29 (76)	6 (16)
	CRB–OIB–MORB	38 (100)	–––	–––	***32*** (84)	1 (3)	5 (13)
Verma and Agrawal (2011); log-ratios of immobile major and trace elements; Figure 10	IAB–CRB+OIB–MORB	23 (100)	3 (13)	***14*** (61)	–––	–––	6 (26)
	IAB–CRB–OIB	23 (100)	5 (22)	–––	***15*** (65)	3 (13)	–––
	IAB–CRB+MORB	23 (100)	2 (9)	–––	***16*** (69)	–––	5 (22)
	IAB–OIB–MORB *	23 (100)	3 (13)	–––	–––	10 (44)	10 (43)
	CRB–OIB–MORB	23 (100)	–––	–––	***12*** (52)	5 (22)	6 (26)

§The groups discriminated in discriminant function-based multidimensional DF1–DF2 diagrams are as follows (B in the tectonic names stands for basic rocks): island arc (IA), continental arc (CA), continental rift (CR), ocean island (OI), and mid-ocean ridge (MOR); the numbers in the parentheses are the percentages of samples plotting in a given field: the correct discrimination (also called % success) can be seen in the column with italic boldface numbers; *: inapplicable diagram.

Table 10. Application of multidimensional diagrams for tectonic discrimination of basic rock samples from the Central American Volcanic Arc (CAVA).

Reference; figure type §; figure no.	Discrimination diagram §	Total no. of samples (%)	Predicted tectonic affinity and number of discriminated samples (%)				
			IAB	CRB+OIB	CRB	OIB	MORB
Verma et al. (2006b); major element log-ratios; Figure 7	IAB–CRB–OIB–MORB	180 (100)	***141*** (78.3)	–––	19 (10.6)	0 (0)	20 (11.1)
	IAB–CRB–OIB	180 (100)	***134*** (74.5)	–––	35 (19.4)	11 (6.1)	–––
	IAB–CRB+MORB	180 (100)	***140*** (77.8)	–––	21 (11.7)	–––	19 (10.5)
	IAB–OIB–MORB	180 (100)	***146*** (81.1)	–––	–––	14 (7.8)	20 (11.1)
	CRB–OIB–MORB *	180 (100)	–––	–––	136 (75.6)	0 (0)	44 (24.4)
Agrawal et al. (2008); log-ratios of immobile trace elements; Figure 9	IAB–CRB+OIB–MORB	61 (100)	**31** (51)	4 (6)	–––	–––	26 (43)
	IAB–CRB–OIB	61 (100)	23 (38)	–––	25 (41)	13 (21)	–––
	IAB–CRB+MORB	61 (100)	**31** (51)	–––	4 (6)	–––	26 (43)
	IAB–OIB–MORB	61 (100)	**31** (51)	–––	–––	2 (3)	28 (46)
	CRB–OIB–MORB	61 (100)	–––	–––	5 (8)	0 (0)	58 (92)
Verma and Agrawal (2011); log-ratios of immobile major and trace elements; Figure 11	IAB–CRB+OIB–MORB	74 (100)	***42*** (57)	9 (12)	–––	–––	23 (31)
	IAB–CRB–OIB	74 (100)	***57*** (77)	–––	17 (23)	0 (0)	–––
	IAB–CRB+MORB	74 (100)	***42*** (57)	–––	9 (12)	–––	23 (31)
	IAB–OIB–MORB	74 (100)	***41*** (55)	–––	–––	5 (7)	28 (38)
	CRB–OIB–MORB *	74 (100)	–––	–––	11 (15)	0 (0)	63 (85)

§ The groups discriminated in discriminant function-based multidimensional DF1–DF2 diagrams are as follows (B in the tectonic names stands for basic rocks): island arc (IA), continental arc (CA), continental rift (CR), ocean island (OI), and mid-ocean ridge (MOR); the numbers in the parentheses are the percentages of samples plotting in a given field: the correct discrimination (also called % success) can be seen in the column with italic boldface numbers; *: inapplicable diagram.

constructing them, most data were compiled from island arcs. The continental arc field, to which the CAVA is likely to belong, is not well represented in them, which may be the reason why the percent success for the arc field is relatively low (Table 10). Nevertheless, an arc affinity for the CAVA rocks is confirmed from these diagrams.

4.2.2. Intermediate rocks

Three sets of five diagrams each indicated a transitional continental rift to collision tectonic setting for the E-MVB (Figures 12, 14, and 16; Table 11) and a continental arc setting for CAVA (Figures 13, 15, and 17; Table 12). In the major element-based diagrams for the E-MVB, the overall %prob estimates for continental rift and collision fields were about 37.0% and 38.6%, respectively (Table 11). In the immobile major and trace element-based diagrams (Figure 14), the E-MVB intermediate rock samples gave %prob of about 32% and 44%, respectively, for continental rift and collision tectonic settings, whereas in the final set of immobile trace element-based diagrams (Figure 16), the E-MVB rocks provided %prob value of about 50% for the continental rift field, followed by only about 24% for the collision tectonic setting (Table 11). Thus, a continental rift or a transitional rift to collision setting is indicated by these diagrams.

For the CAVA intermediate rocks, the major element-based diagrams (Figure 13) indicated a continental arc setting with the %prob value of 57.0% followed by island arc with 38.4% (Table 12). The %prob value for the continental arc setting was higher (60.0% and 66.6%, respectively, for Figures 15 and 17; Table 12) for the other two sets of diagrams based on immobile elements. Thus, the expected continental arc setting is clearly indicated by all diagrams for intermediate magma.

4.2.3. Acid rocks

The indications from multidimensional diagrams for the E-MVB acid rocks are less clear (Figures 18, 20, and 22). The first set based on log-ratios of major elements does not provide a consistent result; the %prob values are distributed among three tectonic settings (27.6% to 35.4%; Table 13). The second set of diagrams based on immobile major and trace elements indicates a transitional within-plate to collision tectonic setting, with %prob values of 40.1% to 49.0%, whereas the third set indicates a transitional continental arc to collision setting, with 39% to 45% (Table 13).

These diagrams, however, seem to work well as documented in the original paper (Verma et al., 2013b) and also for the CAVA acid rocks (Figures 19 and 21; Table 14). The first set of diagrams gave a %prob value of 60.6% (see the first part of results in Table 14). The other two sets of diagrams (Figure 19 and not shown) also indicated a continental arc setting for the CAVA acid rocks (with %prob values of 47% and 49%), although for the last set only two samples with complete data were available. Strictly speaking for such a small number of samples, %prob value for acid rocks should not be calculated or reported (Table 14).

If the diagrams for acid rocks perform well, what could be the reason for inconsistent results for the E-MVB? The acid rocks in the E-MVB may have originated mostly in the heterogeneous continental crust (Figures 3–5) and may therefore indicate the tectonic setting of presumably much older crustal rocks. A dominantly crustal origin for acid rocks was shown for the Sierra de Chichinautzin (Verma, 1999; Velasco-Tapia and Verma, 2013) and Sierra de Las Cruces (Velasco-Tapia, 2014), both located in the central part of the MVB. A larger crustal component in acid rocks from the Los Humeros caldera in the E-MVB than basic and intermediate rocks has also been documented (Verma, 2000a). It can also be postulated that the collision of the Yucatán block with southern Mexico during the Miocene envisioned for southern Mexico (Kim et al., 2011) may have affected the E-MVB as well.

In summary, the basic rocks from the E-MVB indicate a continental rift setting. The intermediate rocks are consistent with a continental rift or a rift to collision transitional setting. Although the acid rocks provide a less consistent result, they may also indicate a transition from rift (or arc) to collision setting. All types of volcanic rocks from basic to acid from the CAVA indicate a continental arc setting, which once again confirms good performance of these 45 diagrams for tectonic discrimination. Their use in geological research is therefore recommended.

4.3. Application of discordancy and significance tests

An objective comparison of the different magma types from these two provinces (E-MVB and CAVA) may throw light on the results of tectonomagmatic discrimination diagrams. The conventional chemical parameters as well as the log-ratios were evaluated from the Fisher F and Student t tests (Verma, 2005; Verma et al., 2013a) applied to discordant outlier-free data (Verma and Díaz-González, 2012). The application of the F test prior to the t test is simply to decide the correct version of the t test (Verma et al., 2013a). In fact, for the t test option, UDASYS internally applied the F test and chose the correct version of the t test. The results of the t test applied as both "one-sided" and "two-sided" versions at the strict 99% confidence level are presented in Tables 15, 16, and 17, for basic, intermediate, and acid rocks, respectively.

The conventional parameters include all major elements from $(SiO_2)_{adj}$ to $(P_2O_5)_{adj}$, REEs from La to Lu, and most common trace elements from Ba to Zr (Tables 15–17). The log-ratios are those used in the multidimensional discrimination diagrams. The first block of ratios from $\ln(TiO_2/SiO_2)$ to $\ln(P_2O_5/SiO_2)$ is for major element-based diagrams for all kinds of igneous rocks (Verma et al.,

Table 11. Application of multidimensional tectonic discrimination diagrams (Verma SP and Verma SK, 2013) to intermediate rocks from the eastern part of the Mexican Volcanic Belt (E-MVB).

Area; rocks; figure name §; figure no.	Figure type §	Total number of samples	Number of discriminated samples				
			Arc			Within-plate	Collision
			IA+CA [$\overline{X} \pm S$] (p_{IA+CA}) Θ	IA [$\overline{X} \pm S$] [p_{IA}] Θ	CA [$\overline{X} \pm S$] [p_{CA}] Θ	CR+OI [$\overline{X} \pm S$] [p_{CR+OI}] Θ	Col [$\overline{X} \pm S$] [p_{Col}] Θ
Eastern part of the Mexican Volcanic Belt (E-MVB); intermediate rocks; all major elements (mint); Figure 12	IA+CA–CR+OI–Col	115	20 [0.602 ± 0.133] (0.3965 – 0.8559)	–––	–––	47 [0.734 ± 0.181] (0.4126–0.9864)	48 [0.753 ± 0.161] (0.3558–0.9826)
	IA–CA–CR+OI	115	–––	3 [0.656 ± 0.199] (0.5279–0.8852)	55 [0.699 ± 0.152] (0.4429–0.9758)	57 [0.815 ± 0.147] (0.4810–0.9926)	–––
	IA–CA–Col	115	–––	2 [0.658 ± 0.224] (0.5000, 0.8164)	43 [0.579 ± 0.088] (0.4325–0.7953)	–––	70 [0.735 ± 0.166] (0.4640–0.9940)
	IA–CR+OI–Col	115	–––	13 [0.571 ± 0.162] (0.3625–0.8500)	–––	48 [0.755 ± 0.165] (0.4619–0.9873)	54 [0.779 ± 0.181] (0.3908–0.9863)
	CA–CR+OI–Col	115	–––	–––	24 [0.587 ± 0.095] (0.4142–0.7875)	50 [0.688 ± 0.179] (0.4186–0.9793)	41 [0.695 ± 0.150] (0.3735–0.9458)
E-MVB 1a. All major element-based diagrams	{Σn} {Σprob} **[%prob]**	**{575}**	**{20} {12.0393}** [–––]	**{18} {10.7095} [3.0%]**	**{122} {77.4386} [21.5%]**	**{202} {151.5928} [37.0%]**	**{213} {158.1203} [38.6%]**
Eastern part of the Mexican Volcanic Belt (E-MVB); intermediate rocks; immobile major and trace elements (mtint); Figure 14	IA+CA–CR+OI–Col	28	3 [0.716 ± 0.136] (0.5649–0.8293)	–––	–––	10 [0.663 ± 0.195] (0.4153–0.9760)	15 [0.618 ± 0.122] (0.3759–0.7941)
	IA–CA–CR+OI	28	–––	0	12 [0.604 ± 0.142] (0.4140–0.7969)	16 [0.659 ± 0.194] (0.3604–0.9996)	–––
	IA–CA–Col	28	–––	0	8 [0.595 ± 0.181] (0.4091–0.9510)	–––	20 [0.663 ± 0.167] (0.4286–0.9899)
	IA–CR+OI–Col	28	–––	3 [0.592 ± 0.109] (0.4932–0.7085)	–––	10 [0.685 ± 0.196] (0.4445–0.9708)	15 [0.629 ± 0.118] (0.4016–0.7949)
	CA–CR+OI–Col	28	–––	–––	9 [0.667 ± 0.191] (0.4083–0.9966)	7 [0.710 ± 0.174] (0.4580–0.9966)	12 [0.658 ± 0.093] (0.4909–0.8312)
E-MVB 1b. All immobile major and trace element-based diagrams	{Σn} {Σprob} **[%prob]**	**{140}**	**{3} {2.1479}** [–––]	**{3} {1.7772} [2.2%]**	**{29} {18.1030} [22.0%]**	**{43} {28.9901} [31.9%]**	**{62} {39.8503} [43.9%]**
Eastern part of the Mexican Volcanic Belt (E-MVB); intermediate rocks; immobile trace elements (tint); Figure 16	IA+CA–CR+OI–Col	30	7 [0.591 ± 0.193] (0.4347–0.9976)	–––	–––	18 [0.707 ± 0.186] (0.4110–0.9842)	5 [0.645 ± 0.190] (0.5141–0.9773)
	IA–CA–CR+OI	30	–––	2 [0.633 ± 0.279] (0.4350, 0.8300)	8 [0.660 ± 0.150] (0.4649–0.9402)	20 [0.819 ± 0.191] (0.5246–0.9966)	–––
	IA–CA–Col	30	–––	1 (0.8384)	10 [0.645 ± 0.118] (0.4589–0.7872)	–––	19 [0.739 ± 0.189] (0.3606–0.9931)
	IA–CR+OI–Col	30	–––	4 [0.593 ± 0.277] (0.3724–0.9975)	–––	18 [0.722 ± 0.169] (0.4503–0.9755)	8 [0.570 ± 0.181] (0.3962–0.9779)
	CA–CR+OI–Col	30	–––	–––	12 [0.587 ± 0.183] (0.3431–0.9955)	13 [0.757 ± 0.164] (0.4404–0.9753)	5 [0.616 ± 0.209] (0.4301–0.9578)
E-MVB 1c. All immobile trace element-based diagrams	{Σn} {Σprob} **[%prob]**	**{150}**	**{7} {4.1379}** [–––]	**{7} {4.4735} [5.1%]**	**{30} {18.7736} [21.2%]**	**{69} {51.9352} [49.8%]**	**{37} {24.9081} [23.9%]**

§ "Figure name" corresponds to one of the three sets of diagrams based on major elements, immobile major and trace elements, and immobile trace elements, respectively, whereas "figure type" gives the tectonic fields being discriminated where the tectonic groups are as follows: IA–island arc, CA–continental arc, CR–continental rift, and OI–ocean island together as within-plate, Col–collision; $\overline{X} \pm S$ –mean ± one standard deviation of the probability estimates for all samples discriminated in a given tectonic setting, reported in []; Θ probability estimates for different tectonic groups are summarized after the number of discriminated samples as follows: [p_{IA+CA}]–range of probability values estimated for IA+CA combined setting, [p_{IA}]–for IA, [p_{CA}]–for CA, [p_{CR+OI}]–for CR+OI, and [p_{Col}]–for Col. Boldface font shows the expected or more probable tectonic setting; the final row gives a synthesis of results as {Σn} {Σprob} **[%prob]** where {Σn}–number of samples plotting in all five diagrams are reported in the column of total number of samples whereas the sum of samples plotting in a given tectonic field are reported in the respective tectonic field column, {Σprob}–sum of probability values for all samples plotting in a given tectonic field are reported in the respective tectonic field column, **[%prob]**–total probability of a given tectonic setting expressed in percent after assigning the probability of IA+CA to IA and CA (see text for weighing factors).

Table 12. Application of multidimensional tectonic discrimination diagrams (Verma SP and Verma SK, 2013) to intermediate rocks from the Central American Volcanic Arc (CAVA).

Area; rocks; figure name §; figure no.	Figure type §	Total number of samples	Number of discriminated samples				
			Arc			Within-plate CR+OI	Collision Col
			IA+CA [$\overline{x} \pm S$] (p_{IA+CA}) Θ	IA [$\overline{x} \pm S$] [p_{IA}] Θ	CA [$\overline{x} \pm S$] [p_{CA}] Θ	[$\overline{x} \pm S$] [p_{CR+OI}] Θ	[$\overline{x} \pm S$] [p_{Col}] Θ
Central American Volcanic Arc (CAVA); intermediate rocks; all major elements (mint); Figure 13	IA+CA–CR+OI–Col	413	389 [0.911 ± 0.132] (0.3504–0.9992)	---	---	18 [0.735 ± 0.180] (0.3820–0.9827)	6 [0.602 ± 0.110] (0.4942–0.8019)
	IA–CA–CR+OI	413	---	108 [0.664 ± 0.165] (0.3918–0.9779)	286 [0.643 ± 0.096] (0.3869–0.9938)	19 [0.662 ± 0.191] (0.3922–0.9862)	---
	IA–CA–Col	413	---	105 [0.681 ± 0.174] (0.4000–0.9915)	306 [0.645 ± 0.090] (0.3777–0.8714)	---	2 [0.688 ± 0.100] (0.6175, 0.7589)
	IA–CR+OI–Col	413	---	376 [0.915 ± 0.125] (0.4303–0.9996)	---	21 [0.708 ± 0.196] (0.3627, 0.9867)	16 [0.641 ± 0.171] (0.3909–0.9029)
	CA–CR+OI–Col	413	---	---	385 [0.889 ± 0.146] (0.4113–0.9996)	21 [0.735 ± 0.150] (0.4636–0.9465)	7 [0.546 ± 0.062] (0.4721–0.6282)
CAVA 1a. All major element-based diagrams	**{Σn} {Σprob} [%prob]**	**2065**	**{389} {354.2382} [---]**	**{589} {487.2821} [38.4%]**	**{977} {723.3053} [57.0%]**	**{79} {56.1179} [3.4%]**	**{31} {19.0617} [1.2%]**
Central American Volcanic Arc (CAVA); intermediate rocks; immobile major and trace elements (mtint); Figure 15	IA+CA–CR+OI–Col	185	176 [0.906 ± 0.099] (0.3860–0.9962)	---	---	2 [0.766 ± 0.260] (0.5820, 0.9494)	7 [0.704 ± 0.110] (0.5847–0.8987)
	IA–CA–CR+OI	185	---	47 [0.702 ± 0.113] (0.5287–0.9932)	137 [0.697 ± 0.075] (0.3803–0.8916)	1 (0.9933)	---
	IA–CA–Col	185	---	43 [0.668 ± 0.109] (0.4458–0.9723)	134 [0.688 ± 0.086] (0.4200–0.8971)	---	8 [0.597 ± 0.187] (0.4291–0.9576)
	IA–CR+OI–Col	185	---	172 [0.882 ± 0.090] (0.5176–0.9955)	---	3 [0.662 ± 0.244] (0.4608–0.9335)	10 [0.645 ± 0.120] (0.5110–0.8211)
	CA–CR+OI–Col	185	---	---	176 [0.940 ± 0.096] (0.4270–0.9997)	3 [0.705 ± 0.203] (0.5181–0.9209)	6 [0.862 ± 0.144] (0.5828–0.9978)
CAVA 1b. All immobile major and trace element-based diagrams	**{Σn} {Σprob} [%prob]**	**925**	**{176} {159.4445} [---]**	**{262} {213.4546} [36.3%]**	**{447} {352.9250} [60.0%]**	**{9} {6.6269} [0.9%]**	**{31} {21.3202} [2.8%]**
Central American Volcanic Arc (CAVA); intermediate rocks; immobile trace elements (tint); Figure 17	IA+CA–CR+OI–Col	196	185 [0.891 ± 0.096] (0.5140–0.9964)	---	---	7 [0.737 ± 0.157] (0.5440–0.9136)	4 [0.698 ± 0.108] (0.5776–0.8046)
	IA–CA–CR+OI	196	---	43 [0.679 ± 0.134] (0.4357–0.9218)	148 [0.835 ± 0.112] (0.5130–0.9522)	5 [0.736 ± 0.190] (0.4273–0.9468)	---
	IA–CA–Col	196	---	40 [0.685 ± 0.109] (0.4839–0.9065)	152 [0.813 ± 0.103] (0.4341–0.9233)	---	4 [0.666 ± 0.107] (0.5710–0.8136)
	IA–CR+OI–Col	196	---	179 [0.730 ± 0.167] (0.4123–0.9966)	---	9 [0.715 ± 0.177] (0.4070–0.9439)	8 [0.661 ± 0.118] (0.4774–0.8223)
	CA–CR+OI–Col	196	---	---	189 [0.928 ± 0.092] (0.4578–0.9993)	5 [0.819 ± 0.136] (0.5903–0.9170)	2 [0.556 ± 0.086] (0.4945–0.6168)
CAVA 1c. All immobile trace element-based diagrams	**{Σn} {Σprob} [%prob]**	**980**	**{185} {164.8031} [---]**	**{262} {187.2098} [29.5%]**	**{489} {422.5776} [66.6%]**	**{26} {19.3705} [2.4%]**	**{18} {11.8571} [1.5%]**

For explanation see footnote of Table 11.

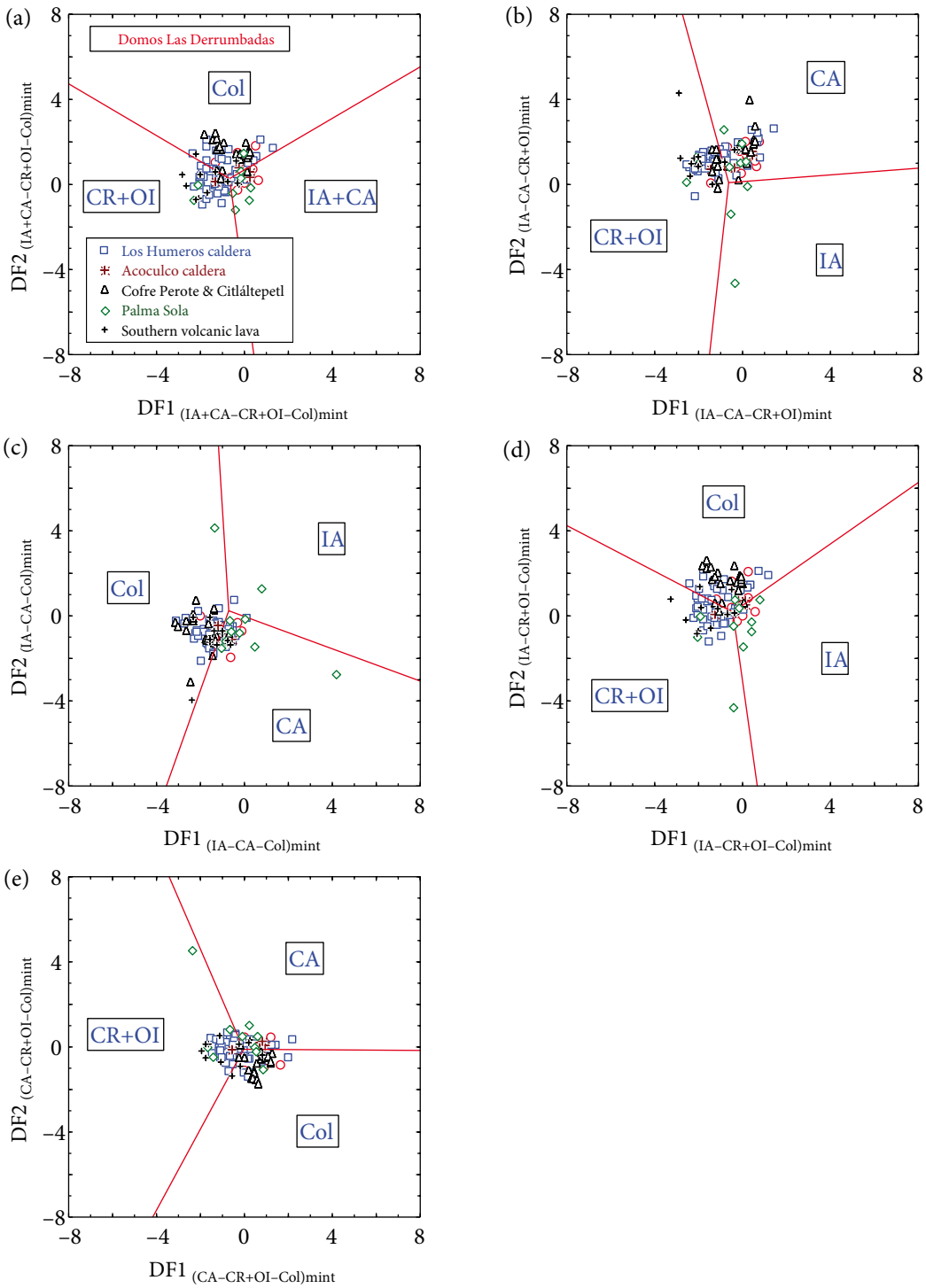

Figure 12. Application of the set of five multidimensional DF1–DF2 diagrams based on log-ratios of major elements (see the subscript mint in all these diagrams; Verma SP and Verma SK, 2013) for intermediate rock samples from the eastern part of the Mexican Volcanic Belt (E-MVB). The tectonic settings being discriminated are of island arc (IA), continental arc (CA), combined continental rift and ocean island (CR+OI), and collision (Col). The symbols are shown as inset in (a). **(a)** Three tectonic settings IA+CA–CR+OI–Col; **(b)** three tectonic settings IA–CA–CR+OI; **(c)** three tectonic settings IA–CA–Col; **(d)** three tectonic settings IA– CR+OI–Col; **(e)** three tectonic settings CR–CR+OI–Col.

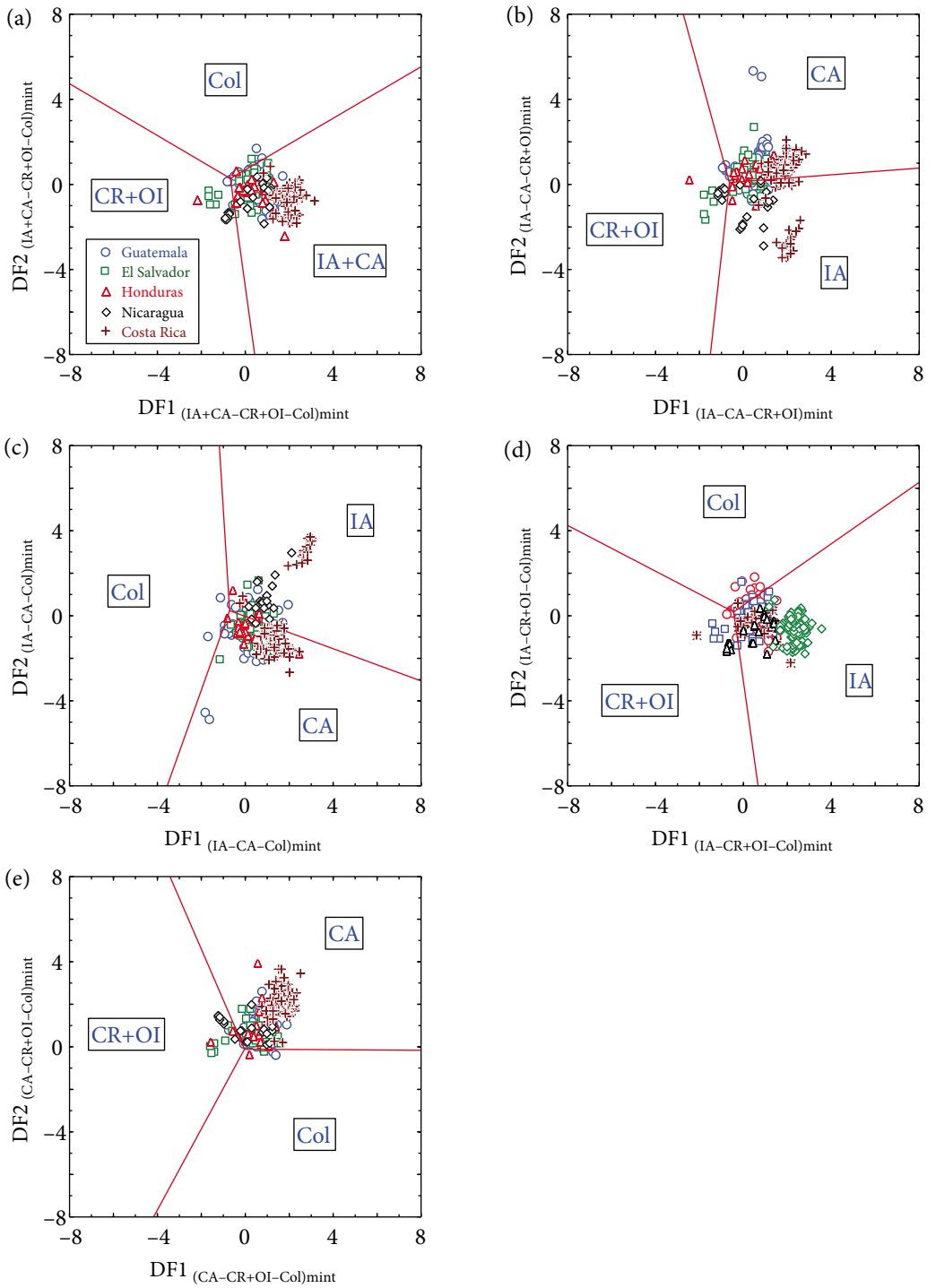

Figure 13. Application of the set of five multidimensional DF1–DF2 diagrams based on log-ratios of major elements for intermediate rock samples from the Central American Volcanic Arc (CAVA). More details are given in Figure 12.

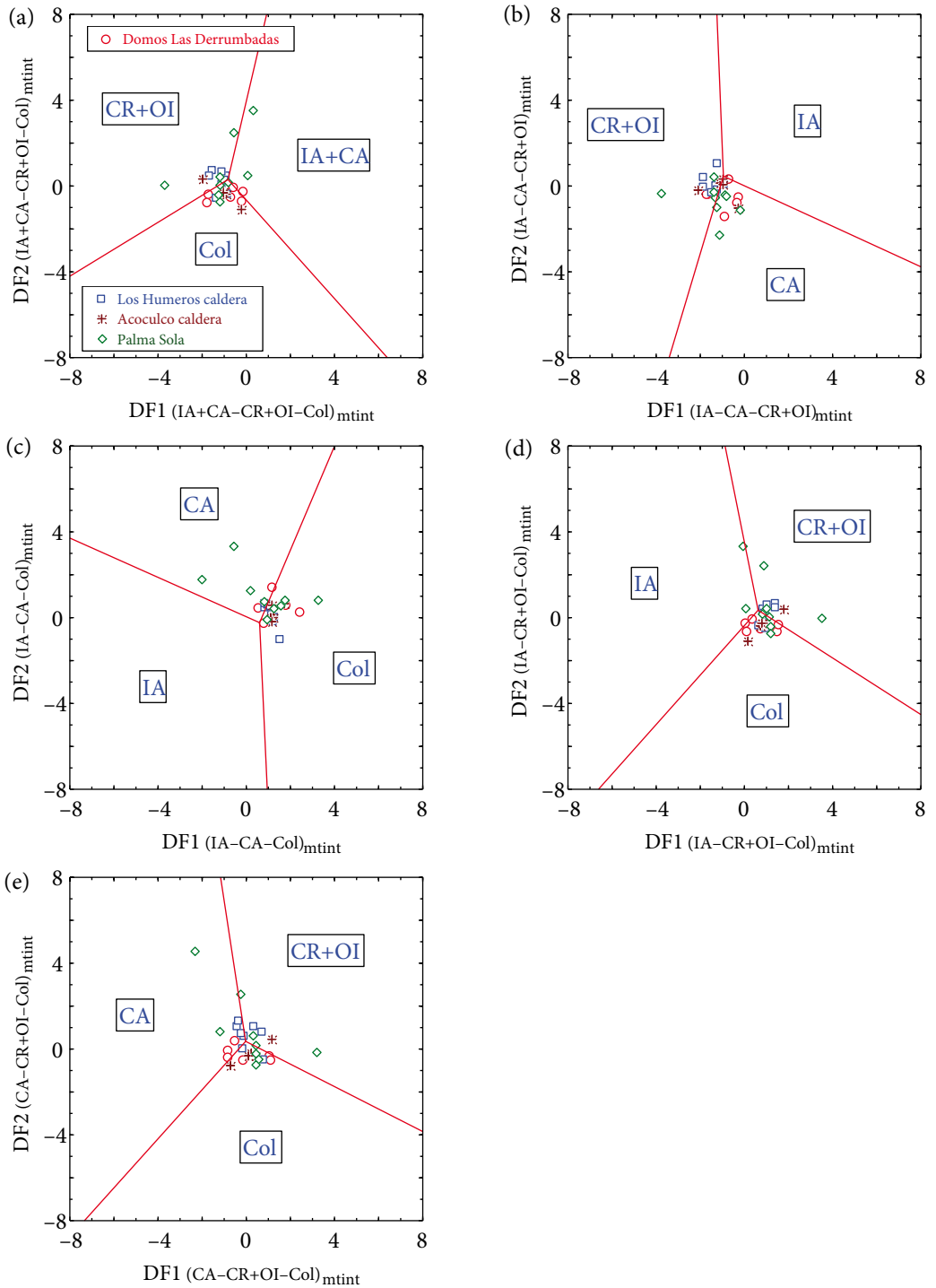

Figure 14. Application of the set of five multidimensional DF1–DF2 diagrams based on log-ratios of immobile major and trace elements (see the subscript mtint in all these diagrams; Verma SP and Verma SK, 2013) for intermediate rock samples from the eastern part of the Mexican Volcanic Belt (E-MVB). **(a)** Three tectonic settings IA+CA–CR+OI–Col; **(b)** three tectonic settings IA–CA–CR+OI; **(c)** three tectonic settings IA–CA–Col; **(d)** three tectonic settings IA–CR+OI–Col; **(e)** three tectonic settings CR–CR+OI–Col.

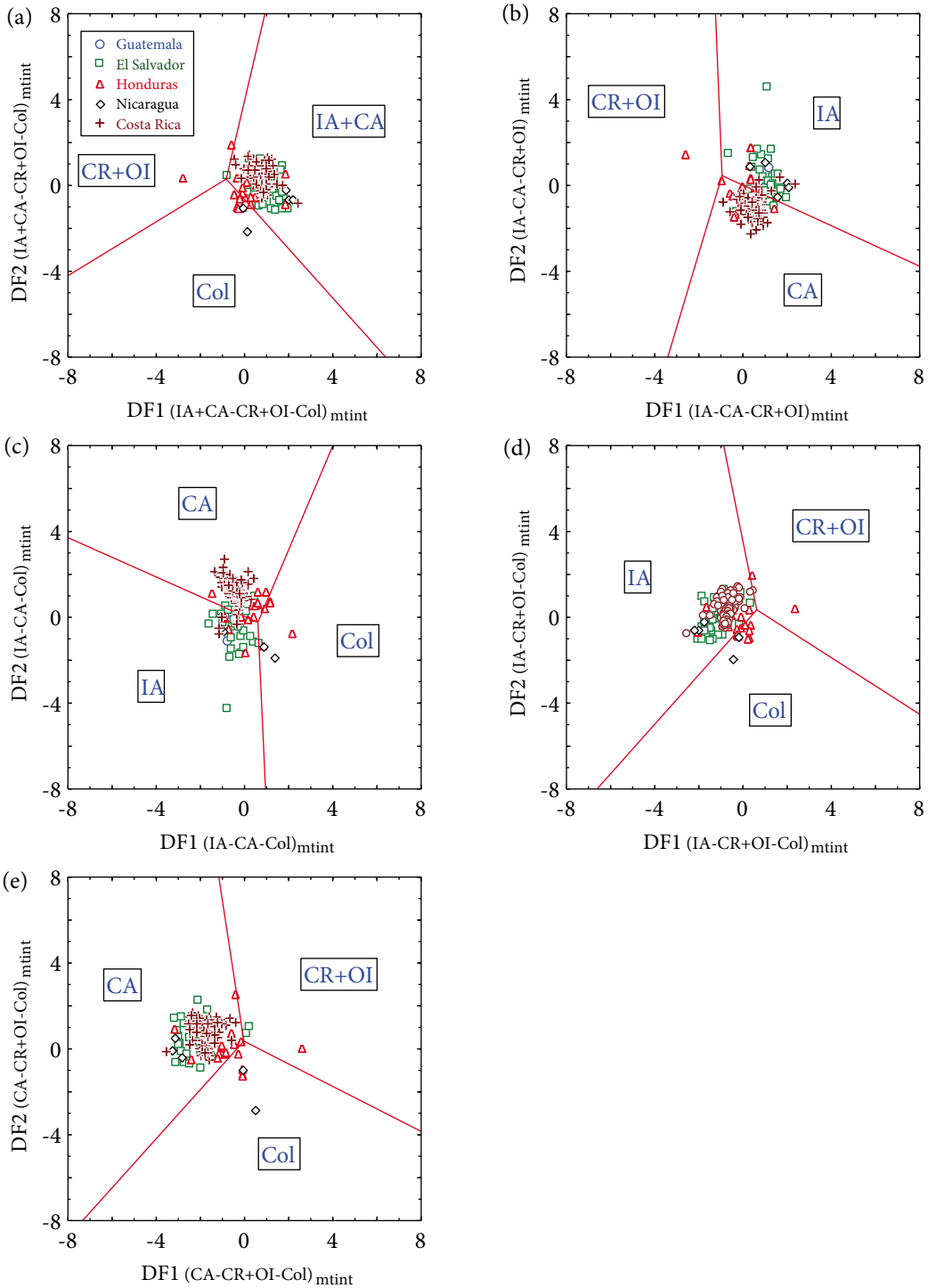

Figure 15. Application of the set of five multidimensional DF1–DF2 diagrams based on log-ratios of immobile major and trace elements for intermediate rock samples from the Central American Volcanic Arc (CAVA). More details are given in Figure 14.

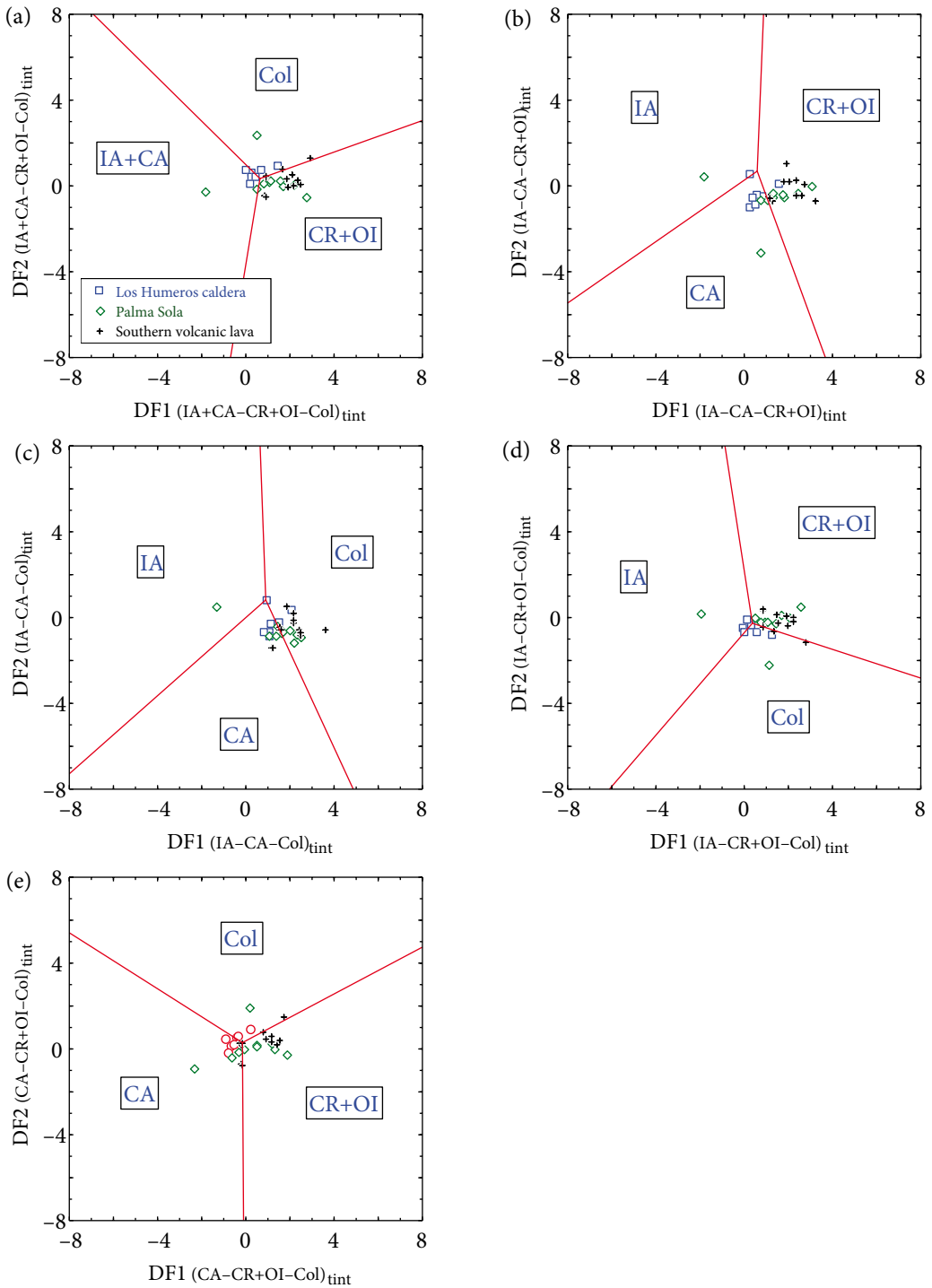

Figure 16. Application of the set of five multidimensional DF1–DF2 diagrams based on log-ratios of immobile trace elements (see the subscript tint in all these diagrams; Verma SP and Verma SK, 2013) for intermediate rock samples from the eastern part of the Mexican Volcanic Belt (E-MVB). **(a)** Three tectonic settings IA+CA–CR+OI–Col; **(b)** three tectonic settings IA–CA–CR+OI; **(c)** three tectonic settings IA–CA–Col; **(d)** three tectonic settings IA–CR+OI–Col; **(e)** three tectonic settings CR–CR+OI–Col.

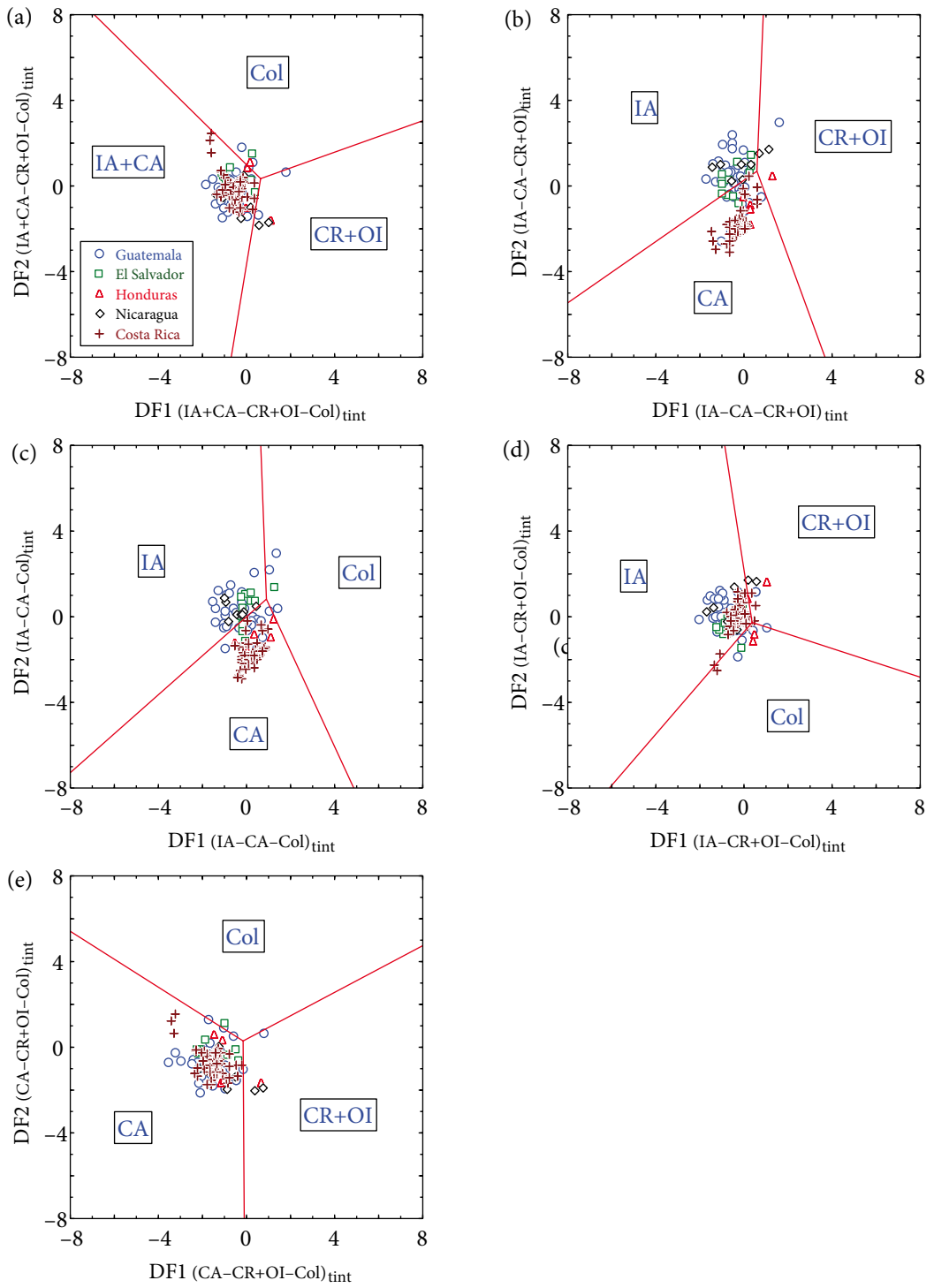

Figure 17. Application of the set of five multidimensional DF1–DF2 diagrams based on log-ratios of immobile trace elements for intermediate rock samples from the Central American Volcanic Arc (CAVA). More details are given in Figure 16.

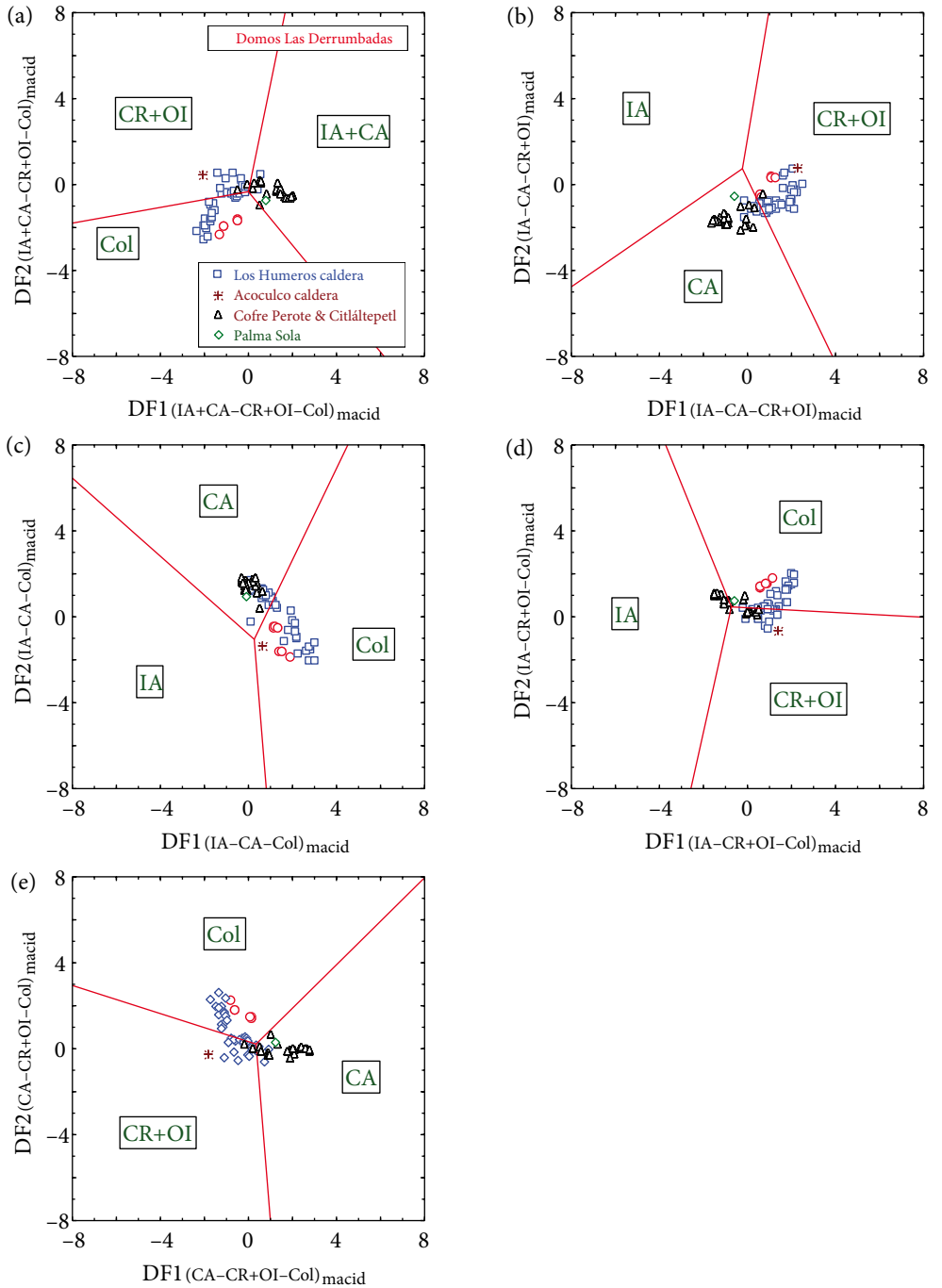

Figure 18. Application of the set of five multidimensional DF1–DF2 diagrams based on log-ratios of major elements (see the subscript macid in all these diagrams; Verma et al., 2013b) for acid rock samples from the eastern part of the Mexican Volcanic Belt (E-MVB). **(a)** Three tectonic settings IA+CA–CR+OI–Col; **(b)** three tectonic settings IA–CA–CR+OI; **(c)** three tectonic settings IA–CA–Col; **(d)** three tectonic settings IA– CR+OI–Col; **(e)** three tectonic settings CR–CR+OI–Col.

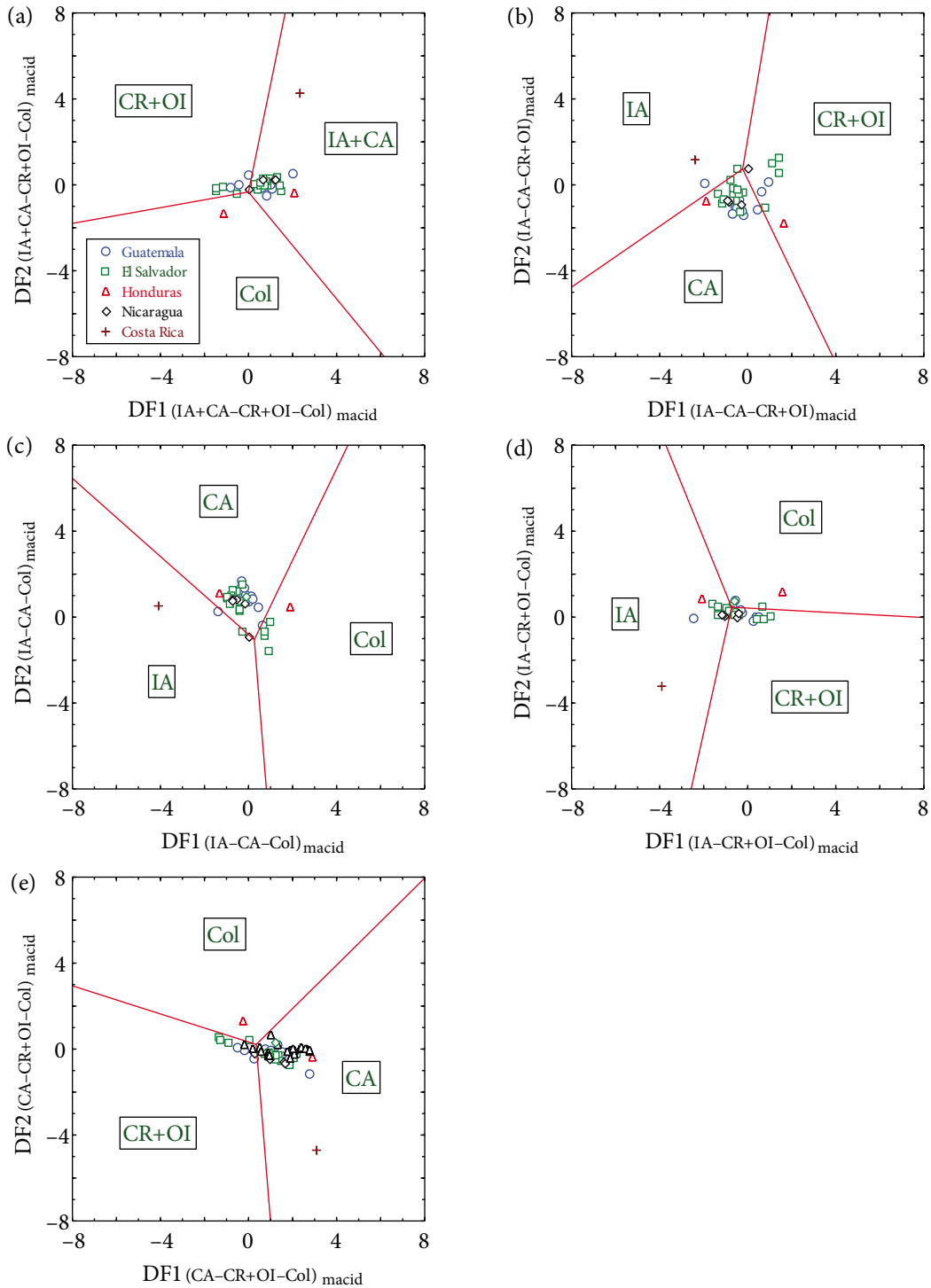

Figure 19. Application of the set of five multidimensional DF1–DF2 diagrams based on log-ratios of major elements for acid rock samples from the Central American Volcanic Arc (CAVA). More details are given in Figure 18.

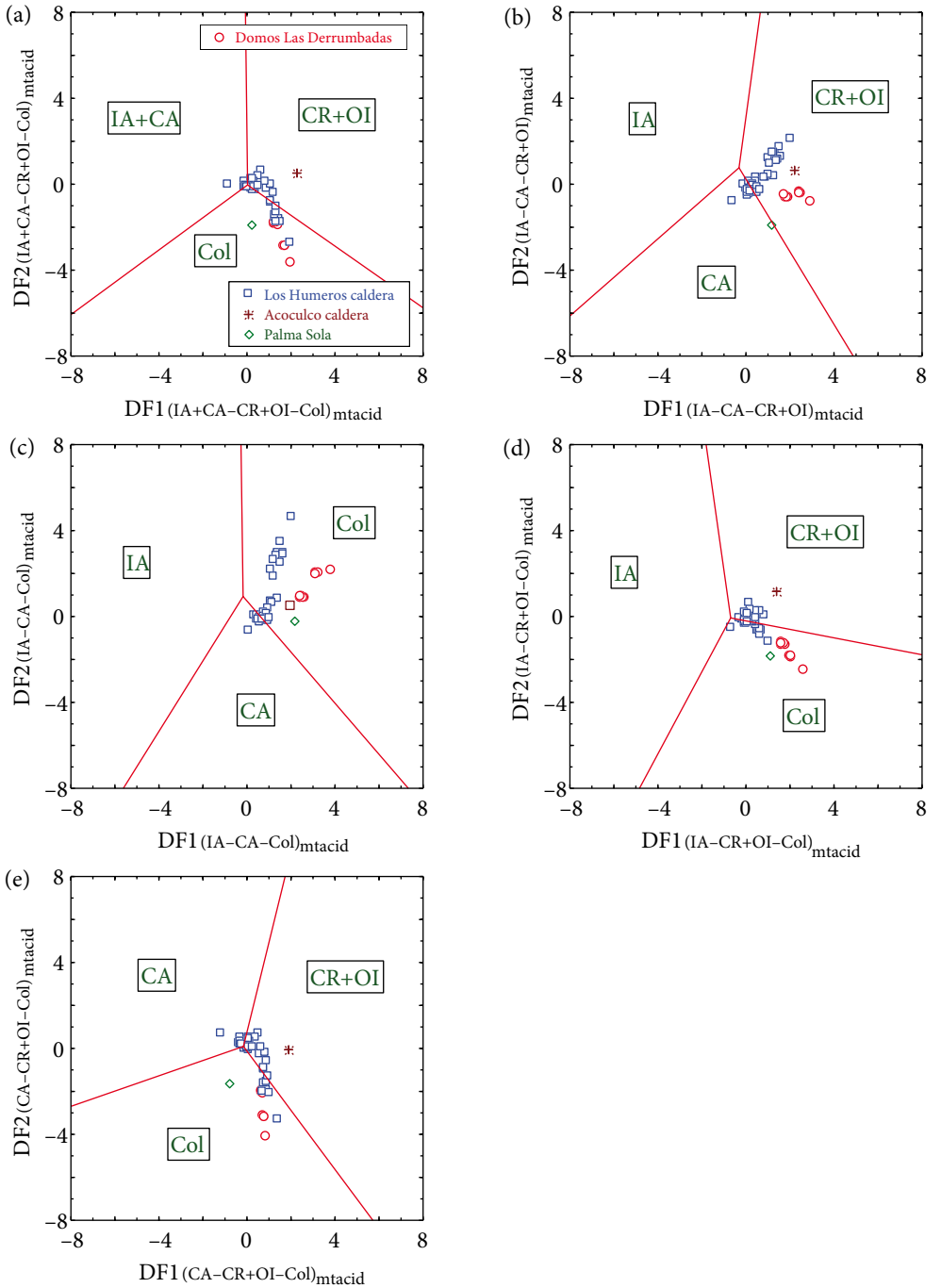

Figure 20. Application of the set of five multidimensional DF1–DF2 diagrams based on log-ratios of immobile major and trace elements (see the subscript mtacid in all these diagrams; Verma et al., 2013b) for acid rock samples from the eastern part of the Mexican Volcanic Belt (E-MVB). **(a)** Three tectonic settings IA+CA–CR+OI–Col; **(b)** three tectonic settings IA–CA–CR+OI; **(c)** three tectonic settings IA–CA–Col; **(d)** three tectonic settings IA–CR+OI–Col; **(e)** three tectonic settings CR–CR+OI–Col.

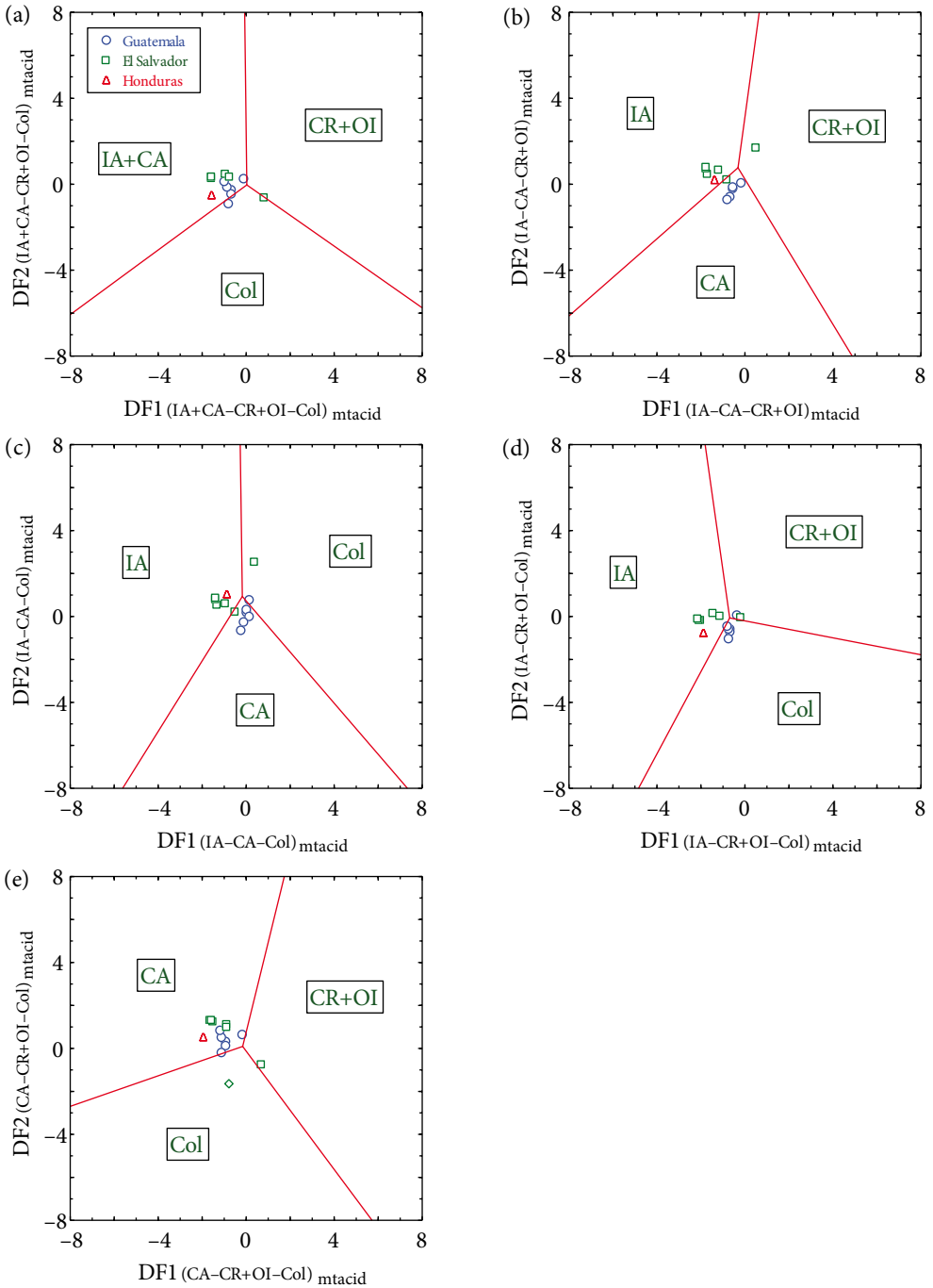

Figure 21. Application of the set of five multidimensional DF1–DF2 diagrams based on log-ratios of immobile major and trace elements for acid rock samples from the Central American Volcanic Arc (CAVA). More details are given in Figure 20.

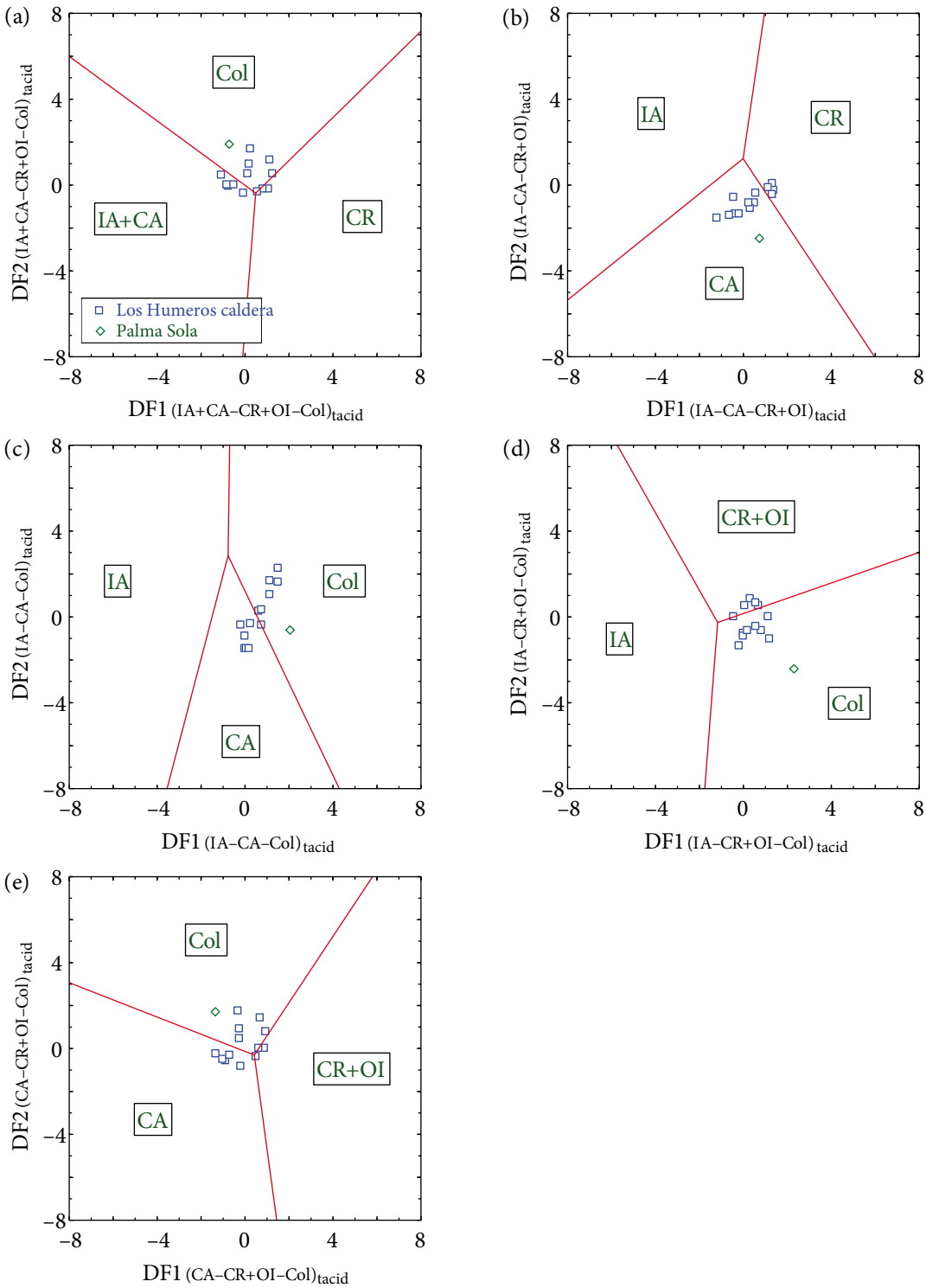

Figure 22. Application of the set of five multidimensional DF1–DF2 diagrams based on log-ratios of immobile trace elements (see the subscript tacid in all these diagrams; Verma et al., 2013b) for acid rock samples from the eastern part of the Mexican Volcanic Belt (E-MVB). **(a)** Three tectonic settings IA+CA–CR+OI–Col; **(b)** three tectonic settings IA–CA–CR+OI; **(c)** three tectonic settings IA–CA–Col; **(d)** three tectonic settings IA–CR+OI–Col; **(e)** three tectonic settings CR–CR+OI–Col.

Table 13. Application of multidimensional tectonic discrimination diagrams (Verma et al., 2013b) to acid rocks from the eastern part of the Mexican Volcanic Belt (E-MVB).

Area; rocks; figure name §; figure no.	Figure type §	Total number of samples	Number of discriminated samples				
			Arc			Within-plate	Collision
			IA+CA	IA	CA	CR+OI	Col
			$[\overline{x} \pm s]$	$[\overline{x} \pm s]$	$[\overline{x} \pm s]$	$[\overline{x} \pm s]$	$[\overline{x} \pm s]$
			(p_{IA+CA}) Θ	$[p_{IA}]$ Θ	$[p_{CA}]$ Θ	$[p_{CR+OI}]$ Θ	$[p_{Col}]$ Θ
Eastern part of the Mexican Volcanic Belt (E-MVB); acid rocks; all major elements (macid); Figure 18	IA+CA–CR+OI–Col	86	26 [0.803 ± 0.1887 (0.3890–0.9805)	–––	–––	25 [0.577 ± 0.154] (0.4147–0.9337)	35 [0.796 ± 0.199] (0.3597–0.9873)
	IA–CA–CR+OI	86	–––	0	31 [0.838 ± 0.129] (0.4944–0.9524)	55 [0.791 ± 0.176] (0.5080–0.9958)	–––
	IA–CA–Col	86	–––	0	53 [0.839 ± 0.129] (0.5154–0.9547)	–––	33 [0.883 ± 0.149] (0.5092–0.9995)
	IA–CR+OI–Col	86	–––	14 [0.603 ± 0.171] (0.3798–0.8442)	–––	29 [0.626 ± 0.113] (0.4930–0.8833)	43 [0.749 ± 0.179] (0.3939–0.9714)
	CA–CR+OI–Col	86	–––	–––	26 [0.822 ± 0.194] (0.3852–0.9926)	26 [0.550 ± 0.149] (0.3504–0.9140)	34 [0.788 ± 0.173] (0.4446–0.9777)
E-MVB 2a. All major element-based diagrams	**{Σn} {Σprob} [%prob]**	**{430}**	**{26} {20.8880} [–––]**	**{14} {8.4422} [3.1%]**	**{110} {91.8057} [33.9%]**	**{135} {90.3711} [27.6%]**	**{145} {116.0108} [35.4%]**
Eastern part of the Mexican Volcanic Belt (E-MVB); acid rocks; immobile major and trace elements (mtacid); Figure 20	IA+CA–CR+OI–Col	48	7 [0.437 ± 0.127] (0.3684–0.7194)	–––	–––	17 [0.574 ± 0.160] (0.3788–0.9754)	24 [0.726 ± 0.193] (0.3699–0.9791)
	IA–CA–CR+OI	48	–––	0	9 [0.600 ± 0.085] (0.5327–0.8098)	39 [0.808 ± 0.193] (0.4907–0.9965)	–––
	IA–CA–Col	48	–––	0	10 [0.550 ± 0.067] (0.5012–0.7291)	–––	38 [0.819 ± 0.197] (0.4857–0.9988)
	IA–CR+OI–Col	48	–––	0	–––	21 [0.616 ± 0.125] (0.4592–0.9566)	27 [0.685 ± 0.167] (0.4709–0.9650)
	CA–CR+OI–Col	48	–––	–––	8 [0.495 ± 0.130] (0.3984–0.8070)	22 [0.534 ± 0.148] (0.3524–0.9497)	18 [0.758 ± 0.119] (0.5447–0.9643)
E-MVB 2b. All immobile major and trace element-based diagrams	**{Σn} {Σprob} [%prob]**	**{240}**	**{7} {3.0601} [–––]**	**{0} {0} [0%]**	**{27} {14.8625} [10.9%]**	**{99} {65.9471} [40.1%]**	**{107} {80.6608} [49.0%]**
Eastern part of the Mexican Volcanic Belt (E-MVB); acid rocks; immobile trace elements (tacid); Figure 22	IA+CA–CR+OI–Col	14	5 [0.561 ± 0.055] (0.5821–0.7075)	–––	–––	3 [0.471 ± 0.100] (0.3727–0.5719)	6 [0.767 ± 0.151] (0.5191–0.9250)
	IA–CA–CR+OI	14	–––	0	10 [0.940 ± 0.071] (0.7585–0.9893)	4 [0.724 ± 0.066] (0.6583–0.8067)	–––
	IA–CA–Col	14	–––	0	6 [0.787 ± 0.073] (0.6460–0.8436)	–––	8 [0.759 ± 0.171] (0.5017–0.9461)
	IA–CR+OI–Col	14	–––	0	–––	4 [0.696 ± 0.097] (0.5878–0.8162)	10 [0.887 ± 0.148] (0.4952–0.9999)
	CA–CR+OI–Col	14	–––	–––	5 [0.727 ± 0.046] (0.6680–0.7764)	3 [0.456 ± 0.091] (0.3839–0.5581)	6 [0.776 ± 0.148] (0.5491–0.9346)
E-MVB 2c. All immobile trace element-based diagrams	**{Σn} {Σprob} [%prob]**	**{70}**	**{5} {3.2526} [–––]**	**{0} {0} [0%]**	**{21} {17.7626} [39%]**	**{14} {8.4581} [16%]**	**{30} {24.1951} [45%]**

For explanation see footnote of Table 11.

Table 14. Application of multidimensional tectonic discrimination diagrams (Verma et al., 2013b) to acid rocks from the Central American Volcanic Arc (CAVA).

Area; rocks; figure name §; figure no.	Figure type §	Total number of samples	Number of discriminated samples				
			Arc			Within-plate	Collision
			IA+CA	IA	CA	CR+OI	Col
			$[\overline{x} \pm s]$	$[\overline{x} \pm s]$	$[\overline{x} \pm s]$	$[\overline{x} \pm s]$	$[\overline{x} \pm s]$
			$(p_{IA+CA})\ \Theta$	$[p_{IA}]\ \Theta$	$[p_{CA}]\ \Theta$	$[p_{CR+OI}]\ \Theta$	$[p_{Col}]\ \Theta$
Central American Volcanic Arc (CAVA); acid rocks; all major elements (macid); Figure 19	IA+CA–CR+OI–Col	36	27 [0.824 ± 0.119] (0.5712–0.9900)	—	—	7 [0.612 ± 0.109] (0.3980–0.7101)	2 [0.662 ± 0.281] (0.4631–0.8608)
	IA–CA–CR+OI	36	—	3 [0.692 ± 0.262] (0.4324–0.9562)	25 [0.766 ± 0.103] (0.5102–0.9039)	8 [0.793 ± 0.185] (0.5054–0.9799)	—
	IA–CA–Col	36	—	4 [0.614 ± 0.242] (0.4267–0.9664)	26 [0.826 ± 0.072] (0.7057–0.9483)	—	6 [0.696 ± 0.151] (0.4823–0.8969)
	IA–CR+OI–Col	36	—	15 [0.705 ± 0.194] (0.4326–0.9997)	—	17 [0.581 ± 0.119] (0.3742–0.7615)	4 [0.572 ± 0.204] (0.3702–0.8561)
	CA–CR+OI–Col	36	—	—	27 [0.855 ± 0.116] (0.5912–0.9976)	7 [0.599 ± 0.082] (0.4512–0.6792)	2 [0.626 ± 0.285] (0.4246–0.8281)
CAVA 2a. All major element-based diagrams	**{Σn} {Σprob} [%prob]**	**180**	**{27} {22.2407} [—]**	**{22} {15.1031} [14.4%]**	**{78} {63.6863} [60.6%]**	**{39} {24.6994} [18.3%]**	**{14} {9.0403} [6.7%]**
Central American Volcanic Arc (CAVA); acid rocks; immobile major and trace elements (mtacid); Figure 21	IA+CA–CR+OI–Col	13	11 [0.741 ± 0.160] (0.4711–0.9231)	—	—	0	2 [0.520 ± 0.062] (0.4767–0.5639)
	IA–CA–CR+OI	13	—	5 [0.778 ± 0.103] (0.6435–0.8759)	7 [0.641 ± 0.107] (0.4800–0.7790)	1 (0.8502)	—
	IA–CA–Col	13	—	5 [0.791 ± 0.085] (0.6841–0.8695)	6 [0.578 ± 0.099] (0.4849–0.7347)	—	2 [0.628 ± 0.245] (0.4549–0.8011)
	IA–CR+OI–Col	13	—	6 [0.880 ± 0.128] (0.6388–0.9721)	—	2 [0.5005 ± 0.0109] (0.4929–0.5082)	5 [0.552 ± 0.096] (0.4385–0.6946)
	CA–CR+OI–Col	13	—	—	12 [0.748 ± 0.164] (0.4824–0.9353)	1(0.5702)	0
CAVA 2b. All immobile major and trace element-based diagrams	**{Σn} {Σprob} [%prob]**	**65**	**{11} {8.1481} [—]**	**{16} {13.1188} [37%]**	**{25} {16.9290} [47%]**	**{4} {2.4214} [5%]**	**{9} {5.0557} [11%]**
Central American Volcanic Arc (CAVA); acid rocks; immobile trace elements (tacid); no figure (only two samples)	IA+CA–CR+OI–Col	2	2 [0.775 ± 0.275] (0.5810–0.9693)	—	—	0	0
	IA–CA–CR+OI	2	—	1 (0.9286)	1 (0.8474)	0	—
	IA–CA–Col	2	—	1 (0.9326)	1 (0.8608)	—	0
	IA–CR+OI–Col	2	—	1 (0.9998)	—	1 (0.8908)	0
	CA–CR+OI–Col	2	—	—	2 [0.834 ± 0.231] (0.6709–0.9974)	0	0
CAVA 2c. All immobile trace element-based diagrams	**{Σn} {Σprob} [%prob]**	**10**	**{2} {1.5504} [—]**	**{3} {2.8610} [41%]**	**{4} {3.3765} [49%]**	**{1} {0.8908} [10%]**	**{0} {0} [0%]**

For explanation see footnote of Table 11.

Table 15. Application of significance tests (software: UDASYS; Verma et al., 2013a) to the traditional as well as log-transformed chemical data for basic volcanic rock samples from the eastern part of the Mexican Volcanic Belt (E-MVB) and the Central American Volcanic Arc (CAVA).

Parameter §	Group A (E-MVB)	Group B (CAVA)	nA (E-MVB)	nB (CAVA)	df	Sign	t_calc	t_crit One–Sided	H0 One–Sided	CL_t One–Sided	t_crit Two–Sided	H0 Two–Sided	CL_t Two–Sided
$(SiO_2)_{adj}$	Gr1	Gr11	50	175	71.319	–	5.9979067	2.3797593	false	>99.9	2.6465090	false	>99.9
$(TiO_2)_{adj}$	Gr1	Gr11	50	178	69.253	+	11.8649599	2.3813891	false	>99.9	2.6486740	false	>99.9
$(Al_2O_3)_{adj}$	Gr1	Gr11	50	176	132.875	–	8.8562374	2.3547333	false	>99.9	2.6133329	false	>99.9
$(Fe_2O_3)_{adj}$	Gr1	Gr11	50	178	66.556	+	3.4022749	2.3836736	false	99.94	2.6517095	false	99.89
$(FeO)_{adj}$	Gr1	Gr11	50	179	73.809	+	3.1978572	2.3779185	false	99.9	2.6440644	false	99.8
$(MnO)_{adj}$	Gr1	Gr11	49	174	89.631	–	2.2548417	2.3686548	true	98.67	2.6317722	true	97.34
$(MgO)_{adj}$	Gr1	Gr11	50	178	78.886	+	5.9897185	2.3745322	false	>99.9	2.6395690	false	>99.9
$(CaO)_{adj}$	Gr1	Gr11	50	176	133.820	–	6.7680069	2.3545306	false	>99.9	2.6130649	false	>99.9
$(Na_2O)_{adj}$	Gr1	Gr11	50	179	101.561	+	7.3732306	2.3636098	false	>99.9	2.6250852	false	>99.9
$(K_2O)_{adj}$	Gr1	Gr11	50	172	74.952	+	5.2114068	2.3771155	false	>99.9	2.6429981	false	>99.9
$(P_2O_5)_{adj}$	Gr1	Gr11	50	171	55.852	+	6.7160112	2.3949760	false	>99.9	2.6667422	false	>99.9
$(Fe_2O_3^t)_{adj}$	Gr1	Gr11	50	179	74.112	+	3.6886464	2.3777032	false	99.97	2.6437785	false	99.95
$(Na_2O+K_2O)_{adj}$	Gr1	Gr11	50	176	107.443	+	7.7770339	2.3615413	false	>99.9	2.6223451	false	>99.9
Mg #	Gr1	Gr11	50	174	84.242	+	5.1321007	2.3714116	false	>99.9	2.6354285	false	>99.9
La	Gr1	Gr11	47	126	57.003	+	7.9217222	2.3935509	false	>99.9	2.6648454	false	>99.9
Ce	Gr1	Gr11	47	128	57.236	+	8.4288136	2.3932699	false	>99.9	2.6644715	false	>99.9
Pr	Gr1	Gr11	34	42	44.115	+	7.0575430	2.4138980	false	>99.9	2.6919622	false	>99.9
Nd	Gr1	Gr11	47	115	61.532	+	7.9808820	2.3884762	false	>99.9	2.6580943	false	>99.9
Sm	Gr1	Gr11	47	115	68.167	+	7.6457250	2.3822870	false	>99.9	2.6498669	false	>99.9
Eu	Gr1	Gr11	47	118	61.045	+	8.6075117	2.3889842	false	>99.9	2.6587699	false	>99.9
Gd	Gr1	Gr11	42	107	147.000	+	6.7256834	2.3519815	false	>99.9	2.6096931	false	>99.9
Tb	Gr1	Gr11	47	53	71.196	+	10.3872197	2.3798538	false	>99.9	2.6466345	false	>99.9
Dy	Gr1	Gr11	24	99	63.818	+	7.9668005	2.3861947	false	>99.9	2.6550606	false	>99.9
Ho	Gr1	Gr11	43	48	89.000	+	6.5088656	2.3689600	false	>99.9	2.6321768	false	>99.9
Er	Gr1	Gr11	34	108	97.929	+	2.2872265	2.3650134	true	98.78	2.6269450	true	97.57
Tm	Gr1	Gr11	28	40	66.000	+	4.6999039	2.3841680	false	99.69	2.6523665	false	99.39
Yb	Gr1	Gr11	47	122	141.994	+	2.6213912	2.3528932	false	99.51	2.6108990	false	99.03
Lu	Gr1	Gr11	47	63	108.000	+	4.1788075	2.3613574	false	99.9	2.6221015	false	99.81
Ba	Gr1	Gr11	41	143	182.000	+	0.9192091	2.3470208	true	81.97	2.6031356	true	63.93
Be	Gr1	Gr11	11	38	10.998	+	4.1632740	2.7181636	false	99.92	3.1059107	false	99.84
Co	Gr1	Gr11	42	29	69.000	+	1.7030752	2.3815958	true	95.35	2.6489486	true	90.69
Cr	Gr1	Gr11	45	138	54.530	+	5.1596518	2.3966879	false	>99.9	2.6690212	false	>99.9
Cs	Gr1	Gr11	33	73	42.974	+	5.3700870	2.4163080	false	>99.9	2.6951790	false	>99.9
Cu	Gr1	Gr11	21	81	99.689	–	9.4430770	2.3643201	false	>99.9	2.6260264	false	>99.9
Ga	Gr1	Gr11	15	6	19.0	+	3.1943765	2.5395227	false	99.76	2.8609639	false	99.52
Hf	Gr1	Gr11	37	62	97.000	+	13.0160618	2.3653895	false	>99.9	2.6274436	false	>99.9
Nb	Gr1	Gr11	45	104	125.537	+	5.5926836	2.3564105	false	>99.9	2.6155522	false	>99.9
Ni	Gr1	Gr11	44	137	53.333	+	5.0955890	2.3983144	false	>99.9	2.6711870	false	>99.9
Pb	Gr1	Gr11	14	71	83.000	+	2.2296504	2.3720987	true	98.58	2.6363399	true	97.15
Rb	Gr1	Gr11	41	144	47.021	+	6.0986364	2.4083027	false	>99.9	2.6844978	false	>99.9
Sb	Gr1	Gr11	14	3	2.023	–	1.0750052	6.8720722	true	80.39	9.7913502	true	60.77
Sc	Gr1	Gr11	17	115	130.0	–	2.1955833	2.3578186	true	98.5	2.6174183	true	97.0
Sr	Gr1	Gr11	46	150	54.457	+	4.5839119	2.3967848	false	99.81	2.6691502	false	99.63

Table 15. (Ccontinued).

Parameter §	Group A (E-MVB)	Group B (CAVA)	nA (E-MVB)	nB (CAVA)	df	Sign	t_calc	t_crit One–Sided	H0 One–Sided	CL_t One–Sided	t_crit Two–Sided	H0 Two–Sided	CL_t Two–Sided
Ta	Gr1	Gr11	37	37	38.925	+	10.6755706	2.4260466	false	>99.9	2.7081883	false	>99.9
Th	Gr1	Gr11	35	87	36.517	+	9.8440329	2.4329082	false	>99.9	2.7173645	false	>99.9
U	Gr1	Gr11	35	83	39.405	+	9.1444128	2.4247837	false	>99.9	2.7065002	false	>99.9
V	Gr1	Gr11	23	103	50.517	–	3.4461650	2.4024532	false	99.94	2.6160510	true	98.93
Y	Gr1	Gr11	46	131	162.981	+	5.3522845	2.3494495	false	>99.9	2.6063454	false	>99.9
Zn	Gr1	Gr11	21	36	21.871	+	3.3069123	2.5094988	false	99.84	2.8203455	false	99.68
Zr	Gr1	Gr11	46	136	180.0	+	10.0226666	2.3498862	false	>99.9	2.6069102	false	>99.9
$\ln(TiO_2/SiO_2)$	Gr1	Gr11	50	180	90.165	+	14.1560942	2.3683997	false	>99.9	2.6314339	false	>99.9
$\ln(Al_2O_3/SiO_2)$	Gr1	Gr11	50	180	100.765	–	6.2156682	2.3639088	false	>99.9	2.6254814	false	>99.9
$\ln(Fe_2O_3/SiO_2)$	Gr1	Gr11	50	180	70.108	+	4.1106305	2.3807028	false	99.95	2.6477623	false	99.89
$\ln(FeO/SiO_2)$	Gr1	Gr11	50	180	74.463	+	3.9575702	2.3774555	false	99.97	2.6434496	false	99.93
$\ln(MnO/SiO_2)$	Gr1	Gr11	49	177	82.299	–	0.2673031	2.3724961	true	<50	2.6368671	true	<50
$\ln(MgO/SiO_2)$	Gr1	Gr11	50	178	102.796	+	7.3778924	2.3631557	false	>99.9	2.6244836	false	>99.9
$\ln(CaO/SiO_2)$	Gr1	Gr11	50	177	103.416	–	3.8451985	2.3629316	false	99.97	2.6241867	false	99.94
$\ln(Na_2O/SiO_2)$	Gr1	Gr11	50	179	123.667	+	9.5497077	2.3568703	false	>99.9	2.6161607	false	>99.9
$\ln(K_2O/SiO_2)$	Gr1	Gr11	50	174	107.557	+	6.7614014	2.3615035	false	>99.9	2.6222950	false	>99.9
$\ln(P_2O_5/SiO_2)$	Gr1	Gr11	47	179	84.844	+	10.2241281	2.3710861	false	>99.9	2.6349966	false	>99.9
ln(La/Th)	Gr1	Gr11	37	94	100.275	–	7.2873068	2.3640948	false	>99.9	2.6257279	false	>99.9
ln(Sm/Th)	Gr1	Gr11	37	88	88.321	–	10.2919152	2.3692932	false	>99.9	2.6326187	false	>99.9
ln(Yb/Th)	Gr1	Gr11	37	91	126.000	–	12.3172009	2.3562988	false	>99.9	2.6154045	false	>99.9
ln(Nb/Th)	Gr1	Gr11	37	67	101.856	+	1.3415380	2.3635004	true	90.86	2.6249402	true	81.73
$\ln(Nb/(TiO_2)_{adj})$	Gr1	Gr11	46	106	147.036	+	7.4447517	2.3519751	false	>99.9	2.6096847	false	>99.9
$\ln(V/(TiO_2)_{adj})$	Gr1	Gr11	22	105	89.309	–	11.6418532	2.3688100	false	>99.9	2.6319780	false	>99.9
$\ln(Y/(TiO_2)_{adj})$	Gr1	Gr11	46	133	177.000	–	10.2619195	2.3476082	false	>99.9	2.6039119	false	>99.9
$\ln(Zr/(TiO_2)_{adj})$	Gr1	Gr11	46	142	126.814	+	7.2747394	2.3561045	false	>99.9	2.6151473	false	>99.9
$\ln(MgO/TiO_2)_{adj}$	Gr1	Gr11	50	179	80.122	–	5.2895353	2.3737745	false	>99.9	2.6385635	false	>99.9
$\ln(P_2O_5/TiO_2)_{adj}$	Gr1	Gr11	47	180	95.188	+	4.1501677	2.3661446	false	99.92	2.6284443	false	99.84
$\ln(Ni/(TiO_2)_{adj})$	Gr1	Gr11	46	135	179.000	+	0.5939694	2.3473693	true	<50	2.6035961	true	<50
ln(La/Yb)	Gr1	Gr11	47	122	71.720	+	9.4735982	2.3794542	false	>99.9	2.6461037	false	>99.9
ln(Ce/Yb)	Gr1	Gr11	47	121	166.000	+	11.7878820	2.3490264	false	>99.9	2.6057862	false	>99.9
ln(Sm/Yb)	Gr1	Gr11	47	120	55.906	+	8.9245997	2.3949074	false	>99.9	2.6666510	false	>99.9
ln(Nb/Yb)	Gr1	Gr11	43	98	123.506	+	10.4227722	2.3569105	false	>99.9	2.6162139	false	>99.9
ln(Th/Yb)	Gr1	Gr11	37	91	126.000	+	12.3172009	2.3562988	false	>99.9	2.6154045	false	>99.9
ln(Y/Yb)	Gr1	Gr11	41	126	165.000	+	4.8657890	2.3491648	false	99.18	2.6059691	false	98.36
Ln(Zr/Yb)	Gr1	Gr11	43	120	132.876	+	16.2121853	2.3547330	false	>99.9	2.6133326	false	>99.9

§ The subscript adj refers to the adjusted data from the SINCLAS or IgRoCS computer programs (Verma et al., 2002; Verma and Rivera-Gómez, 2013a). The outcome of the Student's t test: One–Sided H_0 false means that this parameter for one group is either higher or lower than for the other group at 99% confidence level (CL); One–Sided H_0 true means that this parameter for one group is not higher or lower than the other group at 99% confidence level; Two–Sided H_0 false means that this parameter shows a significant difference between the two areas or groups at 99% confidence level; Two–Sided H_0 true means that this parameter does not show a significant difference between the two areas or groups at 99% confidence level. Remember also that instead of "true" or "false", the outcome could have been stated, respectively, as "accept" or "reject", or even as "valid" or "invalid".

Table 16. Application of significance tests (software: UDASYS; Verma et al., 2013a) to the traditional as well as log-transformed chemical data for intermediate volcanic rock samples from the eastern part of the Mexican Volcanic Belt (E-MVB) and the Central American Volcanic Arc (CAVA).

Parameter §	Group A (E-MVB)	Group B (CAVA)	nA (E-MVB)	nB (CAVA)	df	Sign	t_calc	t_crit One–Sided	H0 One–Sided	CL_t One–Sided	t_crit Two–Sided	H0 Two–Sided	CL_t Two–Sided
$(SiO_2)_{adj}$	Gr2	Gr12	115	388	155.999	+	4.9766946	2.3504911	false	98.99	2.6077224	false	97.98
$(TiO_2)_{adj}$	Gr2	Gr12	115	404	148.434	+	14.0827705	2.3517317	false	>99.9	2.6093628	false	>99.9
$(Al_2O_3)_{adj}$	Gr2	Gr12	111	406	239.011	–	13.3818891	2.3420713	false	>99.9	2.5965973	false	>99.9
$(Fe_2O_3)_{adj}$	Gr2	Gr12	114	406	150.218	–	2.9633574	2.3514278	false	99.82	2.6089610	false	99.65
$(FeO)_{adj}$	Gr2	Gr12	110	406	158.137	–	8.4937026	2.3501622	false	>99.9	2.6072876	false	>99.9
$(MnO)_{adj}$	Gr2	Gr12	113	395	154.965	–	14.4886352	2.3506534	false	>99.9	2.6079371	false	>99.9
$(MgO)_{adj}$	Gr2	Gr12	113	406	149.364	–	0.9761996	2.3515724	true	83.45	2.6091522	true	66.9
$(CaO)_{adj}$	Gr2	Gr12	115	406	166.013	–	9.1676358	2.3490246	false	>99.9	2.6057839	false	>99.9
$(Na_2O)_{adj}$	Gr2	Gr12	114	406	167.300	+	12.7641481	2.3488490	false	>99.9	2.6055517	false	>99.9
$(K_2O)_{adj}$	Gr2	Gr12	100	404	165.973	+	16.4500703	2.3490301	false	>99.9	2.6057911	false	>99.9
$(P_2O_5)_{adj}$	Gr2	Gr12	107	381	144.026	+	13.1698130	2.3525155	false	>99.9	2.6103994	false	>99.9
$(Fe_2O_3^t)_{adj}$	Gr2	Gr12	110	406	156.862	–	7.6883922	2.3503573	false	>99.9	2.6075455	false	>99.9
$(Na_2O+K_2O)_{adj}$	Gr2	Gr12	115	405	165.494	+	16.1965612	2.3490961	false	>99.9	2.6058784	false	>99.9
Mg #	Gr2	Gr12	110	406	153.376	+	3.9473253	2.3509073	false	99.95	2.6082728	false	99.9
La	Gr2	Gr12	45	322	46.620	+	9.5379856	2.4090322	false	>99.9	2.6854706	false	>99.9
Ce	Gr2	Gr12	46	327	47.118	+	10.0007800	2.4081295	false	>99.9	2.6842668	false	>99.9
Pr	Gr2	Gr12	30	228	29.539	+	7.1067139	2.4594326	false	>99.9	2.7529135	false	>99.9
Nd	Gr2	Gr12	45	301	47.765	+	9.2147966	2.4069850	false	>99.9	2.6827408	false	>99.9
Sm	Gr2	Gr12	46	282	51.707	+	8.3341038	2.4006467	false	>99.9	2.6742934	false	>99.9
Eu	Gr2	Gr12	48	282	49.123	+	8.5812408	2.4046829	false	>99.9	2.6796718	false	>99.9
Gd	Gr2	Gr12	36	271	38.732	+	7.1988719	2.4265641	false	>99.9	2.7088801	false	>99.9
Tb	Gr2	Gr12	48	231	52.495	+	9.2645170	2.3994986	false	>99.9	2.6727641	false	>99.9
Dy	Gr2	Gr12	16	258	15.726	+	5.0662075	2.5884309	false	>99.9	2.9275214	false	>99.9
Ho	Gr2	Gr12	37	217	41.465	+	7.1535435	2.4197080	false	>99.9	2.6997190	false	>99.9
Er	Gr2	Gr12	32	260	43.532	+	4.6832814	2.4151134	false	99.82	2.6935844	false	99.63
Tm	Gr2	Gr12	30	173	31.420	+	7.1630354	2.4510682	false	>99.9	2.7416900	false	>99.9
Yb	Gr2	Gr12	48	261	63.623	+	6.8120178	2.3863824	false	>99.9	2.6553102	false	>99.9
Lu	Gr2	Gr12	47	235	62.015	+	6.9883736	2.3879795	false	>99.9	2.6574337	false	>99.9
Ba	Gr2	Gr12	52	335	59.686	+	1.1485061	2.3904487	true	87.24	2.6607179	true	74.48
Be	Gr2	Gr12	8	33	39.000	+	4.6595165	2.4258483	false	99.85	2.7079232	false	99.7
Co	Gr2	Gr12	47	159	64.573	–	0.0404038	2.3854770	true	<50	2.6541065	true	<50
Cr	Gr2	Gr12	34	284	52.491	–	2.0720702	2.3995030	true	97.84	2.6727700	true	95.68
Cs	Gr2	Gr12	27	228	27.145	+	5.9762028	2.4718533	false	>99.9	2.7696022	false	>99.9
Cu	Gr2	Gr12	26	179	53.386	–	7.0705327	2.3982409	false	>99.9	2.6710891	false	>99.9
Ga	Gr2	Gr12	10	4	12.0	+	3.2595011	2.6809892	false	99.66	3.0545228	false	99.32
Hf	Gr2	Gr12	30	203	29.535	+	7.6804066	2.4594522	false	>99.9	2.7529398	false	>99.9
Nb	Gr2	Gr12	50	249	52.781	+	12.2739797	2.3990890	false	>99.9	2.6722186	false	>99.9
Ni	Gr2	Gr12	46	280	49.249	+	2.7023849	2.4044762	false	99.53	2.6793963	false	99.06

Table 16. (Continued).

Parameter §	Group A (E-MVB)	Group B (CAVA)	nA (E-MVB)	nB (CAVA)	df	Sign	t_calc	t_crit One–Sided	H0 One–Sided	CL_t One–Sided	t_crit Two–Sided	H0 Two–Sided	CL_t Two–Sided
Pb	Gr2	Gr12	18	216	17.665	+	6.1021428	2.5570749	false	>99.9	2.8848199	false	>99.9
Rb	Gr2	Gr12	55	333	61.664	+	9.8058766	2.3883398	false	>99.9	2.6579129	false	>99.9
Sb	Gr2	Gr12	12	7	6.159	–	2.6248513	3.1157483	true	98.08	3.6685403	true	96.16
Sc	Gr2	Gr12	16	285	299.000	–	1.7410029	2.3389085	true	95.86	2.5924202	true	91.73
Sr	Gr2	Gr12	61	336	71.332	–	3.2152371	2.3797493	false	99.9	2.6464957	false	99.8
Ta	Gr2	Gr12	30	170	29.099	+	6.3432040	2.4615559	false	>99.9	2.7557644	false	>99.9
Th	Gr2	Gr12	31	283	30.127	+	7.1884610	2.4567009	false	>99.9	2.7492467	false	>99.9
U	Gr2	Gr12	29	282	28.372	+	6.0866295	2.4652118	false	>99.9	2.7606752	false	>99.9
V	Gr2	Gr12	37	218	54.872	–	0.9956984	2.3962373	true	83.79	2.6684212	true	67.58
Y	Gr2	Gr12	59	310	89.938	+	7.2123584	2.3685080	false	>99.9	2.6315774	false	>99.9
Zn	Gr2	Gr12	27	134	159.000	+	1.0056211	2.3500320	true	84.18	2.6071156	true	68.37
Zr	Gr2	Gr12	58	333	61.436	+	11.8831462	2.3885753	false	>99.9	2.6582260	false	>99.9
$\ln(TiO_2/SiO_2)$	Gr2	Gr12	115	413	174.971	+	13.9763792	2.3478563	false	>99.9	2.6042397	false	>99.9
$\ln(Al_2O_3/SiO_2)$	Gr2	Gr12	115	413	192.100	–	9.8147537	2.3459283	false	>99.9	2.6016920	false	>99.9
$\ln(Fe_2O_3/SiO_2)$	Gr2	Gr12	115	413	147.639	–	3.5994572	2.3518695	false	99.97	2.6095451	false	99.95
$\ln(FeO/SiO_2)$	Gr2	Gr12	115	406	144.006	–	7.0039468	2.3525191	false	>99.9	2.6104041	false	>99.9
$\ln(MnO/SiO_2)$	Gr2	Gr12	115	405	132.122	–	11.7915869	2.3548966	false	>99.9	2.6135490	false	>99.9
$\ln(MgO/SiO_2)$	Gr2	Gr12	114	406	149.946	–	1.8125967	2.3514737	true	96.41	2.6090217	true	92.81
$\ln(CaO/SiO_2)$	Gr2	Gr12	115	405	152.753	–	7.9108425	2.3510083	false	>99.9	2.6084062	false	>99.9
$\ln(Na_2O/SiO_2)$	Gr2	Gr12	110	406	204.730	+	15.5046203	2.3447148	false	>99.9	2.6000889	false	>99.9
$\ln(K_2O/SiO_2)$	Gr2	Gr12	110	403	317.291	+	22.0803477	2.3381823	false	>99.9	2.5914611	false	>99.9
$\ln(P_2O_5/SiO_2)$	Gr2	Gr12	113	386	166.111	+	12.5183097	2.3490111	false	>99.9	2.6057660	false	>99.9
ln(La/Th)	Gr2	Gr12	32	281	46.046	–	11.2692078	2.4100996	false	>99.9	2.6868943	false	>99.9
ln(Sm/Th)	Gr2	Gr12	30	261	289.000	–	13.7437146	2.3393444	false	>99.9	2.5929959	false	>99.9
ln(Yb/Th)	Gr2	Gr12	30	281	32.321	–	13.7591049	2.4474219	false	>99.9	2.7368011	false	>99.9
ln(Nb/Th)	Gr2	Gr12	32	211	44.034	–	0.9638711	2.4140642	true	82.93	2.6921840	true	65.87
$\ln(Nb/(TiO_2)_{adj})$	Gr2	Gr12	60	254	78.142	+	10.3226780	2.3750007	false	>99.9	2.6401907	false	>99.9
$\ln(V/(TiO_2)_{adj})$	Gr2	Gr12	35	218	56.566	–	11.6902043	2.3940846	false	>99.9	2.6655557	false	>99.9
$\ln(Y/(TiO_2)_{adj})$	Gr2	Gr12	60	316	80.582	–	8.9063023	2.3734987	false	>99.9	2.6381974	false	>99.9
$\ln(Zr/(TiO_2)_{adj})$	Gr2	Gr12	59	335	77.196	+	9.7771024	2.3756093	false	>99.9	2.6409986	false	>99.9
$\ln(MgO/TiO_2)_{adj}$	Gr2	Gr12	110	406	164.453	–	14.0819241	2.3492412	false	>99.9	2.6060702	false	>99.9
$\ln(P_2O_5/TiO_2)_{adj}$	Gr2	Gr12	98	387	305.568	–	1.7372725	2.3386377	true	95.83	2.5920626	true	91.67
$\ln(Ni/(TiO_2)_{adj})$	Gr2	Gr12	48	293	58.524	–	0.7033540	2.3917566	true	73.69	2.6624578	true	47.38
ln(La/Yb)	Gr2	Gr12	48	307	65.909	+	13.1721846	2.3842501	false	>99.9	2.6524758	false	>99.9
ln(Ce/Yb)	Gr2	Gr12	48	305	67.150	+	14.6977668	2.3831538	false	>99.9	2.6510187	false	>99.9
ln(Sm/Yb)	Gr2	Gr12	48	292	54.244	+	9.4483890	2.3970705	false	>99.9	2.6695306	false	>99.9
ln(Nb/Yb)	Gr2	Gr12	42	228	49.408	+	13.5943507	2.4042166	false	>99.9	2.6790503	false	>99.9
ln(Th/Yb)	Gr2	Gr12	30	281	32.321	+	13.7591049	2.4474219	false	>99.9	2.7368011	false	>99.9
ln(Y/Yb)	Gr2	Gr12	43	304	49.492	+	2.1640670	2.4040795	true	98.23	2.6788676	true	96.47
Ln(Zr/Yb)	Gr2	Gr12	41	304	343.000	+	18.0841603	2.3372924	false	>99.9	2.5902857	false	>99.9

For more information see footnote of Table 15.

Table 17. Application of significance tests (software: UDASYS; Verma et al., 2013a) to the traditional as well as log-transformed chemical data for acid volcanic rock samples from the eastern part of the Mexican Volcanic Belt (E-MVB) and the Central American Volcanic Arc (CAVA).

Parameter §	Group A (E-MVB)	Group B (CAVA)	nA (E-MVB)	nB (CAVA)	df	Sign	t_calc	t_crit One–Sided	H0 One–Sided	CL_t One–Sided	t_crit Two–Sided	H0 Two–Sided	CL_t Two–Sided
$(SiO_2)_{adj}$	Gr3	Gr13	90	36	124.000	+	3.0026890	2.3567873	false	99.84	2.6160510	false	99.68
$(TiO_2)_{adj}$	Gr3	Gr13	90	36	106.731	–	1.4627060	2.3617795	true	92.67	2.6226606	true	85.35
$(Al_2O_3)_{adj}$	Gr3	Gr13	91	35	105.545	–	4.1356673	2.3621833	false	99.92	2.6231955	false	99.84
$(Fe_2O_3)_{adj}$	Gr3	Gr13	91	36	125.000	–	4.6853485	2.3565411	false	99.53	2.6157251	false	99.06
$(FeO)_{adj}$	Gr3	Gr13	90	36	124.000	–	5.4067230	2.3567873	false	>99.9	2.6160510	false	>99.9
$(MnO)_{adj}$	Gr3	Gr13	90	35	48.228	–	9.9892707	2.4061844	false	>99.9	2.6816734	false	>99.9
$(MgO)_{adj}$	Gr3	Gr13	83	36	117.000	–	3.8258521	2.3586307	false	99.97	2.6184909	false	99.94
$(CaO)_{adj}$	Gr3	Gr13	90	34	77.765	–	3.9521398	2.3752410	false	99.97	2.6405098	false	99.93
$(Na_2O)_{adj}$	Gr3	Gr13	91	36	125.000	+	1.2162072	2.3565411	true	88.69	2.6157251	true	77.38
$(K_2O)_{adj}$	Gr3	Gr13	91	36	125.000	+	4.9717934	2.3565411	false	99.1	2.6157251	false	98.2
$(P_2O_5)_{adj}$	Gr3	Gr13	91	34	123.000	–	1.6095940	2.3570377	true	94.5	2.6163823	true	88.99
$(Fe_2O_3^t)_{adj}$	Gr3	Gr13	90	36	124.000	–	5.3062489	2.3567873	false	>99.9	2.6160510	false	>99.9
$(Na_2O+K_2O)_{adj}$	Gr3	Gr13	90	36	124.000	+	6.4066495	2.3567873	false	>99.9	2.6160510	false	>99.9
Mg #	Gr3	Gr13	91	36	106.664	–	1.2488868	2.3618019	true	89.28	2.6226903	true	78.56
La	Gr3	Gr13	29	14	34.316	+	4.4811929	2.4400567	false	99.93	2.7269330	false	99.85
Ce	Gr3	Gr13	29	13	36.755	+	4.3934208	2.4321876	false	99.94	2.7164004	false	99.87
Pr	Gr3	Gr13	16	3	17.0	–	0.3601082	2.5669522	true	<50	2.8982604	true	<50
Nd	Gr3	Gr13	29	10	37.000	+	0.2783105	2.4314572	true	<50	2.7154234	true	<50
Sm	Gr3	Gr13	29	8	35.0	–	1.6107406	2.4377385	true	94.19	2.7238535	true	88.38
Eu	Gr3	Gr13	29	10	37.000	–	3.8059346	2.4314572	false	99.97	2.7154234	false	99.94
Gd	Gr3	Gr13	25	8	31.000	–	1.5699752	2.4528428	true	93.67	2.7440702	true	87.34
Tb	Gr3	Gr13	29	6	33.000	–	1.2239249	2.4448100	true	88.52	2.7333006	true	77.04
Dy	Gr3	Gr13	16	3	17.0	–	1.9102035	2.5669522	true	96.34	2.8982604	true	92.69
Ho	Gr3	Gr13	16	8	22.0	–	3.2689220	2.5083545	false	99.82	2.8187994	false	99.65
Er	Gr3	Gr13	15	2	15.0	–	1.8707205	2.6024840	true	95.95	2.9467167	true	91.9
Tm	Gr3	Gr13	29	10	37.000	–	1.5503172	2.4314572	true	93.52	2.7154234	true	87.04
Yb	Gr3	Gr13	29	5	32.000	–	0.4396106	2.4486949	true	<50	2.7385076	true	<50
Lu	Gr3	Gr13	90	36	124.000	+	3.0026890	2.3567873	false	99.84	2.6160510	false	99.68
Ba	Gr3	Gr13	38	19	55.0	–	3.9201385	2.3960813	false	99.97	2.6682150	false	99.95
Co	Gr3	Gr13	25	9	8.459	–	3.6750666	2.8593663	false	99.72	3.3030861	false	99.43
Cr	Gr3	Gr13	17	10	25.0	+	2.2576468	2.4850622	true	98.35	2.7874162	true	96.7
Cs	Gr3	Gr13	13	2	1.021	+	2.8604545	31.8211700	true	89.3	63.6605000	true	78.6
Cu	Gr3	Gr13	12	4	3.249	–	5.0283106	4.2734100	false	99.38	5.4176040	true	98.75
Hf	Gr3	Gr13	14	5	17.0	+	3.1062036	2.5669522	false	99.68	2.8982604	false	99.36
Nb	Gr3	Gr13	46	13	57.000	+	12.9468979	2.3935544	false	>99.9	2.6648502	false	>99.9
Ni	Gr3	Gr13	14	14	26.0	+	3.6894620	2.4786262	false	99.95	2.7787488	false	99.9
Rb	Gr3	Gr13	48	19	65.0	+	11.1907409	2.3850803	false	>99.9	2.6535726	false	>99.9

Table 17. (Continued).

Parameter §	Group A (E-MVB)	Group B (CAVA)	nA (E-MVB)	nB (CAVA)	df	Sign	t_calc	t_crit One–Sided	H0 One–Sided	CL_t One–Sided	t_crit Two–Sided	H0 Two–Sided	CL_t Two–Sided
Sc	Gr3	Gr13	13	5	4.262	–	2.5428073	3.6228458	true	97.0	4.4164113	true	93.99
Sr	Gr3	Gr13	47	22	67.000	–	7.5825579	2.3832844	false	>99.9	2.6511923	false	>99.9
Ta	Gr3	Gr13	14	2	14.0	+	5.1602266	2.6245068	false	>99.9	2.9768513	false	>99.9
Th	Gr3	Gr13	14	8	20.0	+	7.2448974	2.5279932	false	>99.9	2.8453151	false	>99.9
U	Gr3	Gr13	14	8	20.0	+	9.0217927	2.5279932	false	>99.9	2.8453151	false	>99.9
V	Gr3	Gr13	26	12	13.501	–	1.9284075	2.6368443	true	96.25	2.9937723	true	92.49
Y	Gr3	Gr13	48	18	64.000	–	1.9659858	2.3860201	true	97.32	2.6548284	true	94.64
Zr	Gr3	Gr13	48	22	64.816	+	3.1328250	2.3852506	false	99.87	2.6538055	false	99.74
$ln(TiO_2/SiO_2)$	Gr3	Gr13	91	36	121.715	–	2.8897804	2.3573654	false	99.77	2.6168160	false	99.54
$ln(Al_2O_3/SiO_2)$	Gr3	Gr13	91	36	105.118	–	3.5978191	2.3623309	false	99.97	2.6233910	false	99.94
$ln(Fe_2O_3/SiO_2)$	Gr3	Gr13	91	36	106.644	–	5.1644041	2.3618089	false	>99.9	2.6226995	false	>99.9
$ln(FeO/SiO_2)$	Gr3	Gr13	90	36	99.640	–	5.5763360	2.3643394	false	>99.9	2.6260519	false	>99.9
$ln(MnO/SiO_2)$	Gr3	Gr13	89	35	69.076	–	7.8562375	2.3815338	false	>99.9	2.6488662	false	>99.9
$ln(MgO/SiO_2)$	Gr3	Gr13	91	36	110.843	–	3.7602242	2.3604475	false	99.97	2.6208964	false	99.95
$ln(CaO/SiO_2)$	Gr3	Gr13	91	34	104.778	–	4.6507041	2.3624494	false	99.61	2.6235480	false	99.22
$ln(Na_2O/SiO_2)$	Gr3	Gr13	91	36	125.000	+	0.0736105	2.3565411	true	<50	2.6157251	true	<50
$ln(K_2O/SiO_2)$	Gr3	Gr13	90	35	123.000	+	4.9635284	2.3570377	false	99.12	2.6163823	false	98.25
$ln(P_2O_5/SiO_2)$	Gr3	Gr13	87	36	47.178	–	0.3606840	2.4080209	true	<50	2.6841220	true	<50
ln(La/Th)	Gr3	Gr13	13	5	4.223	–	2.6498122	3.6398800	true	97.3	4.4420587	true	94.61
ln(Sm/Th)	Gr3	Gr13	13	3	2.045	–	2.8270116	6.7729756	true	94.72	9.6145188	true	89.43
ln(Yb/Th)	Gr3	Gr13	14	5	4.132	–	3.5877805	3.6815744	true	98.91	4.5049712	true	97.82
ln(Nb/Th)	Gr3	Gr13	13	7	18.0	–	5.1622933	2.5523976	false	>99.9	2.8784619	false	>99.9
$ln(Nb/(TiO_2)_{adj})$	Gr3	Gr13	48	13	59.000	+	6.1876595	2.3912145	false	>99.9	2.6617365	false	>99.9
$ln(V/(TiO_2)_{adj})$	Gr3	Gr13	27	12	14.225	–	0.4207192	2.6192512	true	<50	2.7154234	true	<50
$ln(Y/(TiO_2)_{adj})$	Gr3	Gr13	47	17	58.906	+	2.9725994	2.3913213	false	99.79	2.6618786	false	99.57
$ln(Zr/(TiO_2)_{adj})$	Gr3	Gr13	48	20	66.000	+	7.9608291	2.3841680	false	>99.9	2.6523665	false	>99.9
$ln(MgO/TiO_2)_{adj}$	Gr3	Gr13	91	36	125.000	–	2.8714834	2.3565411	false	99.76	2.6157251	false	99.52
$ln(P_2O_5/TiO_2)_{adj}$	Gr3	Gr13	88	34	42.844	+	1.4388027	2.4165904	true	92.12	2.6955560	true	84.25
$ln(Ni/(TiO_2)_{adj})$	Gr3	Gr13	14	14	26.0	+	6.2762243	2.4786262	false	>99.9	2.7787488	false	>99.9
ln(La/Yb)	Gr3	Gr13	27	10	35.0	+	6.2595748	2.4377385	false	>99.9	2.7238535	false	>99.9
ln(Ce/Yb)	Gr3	Gr13	28	10	36.000	+	4.9151405	2.4345054	false	99.75	2.7195016	false	99.51
ln(Sm/Yb)	Gr3	Gr13	27	8	32.904	+	1.1246996	2.4451741	true	86.56	2.7337885	true	73.13
ln(Nb/Yb)	Gr3	Gr13	21	5	24.0	+	3.9245522	2.4921631	false	99.97	2.7969494	false	99.93
ln(Th/Yb)	Gr3	Gr13	14	5	4.132	+	3.5877805	3.6815744	true	98.91	4.5049712	true	97.82
ln(Y/Yb)	Gr3	Gr13	20	9	27.0	+	0.9083106	2.4726494	true	81.25	2.7706877	true	62.49
ln(Zr/Yb)	Gr3	Gr13	21	10	29.0	+	2.6924279	2.4620517	false	99.42	2.7563496	true	98.83

For more information see footnote of Table 15.

2006b, 2012, 2013b; Verma SP and Verma SK, 2013), the second block from ln(La/Th) to ln(Nb/Th) is for immobile trace element-based diagrams for basic and ultrabasic rocks (Agrawal et al., 2008), the third block from ln(Nb/$(TiO_2)_{adj}$) to ln(Ni/$(TiO_2)_{adj}$) is for immobile major and trace element-based diagrams for all kinds of igneous rocks (Verma and Agrawal, 2011; Verma SP and Verma SK, 2013; Verma et al., 2013b), and the last block from ln(La/Yb) to ln(Zr/Yb) is for immobile trace element-based diagrams for intermediate and acid igneous rocks (Verma SP and Verma SK, 2013; Verma et al., 2013b).

Groups A and B are consistently used for the E-MVB and CAVA, respectively (Tables 15–17). Group numbers Gr1, Gr11, etc. are arbitrarily assigned as required by the computer program UDASYS. The number of samples for a given element or parameter in each group is shown in nA and nB columns. The degrees of freedom (df) column gives the respective value for assignment of critical t values ("t_crit One–Sided" and "t_crit Two–Sided"; Tables 15–17) as programmed in the UDASYS software. The minus sign in the "Sign" column and "false" in the column "H0 One–Sided" indicate that the parameter evaluated for Group A (E-MVB) shows a statistically lower concentration or value than for Group B (CAVA), whereas the plus sign and "false" in the column "H0 One–Sided" indicates just the opposite, i.e. the parameter for the E-MVB has a higher value than for CAVA. Finally, the outcome of "false" in the column "H0 Two–Sided" signifies that the parameter in the E-MVB and CAVA has significantly different values, whereas "true" in the column "H0 Two–Sided" indicates that the parameter in the E-MVB and CAVA does not have significantly different values.

4.3.1. Basic rocks

This type of rocks from the E-MVB and CAVA showed statistically significant differences for most (43 out of 50) chemical elements and (25 out of 28) log-ratio parameters (see "false" in columns "H0 One–Sided" and "H0 Two–Sided" in Table 15). For conventional chemical elements, the only exceptions were for MnO, Er, Ba, Co, Pb, Sb, and Sc; in fact, most of these conventional parameters showed significant differences at the 95% confidence level (for five of these elements, see values of >95 in the last column of Table 15). For log-ratios, only three parameters did not show statistically significant differences between the E-MVB and CAVA (Table 15). Because most log-ratio parameters showed significant differences, the E-MVB and CAVA samples plotted in different fields in the discrimination diagrams (Verma et al., 2006b, 2012, 2013b; Agrawal et al., 2008; Verma and Agrawal, 2011; Verma SP and Verma SK, 2013).

4.3.2. Intermediate rocks

Significant differences exist also for intermediate magmas from the E-MVB and CAVA for most (42 out of 50) elements and (23 out of 28) log-ratio parameters (Table 16). The elements with no difference are $(MgO)_{adj}$, Ba, Co, Cr, Sb, Sc, V, and Zn, whereas the ratios are ln(MgO/SiO_2), ln(Nb/Th), ln($P_2O_5/TiO_2)_{adj}$, ln(Ni/$(TiO_2)_{adj}$), and ln(Y/Yb). For intermediate rocks somewhat more parameters were similar for the E-MVB and CAVA than for basic rocks. Nevertheless, the similarities and differences among the log-ratio parameters can also explain the behavior of the E-MVB and CAVA samples in multidimensional diagrams.

4.3.3. Acid rocks

The E-MVB and CAVA showed a lesser number (26 out of 45) of chemical elements and (17 out of 28) log-ratio parameters for acid rocks for which significant differences were observed in their concentrations or values (Table 17). Smaller number of samples with statistically significant differences than for basic and intermediate rocks may be partly due to a very small number of samples of acid rocks compiled from the CAVA (only 2–36; Table 17).

5. Future work

The existing diagrams have been extensively used and tested in the original articles (Verma et al., 2006b, 2012, 2013b; Agrawal et al., 2008; Verma and Agrawal, 2011; Verma SP and Verma SK, 2013), as well as in numerous papers (e.g., Sheth, 2008; Van Kranendonk and Sonntag, 2012; Pandarinath and Verma, 2013; Polat, 2013; Verma, 2013; Verma and Oliveira, 2013, 2014; Verma SK and Verma SP, 2013; Pandarinath, 2014a, 2014b; Velasco-Tapia, 2014; Verma SK et al., 2015; Verma SP et al., 2015). Nevertheless, more work is still needed to fill the gap in these new, efficient, and statistically coherent geochemical tools for better elucidating geological processes. One such need is to distinguish the island and continental arcs in the discrimination diagrams for basic and ultrabasic magmas. This task can now be easily accomplished from an appropriate, representative database, because it has been recently shown (Verma et al., 2013a) from an extensive compilation of data that magmas from these two very similar tectonic settings have statistically significant differences for several log-ratio parameters.

New multidimensional diagrams for sedimentary rocks are also very much needed to complement the geological inference from igneous rocks. Two such diagrams to discriminate three tectonic settings have recently been proposed for siliciclastic sediments (Verma and Armstrong-Altrin, 2013), but more work will certainly help to discriminate five tectonic settings (island arc, continental arc, continental rift, ocean island, and collision) from sedimentary rock data. Similarly, the discrimination of conventional settings of active and passive continental margins is also of much interest.

Only the additive log-ratio (alr) transformation of

Aitchison (1986) has so far been used for discrimination diagrams (Verma et al., 2006b, 2012, 2013b; Agrawal et al., 2008; Verma and Agrawal, 2011; Verma SP and Verma SK, 2013). The other two types of log-ratio transformations (the centered log-ratio (clr) of Aitchison (1986) and isometric log-ratio (ilr) of Egozcue et al. (2003)) should also be evaluated and compared with the results of alr. Although from the same database exactly the same diagrams are obtained, the fulfillment of the multinormality condition required for linear discriminant analysis (Morrison, 1990) could result in slightly different databases, which would warrant the use of all three types of log-ratio transformations (Aitchison, 1986; Egozcue et al., 2003; Verma, unpublished data). Finally, new multidimensional diagrams for the classification of altered rocks are very much needed. Work with the ilr transformation is in progress, and soon new diagrams would be available for a more consistent nomenclature of altered igneous rocks.

6. Conclusions

The use of the conventional multielement and new multidimensional diagrams is successfully documented to decipher the tectonic setting of the E-MVB. Their good functioning is confirmed from the known subduction-related tectonic setting of the CAVA. The application of discordancy and significance tests indicates that a large number of chemical and log-ratio parameters show statistically significant differences between the E-MVB and CAVA, especially for basic and intermediate rocks. These multidimensional diagrams and discordancy and significance tests constitute renewed geochemical tools. The use of these tools is, therefore, highly recommended for future work for deciphering tectonic setting of a geological area under study, as well as for objectively inferring similarities and differences among different geological provinces.

Acknowledgments

This work was partly supported by DGAPA-PAPIIT project grant IN104813. I am also grateful to two anonymous reviewers for suggestions, which helped me to improve an earlier version of this paper.

References

Agostini S, Corti G, Doglioni C, Carminati E, Innocenti F, Tonarini S, Manetti P, Di Vincenzo G, Montanari D (2006). Tectonic and magmatic evolution of the active volcanic front in El Salvador: insight into the Berlín and Ahuachapán geothermal areas. Geothermics 35: 368–408.

Agrawal S (1999). Geochemical discrimination diagrams: a simple way of replacing eye-fitted boundaries with probability based classifier surfaces. J Geol Soc India 54: 335–346.

Agrawal S, Guevara M, Verma SP (2008). Tectonic discrimination of basic and ultrabasic rocks through log-transformed ratios of immobile trace elements. Int Geol Rev 50: 1057–1079.

Agrawal S, Verma SP (2007). Comment on "Tectonic classification of basalts with classification trees" by Pieter Vermeesch (2006). Geochim Cosmochim Acta 71: 3388–3390.

Aitchison J (1981). A new approach to null correlations of proportions. Math Geol 13: 175–189.

Aitchison J (1982). The statistical analysis of compositional data (with discussion). J Roy Stat Soc Ser B (Stat Methodol) 44: 137–177.

Aitchison J (1984). Statistical analysis of geochemical compositions. Math Geol 16: 531–564.

Aitchison J (1986). The Statistical Analysis of Compositional Data. London, UK: Chapman and Hall.

Aitchison J, Barceló-Vidal C, Martín-Fernández JA, Pawlowsky-Glahn V (2000). Logratio analysis and compositional distance. Math Geol 32: 271–275.

Aitchison J, Egozcue JJ (2005). Compositional data analysis: where are we and where should we be heading? Math Geol 37: 829–850.

Alvarado GE, Carr MJ, Turrin BD, Swisher III CC, Schmincke HU, Hudnut KW (2006). Recent volcanic history of Irazú volcano, Costa Rica: alternation and mixing of two magma batches, and pervasive mixing. In: Rose WI, Bluth GJS, Carr MJ, Ewert J, Patino LC, Vallance J, editors. Volcanic Hazards in Central America. Boulder, CO, USA: Geological Society of America, pp. 259–276.

Avellán DR, Macías JL, Pardo N, Scolamacchia T, Rodriguez D (2012). Stratigraphy, geomorphology, geochemistry and hazard implications of the Nejapa volcanic field, western Managua, Nicaragua. J Volcanol Geotherm Res 213–214: 51–71.

Bardintzeff JM, Deniel C (1992). Magmatic evolution of Pacaya and Cerro Chiquito volcanological complex, Guatemala. Bull Volcanol 54: 267–283.

Barnett V, Lewis T (1994). Outliers in Statistical Data. Chichester, UK: John Wiley & Sons.

Blatter DL, Carmichael ISE, Deino AL, Renne PR (2001). Neogene volcanism at the front of the central Mexican volcanic belt: basaltic andesites to dacites, with contemporaneous shoshonites and high-TiO_2 lava. Geol Soc Am Bull 113: 1324–1342.

Bolge LL, Carr MJ, Feigenson MD, Alvarado GE (2006). Geochemical stratigraphy and magmatic evolution at Arenal volcano, Costa Rica. J Volcanol Geotherm Res 157: 34–48.

Buccianti A, Mateau-Figueras G, Pawlowsky-Glahn V (2006). Compositional Data Analysis in the Geosciences: From Theory to Practice. London, UK: Geological Society of London Special Publication 262.

Cameron BI, Walker JA, Carr MJ, Patino LC, Matías O, Feigenson MD (2002). Flux versus decompression melting at stratovolcanoes in southeastern Guatemala. J Volcanol Geotherm Res 119: 21–50.

Carr MJ (1984). Symmetrical and segmented variation of physical and geochemical characteristics of the Central American volcanic front. J Volcanol Geotherm Res 20: 231–252.

Carr MJ, Feigenson MD, Bennett EA (1990). Incompatible element and isotopic evidence for tectonic control of source mixing and melt extraction along the Central American arc. Contrib Mineral Petrol 105: 369–380.

Carr MJ, Rose WI Jr (1986). Centam–a data base of Central American volcanic rocks. J Volcanol Geotherm Res 33: 239–240.

Carr MJ, Rose WI, Stoiber RE (1982). Central America. In: Thorpe RS, editor. Andesites. Chichester, UK: John Wiley & Sons, pp. 149–166.

Carr MJ, Saginor I, Alvarado GE, Bolge LL, Lindsay FN, Milidakis K, Turrin BD, Feigenson MD, Swisher CC 3rd (2007). Element fluxes from the volcanic front of Nicaragua and Costa Rica. Geochem Geophys Geosys 8: Q06001.

Carrasco-Núñez G (2000). Structure and proximal stratigraphy of Citlaltépetl volcano (Pico de Orizaba), Mexico. In: Delgado-Granados H, Aguirre-Díaz G, Stock JM, editors. Cenozoic Tectonics and Volcanism of Mexico. Boulder, CO, USA: Geological Society of America Special Paper, pp. 247–262.

Carrasco-Núñez G, Branney MJ (2005). Progressive assembly of a massive layer of ignimbrite with a normal-to-reverse compositional zoning: the Zaragoza ignimbrite of central Mexico. Bull Volcanol 68: 3–20.

Carrasco-Núñez G, McCurry M, Branney MJ, Norry M, Willcox C (2012). Complex magma mixing, mingling, and withdrawal associated with an intra-Plinian ignimbrite eruption at a large silicic caldera volcano: Los Humeros of central Mexico. Geol Soc Am Bull 124: 1793–1809.

Carrasco-Núñez G, Righter K, Chesley J, Siebert L, Aranda-Gómez JJ (2005). Contemporaneous eruption of calc-alkaline and alkaline lavas in a continental arc (Eastern Mexican Volcanic Belt): chemically heterogeneous but isotopically homogeneous source. Contrib Mineral Petrol 150: 423–440.

Carrasco-Núñez G, Rose WI (1995). Eruption of a major Holocene pyroclastic flow at Citlaltépetl volcano (Pico de Orizaba), México, 8.5-9.0 ka. J Volcanol Geotherm Res 69: 197–215.

Carrasco-Núñez G, Siebert L, Díaz-Castellón R, Vázquez-Selem L, Capra L (2010). Evolution and hazards of a long-quiescent compound shield-like volcano: Cofre de Perote, Eastern Trans-Mexican Volcanic Belt. J Volcanol Geotherm Res 197: 209–224.

Castro Govea R (1990). Historia eruptiva reciente del volcán La Malinche. MSc, Universidad Nacional Autónoma de México, Mexico City, Mexico (in Spanish).

Castro Govea R (2007). Historia eruptiva del volcán La Malinche y estudio del emplazamiento del flujo piroclástico Pilares Superior. PhD, Universidad Nacional Autónoma de México, Mexico City, Mexico (in Spanish).

Cebull SE, Shurbet DH (1987). Mexican Volcanic Belt: an intraplate transform? Geofis Int 26: 1–13.

Chan LH, Leeman WP, You CF (1999). Lithium isotopic composition of Central American Volcanic Arc lavas: implications for modification of subarc mantle by slab-derived fluids. Chem Geol 160: 255–280.

Chayes F (1960). On correlation between variables of constant sum. J Geophys Res 65: 4185–4193.

Correa Tello JC (2011). Caracterización petrográfica y geoquímica de Campo Volcánica de Santiago Tetlapayac-El Tepozán-Santa Cruz, Hidalgo. BSc, Universidad Nacional Autónoma de México, Mexico City, Mexico (in Spanish).

Cox KG, Bell JD, Pankhurst RJ (1979). The Interpretation of Igneous Rocks. London, UK: George Allen & Unwin.

Cruz-Huicochea R, Verma SP (2013). New critical values for F and their use in the ANOVA and Fisher's F tests for evaluating geochemical reference material granite G-2 (U.S.A.) and igneous rocks from the Eastern Alkaline Province (Mexico). J Iber Geol 39: 13–30.

Dávalos-Elizondo MG (2009) Petrología y geoquímica de xenolitos ultramáficos en Cd. Cerdán, Puebla, porción oriental de la Faja Volcánica Trans-Mexicana. MSc, Universidad Nacional Autónoma de México, Mexico City, Mexico (in Spanish).

De Cserna Z (1971). Precambrian sedimentation, tectonics, and magmatism in Mexico. Geol Rundsch 60: 1488–1513.

Demant A (1981). L'axe néo-volcanique transmexicain, étude volcanologique et pétrographique, signification géodynamique. PhD, Université de Droit, d'Economie et des Sciences d'Aix-Marseille, Marseille, France (in French).

DePaolo DJ (1981). Trace element and isotopic effects of combined wallrock assimilation and fractional crystallization. Earth Planet Sci Lett 53: 189–202.

Duffield WA, Heiken GH, Wohletz KH, Maassen LW, Dengo G, McKee EH, Castañeda O (1992). Geology and geothermal potential of the Tecuamburro volcano area, Guatemala. Geothermics 21: 425–446.

Egozcue JJ, Pawlowsky-Glahn V, Mateu-Figueras G, Barceló-Vidal C (2003). Isometric logratio transformations for compositional data analysis. Math Geol 35: 279–300.

Faure G (1986). Principles of Isotope Geology. New York, NY, USA: Wiley.

Feigenson MD, Carr MJ (1993). The source of Central American lavas: inferences from geochemical inverse modeling. Contrib Mineral Petrol 113: 226–235.

Ferrari L (2004). Slab detachment control on mafic volcanic pulse and mantle heterogeneity in central Mexico. Geology 32: 77–80.

Ferrari L, Petrone CM, Francalanci L (2002). Reply: "Generation of oceanic-island basalt type volcanism in the western Trans-Mexican volcanic belt by slab rollback, asthenosphere infiltration, and variable flux melting". Geology 114: 858–859.

Ferrari L, Rosas-Elguera J (1999). Alkalic (ocean-island basalt type) and calc-alkaline volcanism in the Mexican volcanic belt: a case for plume-related magmatism and propagating rifting at an active margin?: Comment and reply. Geology 27: 1055–1056.

Ferriz H, Mahood GA (1987). Strong compositional zonation in a silicic magmatic system: Los Humeros, Mexican Neovolcanic Belt. J Petrol 28: 171–209.

Floyd PA, Winchester JA (1975). Magma type and tectonic setting discrimination using immobile elements. Earth Planet Sci Lett 27: 211–218.

Floyd PA, Winchester JA (1978). Identification and discrimination of altered and meta-morphosed volcanic rocks using immobile elements. Chem Geol 21: 291–306.

Freeze AR, Cherry JA (1979). Groundwater. Upper Saddle River, NJ, USA: Prentice Hall.

Gómez-Tuena A, LaGatta AB, Langmuir CH, Goldstein SL, Ortega-Gutiérrez F, Carrasco-Núñez G (2003). Temporal control of subduction magmatism in the eastern Trans-Mexican Volcanic Belt: mantle sources, slab contributions, and crustal contamination. G3 4: 8912.

Gómez-Tuena A, Orozco-Esquivel MT, Ferrari L (2007). Igneous petrogenesis of the Trans-Mexican Volcanic Belt. In: Alaniz-Álvarez SA, Nieto-Samaniego ÁF, editors. Geology of Mexico: Celebrating the Centenary of the Geological Society of Mexico. Boulder, CO, USA: Geological Society of America, Colorado, USA, pp. 129–181.

González Partida E, Torres Rodriguez V, Birkle P (1997). Plio-Pleistocene volcanic history of the Ahuachapan geothermal system, El Salvador: the Concepción de Ataco caldera. Geothermics 26: 555–575.

Hall A (1996). Igneous Petrology. Essex, UK: Longman.

Hazlett RW (1987). Geology of San Cristobal volcanic complex, Nicaragua. J Volcanol Geotherm Res 33: 223–230.

Jensen JL, Lake LW, Corbett PWM, Goggin DJ (1997). Statistics for Petroleum Engineers and Geoscientists. Upper Saddle River, NJ, USA: Prentice Hall.

Kim WH, Clayton RW, Keppie F (2011). Evidence of a collision between the Yucatán block and Mexico in the Miocene. Geophys J Int 187: 989–1000.

Kudo AM, Jackson ME, Husler J W (1985). Phase chemistry of recent andesite, dacite, and rhyodacite of Volcan Pico de Orizaba, Mexican Volcanic Belt: evidence for xenolitic contamination. Geofis Int 24: 679–689.

Le Bas MJ (2000). IUGS reclassification of the high-Mg and picritic volcanic rocks. J Petrol 41: 1467–1470.

Le Bas MJ, Le Maitre RW, Streckeisen A, Zanettin B (1986). A chemical classification of volcanic rocks based on the total alkali-silica diagram. J Petrol 27: 745–750.

Le Bas MJ, Streckeisen AL (1991). The IUGS systematics of igneous rocks. J Geol Soc London 148: 825–833.

Leeman WP, Carr MJ (1995). Geochemical constraints on subduction processes in the Central American Volcanic Arc: Implications of boron geochemistry. GSA Special Papers 295: 57–73.

Le Maitre RW, Streckeisen A, Zanettin B, Le Bas MJ, Bonin B, Bateman P, Bellieni G, Dudek A, Schmid R, Sorensen H et al. (2002). Igneous Rocks. A Classification and Glossary of Terms: Recommendations of the International Union of Geological Sciences Subcommission of the Systematics of Igneous Rocks. Cambridge, UK: Cambridge University Press.

López Hernández A (2009) Evolución volcánica del complejo Tulancingo-Acoculco y su sistema hidrotermal, estados de Hidalgo y Puebla, México. PhD, Universidad Nacional Autónoma de México, Mexico City, Mexico (in Spanish).

Márquez A, Oyarzun R, de Ignacio C, Doblas M (2001). Southward migration of volcanic activity in the central Mexican Volcanic Belt: asymmetric extension within a two-layer crustal stretching model. J Volcanol Geotherm Res 112: 175–187.

Márquez A, Oyarzun R, Doblas M, Verma SP (1999a). Alkalic (ocean-island basalt type) and calc-alkalic volcanism in the Mexican Volcanic Belt: a case for plume-related magmatism and propagating rifting at an active margin? Geology 27: 51–54.

Márquez A, Oyarzun R, Doblas M, Verma SP (1999b). Reply (to Comment by L. Ferrari and J. Rosas Elguera on "Alkalic (ocean basalt type) and calc-alkalic volcanism in the Mexican volcanic belt: a case of plume-related magmatism and propagating rift at an active margin?" Comment and Reply. Geology 27: 1055–1056.

McDonough WF, Sun SS (1995). The composition of the Earth. Chem Geol 120: 223–253.

Middlemost EAK (1989). Iron oxidation ratios, norms and the classification of volcanic rocks. Chem Geol 77: 19–26.

Miller JN, Miller JC (2005). Statistics and chemometrics for analytical chemistry. Essex, UK: Pearson Prentice Hall.

Molnar P, Sykes LR (1969). Tectonics of the Caribbean and Middle America regions from focal mechanisms and seismicity. Geol Soc Am Bull 80: 1639–1684.

Moore G, Marone C, Carmichael ISE, Renne P (1994). Basaltic volcanism and extension near the intersection of the Sierra Madre volcanic province and the Mexican Volcanic Belt. Geol Soc Am Bull 106: 383–394.

Mooser F (1969). The Mexican Volcanic Belt-structure and development. Formation of fractures by differential crustal heating. In: Maldonado-Koerdell M, editor. Pan-American Symposium on Upper Mantle. Group II: Upper Mantle Petrology and Tectonics. Mexico City, Mexico: Instituto de Geofísica, UNAM, pp. 15–22.

Mora JC, Macías JL, García-Palomo A, Arce JL, Espíndola JM, Manetti P, Vaselli O, Sánchez JM (2004). Petrology and geochemistry of the Tacaná Volcanic complex, Mexico-Guatemala: evidence for the last 40 000 yr of activity. Geofis Int 43: 331–359.

Morales Barrera WV (2009). Estudio geológico de un depósito ignimbrítico en la región de Xalapa, Veracruz: distribución, estratigrafía, petrografía, y geoquímica. MSc, Universidad Nacional Autónoma de México, Mexico City, Mexico (in Spanish).

Morrison DF (1990). Multivariate Statistical Methods. New York, NY, USA: McGraw-Hill.

Mooser F, Maldonado-Koerdell M (1961). Mexican national report on volcanology. Anal Inst Geofis 7: 45–53.

Negendank JFW, Emmermann R, Krawczyk R, Mooser F, Tobschall H, Werle D (1985). Geological and geochemical investigations on the eastern Trans Mexican Volcanic Belt. Geofis Int 24: 477–575.

Negendank JFW, Emmermann R, Mooser F, Seifert-Kraus U, Tobschall HJ (1981). Evolution of some Tertiary and Quaternary central volcanoes of the Trans-Mexican Volcanic Belt and possible different positions of the Benioff zone. Zentralb Geol Paläont 3/4: 183–194.

Orozco-Esquivel MT (1995). Zur Petrologie des Vulkangebietes von Palma-Sola, Mexiko. Ein Beispiel fuer den Uebergang von anorogenem zu orogenem Vulkanismus. PhD, Universitaet Karlsruhe, Karlsruhe, Germany.

Orozco-Esquivel T, Petrone CM, Ferrari L, Tagami T, Manetti P (2007). Geochemical and isotopic variability in lavas from the eastern Trans-Mexican Volcanic Belt: slab detachment in a subduction zone with varying dip. Lithos 93: 149–174.

Ottonello G (1997). Principles of Geochemistry. New York, NY, USA: Columbia University Press.

Pacheco JF, Singh SK (2010). Seismicity and state of stress in Guerrero segment of the Mexican subduction zone. J Geophys Res 115: B01303.

Pandarinath K (2014a). Testing of the recently developed tectonomagmatic discrimination diagrams from hydrothermally altered igneous rocks of 7 geothermal fields. Turk J Earth Sci 23: 412–426.

Pandarinath K (2014b). Tectonomagmatic origin of Precambrian rocks of Mexico and Argentina inferred from multi-dimensional discriminant-function based discrimination diagrams. J South Am Earth Sci 56: 464–484.

Pandarinath K, Verma SK (2013). Application of four sets of tectonomagmatic discriminant function based diagrams to basic rocks from northwest Mexico. J Iber Geol 39: 181–195.

Pardo M, Suárez G (1995). Shape of the subducted Rivera and Cocos plates in southern Mexico: Seismic and tectonic implications. J Geophys Res 100: 12357–12373.

Pardo N, Avellán DR, Macías JL, Scolamacchia T, Rodríguez D (2008). The ~1245 yr BP Asososca maar: new advances on recent volcanic stratigraphy of Managua (Nicaragua) and hazard implications. J Volcanol Geotherm Res 176: 493–512.

Patino LC, Carr MJ, Feigenson MD (1997). Cross-arc geochemical variations in volcanic fields in Honduras C.A.: progressive changes in source with distance from the volcanic front. Contrib Mineral Petrol 129: 341–351.

Patino LC, Carr MJ, Feigenson MD (2000). Local and regional variations in Central American arc lavas controlled by variations in subducted sediment input. Contrib Mineral Petrol 138: 265–283.

Pearson K (1897). Mathematical contribution to the theory of evolution. - on a form of spurious correlation which may arise when indices are used in the measurement of organs. P R Soc London 60: 489–502.

Pérez-Campos X, Kim Y, Husker A, Davis PM, Clayton RW, Iglesias A, Pacheco JF, Singh SK, Manea VC, Gurnis M (2008). Horizontal subduction and truncation of the Cocos plate beneath central Mexico. Geophys Res Lett 35: L18303.

Polat A (2013). Geochemical variations in Archean volcanic rocks, southwestern Greenland: traces of diverse tectonic settings in the early Earth. Geology 41: 379–380.

Ragland PC (1989). Basic Analytical Petrology. New York, NY, USA: Oxford University Press.

Reagan MK, Gill JB (1989). Coexisting calcalkaline and high-niobium basalts from Turrialba volcano, Costa Rica: implications for residual titanates in arc magma sources. J Geophys Res 94: 4619–4633.

Rodríguez SR, Siebe C, Komorowski JC, Abrams M (2002). The Quetzalapa pumice: a voluminous late Pleistocene rhyolite deposit in the eastern Trans-Mexican Volcanic Belt. J Volcanol Geotherm Res 113: 177–212.

Rollinson HR (1993). Using Geochemical Data: Evaluation, Presentation, Interpretation. Essex, UK: Longman Scientific Technical.

Rossotti A, Carrasco-Núñez G, Rosi M, Di Muro A (2006). Eruptive dynamics of the "Citlaltépetl pumice" at Citlaltépetl volcano, eastern Mexico. J Volcanol Geotherm Res 158: 401–429.

Rotolo SG, Castorina F (1998). Transition from mildly-tholeiitic to calc-alkaline suite: the case of Chicontepec volcanic centre, El Salvador, Central America. J Volcanol Geotherm Res 86: 117–136.

Ryder CH, Gill JB, Tepley F 3rd, Ramos F, Reagan M (2006). Closed-to open-system differentiation at Arenal volcano (1968-2003). J Volcanol Geotherm Res 157: 75–93.

Schaaf P, Carrasco-Núñez G (2010). Geochemical and isotopic profile of Pico de Orizaba (Citlaltépetl) volcano, Mexico: Insights for magma generation processes. J Volcanol Geotherm Res 197: 108–122.

Siebe C, Abrams M, Sheridan MF (1993). Major Holocene block-and-ash fan at the western slope of ice-capped Pico de Orizaba volcano, México: implications for future hazards. J Volcanol Geotherm Res 59: 1–33.

Siebe C, Verma SP (1988). Major element geochemistry and tectonic setting of Las Derrumbadas rhyolitic domes, Puebla, Mexico. Chem Erde 48: 177–189.

Siebert L, Carrasco-Núñez G (2002). Late-Pleistocene to precolumbian behind-the-arc mafic volcanism in the eastern Mexican Volcanic Belt; implications for future hazards. J Volcanol Geotherm Res 115: 179–205.

Sheth HC (2008). Do major oxide tectonic discrimination diagrams work? Evaluating new log-ratio and discriminant-analysis-based diagrams with Indian Ocean mafic volcanics and Asian ophiolites. Terra Nova 20: 229–236.

Sheth HC, Torres-Alvarado IS, Verma SP (2000). Beyond subduction and plumes: a unified tectonic-petrogenetic model for the Mexican Volcanic Belt. Int Geol Rev 42: 1116–1132.

Shurbet DH, Cebull SE (1984). Tectonic interpretation of the Trans-Mexican Volcanic Belt. Tectonophysics 101: 159–165.

Singer BS, Smith KE, Jicha BR, Beard BL, Johnson CM, Rogers NW (2011). Tracking open-system differentiation during growth of Santa María volcano, Guatemala. J Petrol 52: 2335–2363.

Suarez G, Singh SK (1986). Tectonic interpretation of the Trans-Mexican Volcanic Belt—discussion. Tectonophysics 127: 155–160.

Sun SS, McDonough WF (1989). Chemical and isotopic systematics of oceanic basalts: implications for mantle composition and processes. In: Saunders AD, Norry MJ, editors. Magmatism in the Ocean Basins. London, UK: Geological Society Special Publication, pp. 313–345.

Sussman D (1985). Apoyo caldera, Nicaragua: a major Quaternary silicic eruptive center. J Volcanol Geotherm Res 24: 249–282.

Tatsumi Y, Eggins S (1995). Subduction Zone Magmatism. Frontiers in Earth Sciences. Cambridge, MA, USA: Blackwell Science.

Taylor SR, McLennan SM (1985). The Continental Crust: Its Composition and Evolution. Geoscience Texts. Oxford, UK: Blackwell Scientific.

Torres-Alvarado IS, Verma SP (2003). Discussion and reply: Neogene volcanism at the front of the central Mexican Volcanic Belt: basaltic andesites to dacites, with contemporaneous shoshonites and high-TiO_2 lava. Geol Soc Am Bull 115: 1020–1024.

Torres-Alvarado IS, Verma SP, Palacios-Berruete H, Guevara M, González-Castillo OY (2003). DC_Base: a database system to manage Nernst distribution coefficients and its application to partial melting modeling. Comput Geosci 29: 1191–1198.

Van Kranendonk MJ, Sonntag I (2012). Geochemistry and tectonic setting of basalts from the Eastern Goldfields Superterrane. Aust J Earth Sci 59: 707–735.

Velasco-Tapia F (2014). Multivariate analysis, mass balance techniques, and statistical tests as tools in igneous petrology: Application to the Sierra de las Cruces Volcanic Range (Mexican Volcanic Belt). The Scientific World Journal 2014; 2014: 793236.

Velasco-Tapia F, Verma SP (2013). Magmatic processes at the volcanic front of Central Mexican Volcanic Belt: Sierra de Chichinautzin volcanic field (Mexico). Turk J Earth Sci 22: 32–60.

Verma SK, Oliveira EP (2013). Application of multi-dimensional discrimination diagrams and probability calculations to Paleoproterozoic acid rocks from Brazilian cratons and provinces to infer tectonic settings. J South Am Earth Sci 45: 117–146.

Verma SK, Oliveira EP (2014). Tectonic setting of basic igneous and metaigneous rocks of Borborema Province, Brazil using multi-dimensional geochemical discrimination diagrams. J South Am Earth Sci (in press).

Verma SK, Oliveira EP, Verma SP (2015). Plate tectonic settings for Precambrian basic rocks from Brazil by multi-dimensional tectonomagmatic discrimination diagrams and their limitations. Int Geol Rev (in press).

Verma SK, Pandarinath K, Verma SP (2012). Statistical evaluation of tectonomagmatic discrimination diagrams for granitic rocks and proposal of new discriminant-function-based multi-dimensional diagrams for acid rocks. Int Geol Rev 54: 325–347.

Verma SK, Verma SP (2013). Identification of Archaean plate tectonic processes from multidimensional discrimination diagrams and probability calculations. Int Geol Rev 55: 225–248.

Verma SP (1983). Magma genesis and chamber processes at Los Humeros caldera, Mexico–Nd and Sr isotope data. Nature 301: 52–55.

Verma SP (1984). Alkali and alkaline earth element geochemistry of Los Humeros caldera, Puebla, Mexico. J Volcanol Geotherm Res 20: 21–40.

Verma SP (1991a). Determination of thirteen rare-earth elements by high-performance liquid chromatography in thirty and of K, Rb, Cs, Sr and Ba by isotope dilution mass spectrometry in eighteen international geochemical reference samples. Geostand Newslett 15: 129–134.

Verma SP (1991b). Usefulness of liquid chromatography for determination of thirteen rare-earth elements in rocks and minerals. Lanth Actin Res 3: 237–257.

Verma SP (1992). Seawater alteration effects on REE, K, Rb, Cs, Sr, U, Th, Pb and Sr-Nd-Pb isotope systematics of Mid-Ocean Ridge Basalt. Geochem J 26: 159–177.

Verma SP (1999). Geochemistry of evolved magmas and their relationship to subduction-unrelated mafic volcanism at the volcanic front of the central Mexican Volcanic Belt. J Volcanol Geotherm Res 93: 151–171.

Verma SP (2000a). Geochemical evidence for a lithospheric source for magmas from Los Humeros caldera, Puebla, Mexico. Chem Geol 164: 35–60.

Verma SP (2000b). Geochemistry of the subducting Cocos plate and the origin of subduction-unrelated mafic volcanism at the volcanic front of the central Mexican Volcanic Belt. In: Delgado-Granados H, Aguirre-Díaz G, Stock JM, editors. Cenozoic Tectonics and Volcanism of Mexico. Boulder, CO, USA: Geological Society of America Special Papers, pp. 195–222.

Verma SP (2001a). Geochemical evidence for a lithospheric source for magmas from Acoculco caldera, Eastern Mexican Volcanic Belt. Int Geol Rev 43: 31–51.

Verma SP (2001b). Geochemical and Sr-Nd-Pb isotopic evidence for a combined assimilation and fractional crystallisation process for volcanic rocks from the Huichapan caldera, Hidalgo, Mexico. Lithos 56: 141–164.

Verma SP (2002). Absence of Cocos plate subduction-related basic volcanism in southern Mexico: a unique case on Earth? Geology 30: 1095–1098.

Verma SP (2004). Solely extension-related origin of the eastern to west-central Mexican Volcanic Belt (Mexico) from partial melting inversion model. Curr Sci 86: 713–719.

Verma SP (2005). Estadística básica para el manejo de datos experimentales: aplicación en la Geoquímica (Geoquimiometría). Mexico City, Mexico: UNAM (in Spanish).

Verma SP (2006). Extension-related origin of magmas from a garnet-bearing source in the Los Tuxtlas volcanic field, Mexico. Int J Earth Sci 95: 871–901.

Verma SP (2009). Continental rift setting for the central part of the Mexican Volcanic Belt: a statistical approach. Open Geol J 3: 8–29.

Verma SP (2010). Statistical evaluation of bivariate, ternary and discriminant function tectonomagmatic discrimination diagrams. Turk J Earth Sci 19: 185–238.

Verma SP (2012). Application of multi-dimensional discrimination diagrams and probability calculations to acid rocks from Portugal and Spain. Comunicaç Geol 99: 79–93.

Verma SP (2013). Application of 50 multi-dimensional discrimination diagrams and significance tests to decipher compositional similarities and differences between Hawaiian and Icelandic volcanism. Int Geol Rev 55: 1553–1572.

Verma SP, Agrawal S (2011). New tectonic discrimination diagrams for basic and ultrabasic volcanic rocks through log-transformed ratios of high field strength elements and implications for petrogenetic processes. Rev Mex Cienc Geol 28: 24–44.

Verma SP, Armstrong-Altrin JS (2013). New multi-dimensional diagrams for tectonic discrimination of siliciclastic sediments and their application to Precambrian basins. Chem Geol 355: 117–133.

Verma SP, Besch T, Guevara M, Schulz-Dobrich B (1992). Determination of twelve trace elements in twenty-seven and ten major elements in twenty-three geochemical reference samples by X-ray fluorescence spectrometry. Geostand Newslett 16: 301–309.

Verma SP, Cruz-Huicochea R (2013). Alternative approach for precise and accurate Student´s t critical values and application in geosciences. J Iber Geol 39: 31–56.

Verma SP, Cruz-Huicochea R, Díaz-González L (2013a). Univariate data analysis system: deciphering mean compositions of island and continental arc magmas, and influence of underlying crust. Int Geol Rev 55: 1922–1940.

Verma SP, Díaz-González L (2012). Application of the discordant outlier detection and separation system in the geosciences. Int Geol Rev 54: 593–614.

Verma SP, Díaz-González L, González-Ramírez R (2009). Relative efficiency of single-outlier discordancy tests for processing geochemical data on reference materials and application to instrumental calibration by a weighted least-squares linear regression model. Geostand Geoanal Res 33: 29–49.

Verma SP, Díaz-González L, Sánchez-Upton P, Santoyo E (2006a). OYNYL: A new computer program for ordinary, York, and New York least-squares linear regressions. WSEAS Trans Environ Dev 2: 997–1002.

Verma SP, Guevara M, Agrawal S (2006b). Discriminating four tectonic settings: five new geochemical diagrams for basic and ultrabasic volcanic rocks based on log-ratio transformation of major-element data. J Earth Syst Sci 115: 485–528.

Verma SP, Lopez MM (1982). Geochemistry of Los Humeros caldera, Puebla, Mexico. Bull Volcanol 45: 63–79.

Verma SP, Pandarinath K, Verma SK, Agrawal S (2013b). Fifteen new discriminant-function-based multi-dimensional robust diagrams for acid rocks and their application to Precambrian rocks. Lithos 168–169: 113–123.

Verma SP, Quiroz-Ruiz A (2008). Critical values for 33 discordancy test variants for outliers in normal samples of very large sizes from 1,000 to 30,000 and evaluation of different regression models for the interpolation of critical values. Rev Mex Cienc Geol 25: 369–381.

Verma SP, Quiroz-Ruiz A (2011). Corrigendum to Critical values for 22 discordancy test variants for outliers in normal samples up to sizes 100, and applications in science and engineering [Rev. Mex. Cienc. Geol., 23 (2006), 302–319]. Rev Mex Cienc Geol 28: 202.

Verma SP, Quiroz-Ruiz A, Díaz-González L (2008). Critical values for 33 discordancy test variants for outliers in normal samples up to sizes 1000, and applications in quality control in Earth Sciences. Rev Mex Cienc Geol 25: 82–96.

Verma SP, Rivera-Gómez MA (2013a). Computer programs for the classification and nomenclature of igneous rocks. Episodes 36: 115–124.

Verma SP, Rivera-Gómez MA (2013b). New computer program TecD for tectonomagmatic discrimination from discriminant function diagrams for basic and ultrabasic magmas and its application to ancient rocks. J Iber Geol 39: 167–179.

Verma SP, Rodríguez-Ríos R, González-Ramírez R (2010). Statistical evaluation of classification diagrams for altered igneous rocks. Turk J Earth Sci 19: 239–265.

Verma SP, Torres-Alvarado IS, Sotelo-Rodríguez ZT (2002). SINCLAS: Standard igneous norm and volcanic rock classification system. Comput Geosci 28: 711–715.

Verma SP, Torres-Alvarado IS, Velasco-Tapia F (2003). A revised CIPW norm. Schweiz Miner Petrog Mitteil 83: 197–216.

Verma SP, Verma SK (2013). First 15 probability-based multi-dimensional discrimination diagrams for intermediate magmas and their robustness against post-emplacement compositional changes and petrogenetic processes. Turk J Earth Sci 22: 931–995.

Verma SP, Verma SK, Oliveira EP (2015). Application of 55 multi-dimensional tectonomagmatic discrimination diagrams to Precambrian belts. Int Geol Rev (in press).

Verma SP, Verma SK, Pandarinath K, Rivera-Gómez MA (2011). Evaluation of recent tectonomagmatic discrimination diagrams and their application to the origin of basic magmas in Southern Mexico and Central America. Pure Appl Geophys 168: 1501–1525.

Walker JA, Carr MJ, Feigenson MD, Kalamarides RI (1990). The petrogenetic significance of interstratified high- and low-Ti basalts in central Nicaragua. J Petrol 31: 1141–1164.

Walker JA, Patino LC, Cameron BI, Carr MJ (2000). Petrogenetic insights provided by compositional transects across the Central American arc: southeastern Guatemala and Honduras. J Geophys Res 105: 18949–18963.

Walker JA, Patino LC, Carr MJ, Feigenson MD (2001). Slab control over HFSE depletions in central Nicaragua. Earth Planet Sci Lett 192: 533–543.

Wedepohl KH (1971). Geochemistry. New York, NY, USA: Holt, Rinehart and Winston.

Wilson M (1989). Igneous Petrogenesis. A Global Tectonic Approach. London, UK: Harper Collins Academic.

Winchester JA, Floyd PA (1976). Geochemical magma type discrimination: application to altered and metamorphosed basic igneous rocks. Earth Planet Sci Lett 28: 459–469.

Winchester JA, Floyd PA (1977). Geochemical discrimination of different magma series and their differentiation products using immobile elements. Chem Geol 20: 325–343.